

Point-by-point response to reviewers

In the following responses, reviewer comments are in black, author responses are in blue and author changes are highlighted in green.

Response to RC1

I find this paper to be an interesting contribution with a few minor issues. My main concern is with section 6.2 which I think needs some more care in how they infer things from the data. A common issue throughout the paper is that the meanings of things like color ratio and depolarization ratio are given much context (what does a value of X really mean).

Response:

The authors thank the reviewer for comments on the manuscript. As suggested, Section 6.2 has been revised and more care has been taken when interpreting the time evolution of the volcanic aerosols. Upon revisiting the time series analysis we noticed an error in the code that was used to construct the time series from the lidar data. In the original code, the **cumulative** mean was being calculated for each optical property in the time series. The time of each observation was also, incorrectly, calculated as a cumulative mean, which resulted in the incorrect residence time for each data point presented in Fig. 8 of the original manuscript.

In the revised manuscript, this error has been corrected so that the curtain means and root mean square errors are calculated for each CALIOP/AIRS observation and are plotted together with the curtain mean of the time of each observation.

Note that we define the ‘curtain mean’ as the mean of all CALIOP layer optical properties (i.e. S_p , δ_v , δ_p and χ') within a collocated AIRS granule, which equates to a ~ 6 minute subset of a CALIOP granule. This revision only affects the original data plotted in Fig. 8 of the original manuscript. It also impacts the calculation of the e -folding time of the Sarychev depolarization ratios. We have therefore attached the revised version of Fig. 8 (Figure 1 of this document) below.

We have also more explicitly defined both the depolarization ratio and the color ratio in the revised manuscript.

We note, though, that the color ratio is constructed based on only two measurements (532 and 1064 nm attenuated backscatter) and so it is difficult to infer, quantitatively, what the volcanic aerosol particle sizes are without assuming more about the complex refractive index and size distribution of the particles. It can, however, be used to infer relative size. This is explained in more detail in the revised manuscript and in the responses to comments that follow.

Page 7, line 26. Does mean there was effectively no change in the values during measurement period?

Response:

Indeed, there was little change in the optical properties during the measurement period for the Kasatochi case study. We refer the reviewer to the revised Fig. 8 (Figure 1 below), which shows how the optical properties changed over time during the measurement time period.

Page 7, line 28. You commonly refer to layers as either sulfate or ash. While sometimes these

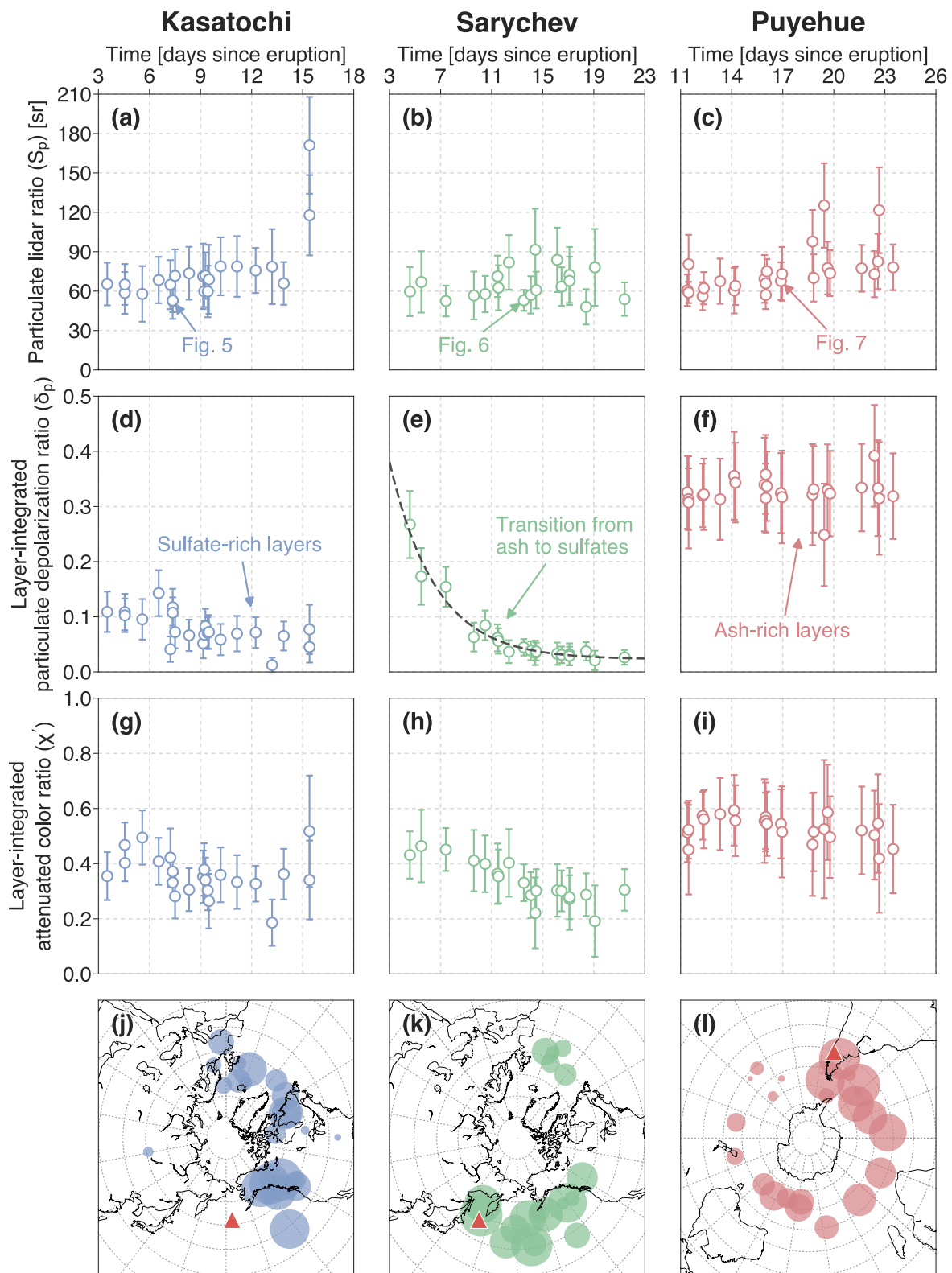


Figure 1: Revised version of Fig. 8 of the original manuscript.

layers separate themselves, other times they can be mixed in a complex fashion. You may wish to define your layers as layers optically dominated by ash or sulfate aerosol rather than imply that they are distinctly one or the other. Is it possible that complex mixing is responsible for the rather large variations in the backscatter to extinction ratio? Alternatively, is it consistent with noise or variability in the sulfate and/or ash itself?

Response:

Thank you for suggesting this.

In the revised manuscript, the authors refer to layers as 'ash-rich', 'sulfate-rich' and as being 'optically dominated' by either ash or sulfate.

To the reviewer's second point: as we are measuring the aerosol layers over a number of days across the globe, it is possible that complex mixing of ambient aerosol will be occurring over time. Sedimentation, dehydration and coagulation processes are also likely to be occurring. Therefore some variability in the lidar ratio should be expected. We note, however, that the lidar ratio retrieval becomes more sensitive (and uncertain) to changes in the return backscatter signal as the two-way transmittance approaches 1 (see Fig. 4 of original manuscript). As the majority of the aerosol layers were optically thin ($\tau_e < 1$), the large variability (high standard deviations) in the lidar ratio PDFs (Fig. 2 of original manuscript) is probably also, in part, due to the high sensitivity to noise in the backscatter return signal. However, based on the observational evidence provided by the color and depolarization ratios, we believe that CALIOP has captured compositional changes in the volcanic aerosols under examination; particularly for the Sarychev case (see Figure 1e of this document). We have included this discussion in the revised manuscript as follows:

"The decay in δ_p corresponds to an e -folding time of 3.6 days (dashed line; Fig 8e) and may indicate that ash particles were being removed from the atmosphere during the measurement period for the Sarychev case study."

Page 8, Some of these figures are much too small to see much detail in. I know I can blow them up to see them but my experience is that ACP makes them into JPGs for the final figures and they are always 'infinite' resolution like some bad TV show.

Response:

To improve readability, we have increased the size of all figures on page 8. We have also increased the font size in all figures.

The majority of our figures are in pdf (vectorised) format and so no resolution will be lost in the ACP typesetting stage for these figures. All other figures are in png (non-lossy) format with a dpi of 600. We have been careful to follow the ACP guidelines on producing high quality figures as described here: http://www.atmospheric-chemistry-and-physics.net/for_authors/manuscript_preparation.html

Page 9, Here I will be a curmudgeon, I hate VEI. People use it like it is a quantitative assessment of volcanic explosivity and I think it is disappointingly far short of that and often is not relevant to stratospheric impact. Check this out (a commercial site but the definition is correct) <http://geology.com/stories/13/volcanic-explosivity-index/> . The definition is a mess.

Response:

Reference to the VEI has been removed in the revised manuscript as the authors agree that its use here is not relevant to the study.

Page 9, How do you avoid ice-rich layers? (line 20) Also, since there is a composition change from sulfate to ash, how sure are you that the changes in the color ratio are due solely to size rather than simply that they are a different color?

Response:

Ice-rich layers are avoided based on the Ash Index (AI) criterion. If a stratospheric layer were ice-rich then we would expect the AI to be strongly negative (Prata et al., 2015). Since our criterion is set so that we only accept $AI \geq 1$ we assume that ice-rich layers have been removed from the analysis.

The explicit definition of the AI has been included in the revised manuscript.

To the reviewer's second point, we never suggest that there is a transition from sulfate to ash, rather, we suggest that there is a composition change from ash to sulfate (based on the depolarization and color ratio changes for the Sarychev case). Sulfate aerosols are generally in the 0.1–1 μm radius size range and ash particles that have resided in the stratosphere for more than 2 weeks would likely be sub-micron to micron size. Indeed, O'Neill et al. (2012) report effective radii of 0.25 μm for the Sarychev aerosols over the Arctic. This means that the size of the particles under examination is less than/comparable to the sampling wavelengths (532 nm and 1064 nm). In this sense, we are talking about scattering and absorption, rather than reflection, which means changes in the 'color' of the particles (in the usual sense of the word) could not be inferred using CALIOP measurements.

The color ratio can change due to changes in the size, complex refractive index and shape of the aerosols being measured. We speculate that ash particles were present in the initial observations of the CALIOP measurements for Sarychev case and so a combination of the sedimentation (contributing to a reduction in particle size) and sulfate formation (contributing to a change in the imaginary part of the refractive index) led to changes in the color ratio. This discussion has been included in the revised manuscript as follows:

"Figure 8h demonstrates that χ' also decreased with time over the measurement period. Changes in χ' can be due to changes in the size, complex refractive index and shape of the aerosols being measured. It is difficult to infer, quantitatively, what the volcanic aerosol particle sizes are without assuming more about the complex refractive index and size distribution of the particles; however, we note that O'Neill et al. (2012) report effective radii of 0.25 μm for the Sarychev aerosols over the Arctic. As the attenuated color ratio is constructed based on two measurements (532 and 1064 nm attenuated backscatter) we can only use it to infer relative changes in particle size. We speculate that ash particles were present in the initial observations of the CALIOP measurements and so a combination of the sedimentation (contributing to a reduction in particle size) and sulfate formation (contributing to a change in the imaginary part of the refractive index) led to a decrease in χ' with time."

Page 13, line 11. I think it would be more proper to say 'unambiguously identifying this layer as containing non-spherical particles. It is not necessarily an either/or situation...

Response:

Accepted. The sentence in the revised manuscript has been amended to read:

"The Puyehue layers (Fig. 7) are quite similar to the sulfate-dominated layers in terms of the geometric thickness; however, the layer-integrated optical properties, along with the AIRS ash signal,

unambiguously identify this layer as containing non-spherical ash particles.”

Section 6.2. I find much of this discussion to be speculative and perhaps the authors are over analyzing their results. Certainly, changes over time that are small compared to the measurement uncertainty is not terribly convincing. They authors seem to forget that they never measure the same aerosol and that for an inhomogeneous cloud they cannot really be sure that some of the differences are not just variability in the cloud. The authors also do not mention that the aerosol is mixing with ambient aerosol throughout this period and so some changes are may be a result to that process. I would not bother with the humidity explanation and the comparisons with the Icelandic eruption are not likely to be particularly relevant. It is extremely common for sulfate aerosol to contain volcanic material (and meteoritic, etc.) while optically suggesting spherical particles. Given the high number densities after an eruption some coagulation between ash and sulfate is bound to occur in mixed layers. Perhaps some of these arguments would hold together if we had any idea of how big the ash particles are (i.e., what does the color ratio mean?). (For that matter how good do the authors believe the color ratios are? My impression of the 1064 nm channel on CALIOP is that it is not very robust though differences are real even if not correct).

Response:

Thank you for this comment. Section 6.2 has been revised to accommodate the reviewers suggestions as follows:

“The particulate lidar ratios for all three case studies were quite variable with time (Figs. 8a–c). Over these timescales (1–2 weeks) it is likely that the volcanic aerosol layers are mixing with ambient aerosol, resulting in fluctuations in the lidar ratio with time. Changes in the lidar ratio may also be a result of sampling different parts of an inhomogeneous aerosol cloud.”

We have also removed the discussion of the changes in layer-integrated attenuated backscatter and the coagulation and condensation processes as we agree that this part of Sect. 6.2 is speculative based on the evidence (see also revised Figure 1 of this document). We have also removed the humidity explanation.

As there are few ground-based observations of the volcanic ash lidar ratio together with the depolarization ratio (at 532 nm), we believe that comparison of the Eyjafjallajökull observations with the Puyehue observations is justified and have thus retained this discussion.

As discussed above, while we are not able to retrieve particle size, the color ratio can indicate relative changes in particle size. For these reasons we can infer that the Puyehue particles were larger than the Kasatochi and Sarychev particles. Reference to O’Neill et al. (2012) has been included in the revised discussion as they report on particle sizes for the Sarychev case.

The quality of the layer-integrated attenuated color ratios depends on the correct identification of the layer-top and base, the reliability of the 532 and 1064 nm calibration constants and the SNR. The 1064 nm channel calibration depends on the assumption that the color ratio for high cirrus clouds is 1. The calibration procedure is described in Section 7.1.2.2 of the level 1 ATBD (Winker et al., 2006) and the assumption of the cirrus cloud color ratio was determined to be justified based on a validation study using the Cloud-Physics Lidar (Vaughan et al., 2010). We therefore believe that, while there may be some variability in the calibration of the 1064 nm channel, the color ratios used here are robust enough to infer relative changes in particle size.

Response to RC2

Review of Lidar ratios of stratospheric volcanic ash and sulfate aerosols retrieved from CALIOP measurements by Prata et al. (2017).

Volcanic aerosol optical depth from satellites are used in numerical simulations, including those presented in the Intergovernmental Panel on Climate Change reports, to assess the impact of volcanic eruptions in climate and separate natural and anthropogenic climate forcing factors. In order to derive this quantity, native backscatter measurements from CALIOP need to be converted into an extinction coefficient using a lidar ratio. The volcanic layer detection approach of this paper is based upon the combined use of AIRS and CALIOP, providing complementary information on volcanic clouds. They calculated statistical parameters associated with the optical properties (lidar ratio, volume depolarization and attenuated color ratio) of three volcanic plumes (Sarychev, Kasatochi and Cordon) based upon the CALIOP level 2 products. They provided a thoughtful assessment of these coefficients associated with a rigorous and clear analysis of the different sources of errors. This is a very well written paper on which I don't have major comments. Thus, I strongly recommend it for publication in ACP.

I have two minor comments:

1) I believe that the proposed threshold (fig 9) to separate volcanic clouds into ash-rich and sulfate-rich categories is optimized for those cases. Indeed, Vernier et al. (2015) has shown that the pdf of the particulate depolarization ratio associated with the Kelud plume observations were indeed between those of Cordon and Sarychev/Kasatochi. Thus, the classification of volcanic cloud based upon their optical properties is challenging since those properties evolve with time depending of the presence of ash and sulfate which can also be mixed. Overall, because volcanic plumes are a mixture of two types of aerosol (external and possibly internally mixed) (sulfate and ash) which evolve with time, it makes them difficult to classify them (e.g. Kelud, Tavurvur). 2) How would you propose to use the lidar ratios calculated in this paper for deriving times series of volcanic aerosol optical depth during the months following those eruption when AIRS is not sensitive enough to detect SO₂ or Ash in contrast to the CALIOP lidar measurements? I think it would be interesting to discuss how your results can be used to derive volcanic aerosol time series.

Very nice paper!

Response:

The authors thank the reviewer for their thoughtful comments on the manuscript. Response to 1) The authors agree that the proposed threshold is optimised for the case studies considered. However, as we attempted to separate ash-rich layers ($AI \geq 1 K$ and $SI < 1 K$) and sulfate-rich layers ($AI < 1 K$ and $SI \geq 1 K$) using AIRS, we expect that the majority of mixed layers (sulfate/ash) would exhibit an $AI > 1 K$ and $SI > 1 K$ and so would have been removed from our analysis. Our depolarization measurement results, therefore, highlight the two extreme cases (i.e. ash-rich or sulfate-rich) and so, as the reviewer has stated, values falling between the Puyehue and Kasatochi/Sarychev values would likely be a mixture of sulfate and ash (e.g. Vernier et al., 2016). Classification of volcanic aerosols into ash-rich and sulfate-rich layers is important as the lidar ratio may change depending on the composition of the layers. We approached this problem with the operational extinction retrieval in mind; when the lidar ratio cannot be retrieved directly, the aerosol must be classified as a predefined type (associated with a predefined lidar ratio). We have proposed a method for detection, using native CALIOP measurements, of sulfates and ash and have given values of the lidar ratio for these particular case studies. We have acknowledged the reviewers point and included reference to the new stratospheric aerosol subtyping scheme (Tackett et al., 2016) in the revised manuscript as

follows:

“We point out that our suggested δ_v threshold of 0.2 has been optimised for the eruption case studies considered here and that a slightly different threshold might be found for a different or larger data set. For example, Tackett et al. (2016) found a slightly lower threshold of $\delta_v = 0.15$ for the cases they examined. We also note that, for the depolarization ratio range $0.075 < \delta_v \leq 0.15$, Tackett et al. (2016) use $\chi' < 0.5$ to identify stratospheric smoke. As volcanic aerosols are often composed of a complex mixture of both ash and sulfate, which changes with time, strict classification using a single threshold is challenging. In the case of ambiguous depolarization ratios ($\delta_v \sim 0.2$), supplementary information from collocated AIRS measurements may provide more insight into the likely composition of stratospheric volcanic aerosol layers.”

Response to 2) This is the reason we explored the use of CALIOP-measured parameters for discriminating volcanic ash from sulfate after first identifying ash-rich and sulfate-rich layers using independent detection from AIRS. The depolarization ratio appears to be the most appropriate parameter for determining whether a stratospheric volcanic layer is sulfate-rich or ash-rich. As we have shown, the lidar ratio varies with time and so the assumption of a constant lidar ratio will likely introduce errors in the retrieval of extinction profiles. We have included a new subsection in the revised manuscript that discusses how one could use our results to derive a volcanic aerosol optical depth time series:

“ 6.4 Deriving an optical depth times series

In cases where the lidar ratio cannot be retrieved directly, the CALIPSO extinction retrieval (Young and Vaughan, 2009) relies on a predefined lidar ratio that is associated with a predefined type. Classification of volcanic aerosols into ash-rich and sulfate-rich layers is therefore important as the lidar ratio may change depending on the composition of the layers. The depolarization ratio appears to be the most appropriate parameter for determining whether a stratospheric volcanic layer is sulfate-rich or ash-rich. As we have shown, the lidar ratio varied with time for the case studies presented here and so the assumption of a constant lidar ratio will likely introduce errors in the retrieval of extinction profiles. Optimum results for a volcanic aerosol optical depth time series could be obtained by following the method presented here and only accepting cases where an extinction retrieval was constrained by an estimate of the two-way transmittance (i.e. extinction quality control flag equal to 1). This would most likely restrict observations to nighttime measurements of layers with optical depths > 0.2 (Fig. 4). In cases where the two-way transmittance method fails, a predefined lidar ratio would have to be used. One could use the the PDFs presented in Fig. 2 to constrain the choice of the lidar ratio. As the PDFs for the lidar ratios are positively skewed, the median lidar ratio would be best suited for this approach. For example, 60 sr for sulfate-rich ($\delta_v < 0.2$) and 67 sr for ash-rich ($\delta_v > 0.2$) layers.”

Response to RC3

The paper by Prata et al. presents lidar ratio of stratospheric volcanic ash and sulfate aerosols retrieved from CALIOP measurements; an important quantity for deriving aerosol properties from a backscatter lidar like CALIOP. The paper is well suited for publication in ACP after consideration of the following comments:

General comments:

The description of the used method is hardly to follow for a reader less experienced with this method. The manuscript often refers to former papers for important equations. The chapter should be reworked in a way that all important points are included in this manuscript. It should also be clearly worked out why the *a priori* lidar ratio which was used for the calculation of the particle backscatter coefficient and the effective two-way transmittance does not affect the retrieved lidar ratio.

Response:

The authors thank the reviewer for this comment.

In the revised manuscript, Sect. 3 has been reworked to include key equations and describes the relevant steps needed to retrieve the lidar ratio using the method of Fernald et al. (1972). Explicit definitions of the AI and SI have now also been included.

In regard to the *a priori* lidar ratio, the reviewer has misunderstood the retrieval method here. The *a priori* lidar ratio is not used to calculate the particulate backscatter coefficient and effective two-way transmittance. This is because the particulate backscatter coefficient, $\beta_p(r)$, does not appear in the two-component lidar ratio solution (see Eq. (3) of original manuscript). Also, the effective two-way transmittance is measured based on the mean attenuated scattering ratio - and so no *a priori* assumptions of the lidar ratio are required to estimate the transmittance. For the top layer, it is measured as the mean attenuated scattering ratio in a clear air region immediately below the layer.

The iterative lidar ratio solution in Eq. (3) (original manuscript, now Eq. (14) in revised manuscript), however, does require an initial estimate of the lidar ratio to begin the iteration. The choice of the initial lidar ratio will affect the number of iterations required for consecutive solutions to converge. As noted in Fernald et al. (1972), in general, Eq. (3) will converge rapidly but will converge more slowly for very clean atmospheres. In practice we have found that solutions converge rapidly when initialising Eq. (3) with the result of Eq. (7) (original manuscript, now Eq. (15) of revised manuscript).

Minor comments: The mean depolarization ratio for Puyehue in the abstract (0.28) differs from the mean value given in Table 2 (0.29).

Response:

This error has now been corrected in the revised manuscript.

You report about an exponential decay in the mean depolarization ratio for the Sarychev layer with time. Do you see changes also in one or more of the other properties?

Response:

Indeed we do see changes in both the lidar ratio and the layer-integrated attenuated color ratio with time for the Sarychev case study. The attenuated color ratio also decreases with time; similar to the depolarization ratio. The lidar ratio is quite variable showing no significant increasing or decreas-

ing trend with time.

We have now made mention of the change in color ratio with time for the Sarychev case in the abstract of the revised manuscript.

Upon revisiting the time series analysis we noticed an error in the code that was used to construct the time series from the lidar data. In the original code, the **cumulative** mean was being calculated for each optical property in the time series. The time of each observation was also, incorrectly, calculated as a cumulative mean, which resulted in the incorrect residence time for each data point presented in Fig. 8 of the original manuscript.

In the revised manuscript, this error has been corrected so that the curtain means and root mean square errors are calculated for each CALIOP/AIRS observation and are plotted together with the curtain mean of the time of each observation.

Note that we define the ‘curtain mean’ as the mean of all CALIOP layer optical properties (i.e. S_p , δ_v , δ_p and χ') within a collocated AIRS granule, which equates to a ~ 6 minute subset of a CALIOP granule. This revision only affects the original data plotted in Fig. 8 of the original manuscript. It also impacts the calculation of the e -folding time of the Sarychev depolarization ratios. We have therefore attached the revised version of Fig. 8 (Figure 1 of this document).

Page 4, line 31: At this point ‘ η ’ is not defined. Please make sure that all variables are defined when using them the first time.

Response:

The multiple scattering factor is defined on page 4 line 18 of the original manuscript (before the line that the reviewer is referring to). However, in Sect. 2 of the revised manuscript we have been more explicit in defining η :

“We note that the effective two-way transmittance profile, $T_{e,\lambda}^2(0, r)$, is related to the particulate two-way transmittance profile via $T_{e,\lambda}^2(0, r) = T_{p,\lambda}^{2\eta}(0, r)$, where η is defined here as the multiple scattering factor (Platt, 1973).”

Section 3.1: How is the BTD algorithm defined? Please give more information about this.

Response:

The BTD algorithms for the AI and SI have been added to Sect. 3.1 of the revised manuscript as follows: “

$$SI = BT(1407.2 \text{ cm}^{-1}) - BT(1371.5 \text{ cm}^{-1}). \quad (1)$$

and

$$AI = BT_1 - BT_2 + BT_3 - BT_4 \quad (2)$$

where

$$BT_1 = \frac{1}{4} [BT(856.44 \text{ cm}^{-1}) + BT(856.75 \text{ cm}^{-1}) \\ + BT(857.06 \text{ cm}^{-1}) + BT(857.37 \text{ cm}^{-1})],$$

$$BT_2 = \frac{1}{4} [BT(964.25 \text{ cm}^{-1}) + BT(965.04 \text{ cm}^{-1}) \\ + BT(965.44 \text{ cm}^{-1}) + BT(966.24 \text{ cm}^{-1})],$$

$$BT_3 = \frac{1}{2} [BT(1131.79 \text{ cm}^{-1}) + BT(1133.96 \text{ cm}^{-1})]$$

and

$$BT_4 = \frac{1}{2} [BT(1080.92 \text{ cm}^{-1}) + BT(1082.41 \text{ cm}^{-1})].$$

Here $BT(\nu)$ is the brightness temperature measured at wavenumber, ν .”

Section 3.1: Why do the conditions differ for the different volcanic layers?

Response:

We assume that the reviewer is referring to the SI and AI threshold conditions. The reason the conditions differ is that we are looking for a volcanic ash signal for the Puyehue case study and an SO₂ signal for the Kasatochi and Sarychev case studies. In order to detect volcanic ash we require that the AI be greater than or equal to 1 K and the SI be less than 1 K to ensure that we are measuring a layer with an ash signal but, importantly, not an SO₂ signal. Similarly, we require that the Kasatochi and Sarychev layers only exhibit an SO₂ signal (SI \geq 1 K) and do not exhibit an ash signal (AI < 1 K). To make this point clear we have revised the relevant part of Section 3.1 as follows:

“For the Puyehue case study, this set of collocated AIRS pixels is scanned for an AI greater than or equal to 1 K and SI below 1 K. These conditions were set to ensure that the volcanic aerosol layers analysed for the Puyehue case study were dominated by an ash signal and, importantly, did not exhibit an SO₂ signal. Similarly, to ensure that observations of volcanic layers for the Kasatochi and Sarychev case studies were dominated by sulfates (and not an ash), the algorithm required an SI greater than or equal to 1 K and an AI below 1 K.”

Section 3.2: What is meant by the ‘mean scattering ratio’?

Response:

Thank you for this comment. The authors meant to refer to the mean of the **attenuated** scattering ratio profile, $R'(r)$. The attenuated scattering ratio profile is defined as the ratio of the total attenuated backscatter profile, $\beta'(r)$, to the attenuated molecular backscatter profile, $\beta'_m(r)$ (Vaughan et al., 2009):

$$R'(r) = \frac{\beta'(r)}{\beta'_m(r)}. \quad (3)$$

We note that Eq. (3) has been corrected from the original RC3 response where we had incorrectly stated that $R'(r) = [\beta'_m + \beta'_p(r)]/\beta'_m(r)$. This is incorrect due to the non-separability of the transmittance factors. However, this change does not affect the revised manuscript as we do not calculate the attenuated scattering ratio in our retrieval procedure.

For the top layer in a given CALIOP profile, the operational algorithm calculates the two way transmittance constraint by taking the mean of $R'(r)$ in the clear air region immediately below the detected aerosol layer i.e. $T_e^2(r_t, r_b) = \langle R'_{below}(r) \rangle$, where the particulate backscatter is assumed to be zero. The clear air region is defined by the ‘clear air analysis depth’, which is determined via an iterative process in the SIBYL algorithm (see Sect. 4.3 of Vaughan et al., 2005). This description is included in Sect. 2.2 of the revised manuscript as follows:

“Finally, the effective two-way transmittance, $T_e^2(r_t, r_b)$, is calculated by taking the ratio of the mean attenuated scattering ratio profiles over regions of clear air detected above and below the layer (Vaughan et al., 2009):

$$T_e^2(r_t, r_b) = \langle R'_{\text{below}}(r) \rangle / \langle R'_{\text{above}}(r) \rangle, \quad (4)$$

where the attenuated scattering ratio profile is defined as $R'(r) = \beta'_{532}(r) / \beta'_{m,532}(r)$. We note that only the top layer in a given profile was considered in the present study so that measurements of $T_e^2(r_t, r_b)$ were not degraded by signal attenuation introduced by overlying cloud/aerosol layers. For the top layer, the operational retrieval assumes a purely molecular atmosphere (i.e. $\langle R'_{\text{above}} \rangle = 1$), and so the effective two-way transmittance is calculated as $T_e^2(r_t, r_b) = \langle R'_{\text{below}} \rangle$. The clear air region is defined by the ‘clear air analysis depth’, which is determined via an iterative process in the CALIPSO level 2 feature detection algorithm (Vaughan et al., 2005). It should also be noted that $T_e^2(r_t, r_b)$ can only be calculated at 532 nm as the molecular scattering signal at 1064 nm is too small (~ 16 times weaker than at 532 nm).”

Section 4.2: Mean color ratio for Sarychev layer does not agree with value given in Table 2.

Response:

This error has been corrected in the revised manuscript.

Section 4.2: In the Abstract it was reported that the depolarization ratio exponentially decreased with time. This is not reported in Section 4.2. As the change in the optical properties is an important point and thus reported in the Abstract it should also be referred to in the description of the Sarychev layer. How do the other optical properties behave? What are the properties in the beginning of the observations (, mid) and end? This is reported quite lately in the manuscript. To which periods does the mean value correspond to? If the mean values are calculated from the whole period what is the significance of this mean value?

Response:

The authors agree that the decrease in the depolarization ratio with time for the Sarychev case study is an important finding. This finding has now been reported in Sect. 4.2 and we report on the change with time for each of the optical properties in Sects. 4.1, 4.2 and 4.3 in the revised manuscript as follows:

Sect. 4.1:

“The lidar ratios (S_p) and color ratios (χ') were quite variable with time; making it difficult to infer any clear trends in these parameters. The particulate depolarization ratios (δ_p) remained largely unchanged during the measurement time period (Fig. 8d).”

Sect. 4.2:

“The mean optical properties of the Sarychev layers shared many similarities with the Kasatochi layers (Fig. 2); however, the Sarychev particulate depolarization ratio exhibited an exponential decrease with time over 3.6 days. A similar decreasing trend was also observed for the attenuated color ratio. The time evolution of all optical properties are discussed in Sect. 6.2 and are shown in Fig. 8.”

Sect. 4.3:

“In contrast to the optical properties of the Kasatochi and Sarychev layers, the Puyehue layers exhibited consistently high depolarization ratios ($\delta_p = 0.33 \pm 0.03$; Table 2), indicating aerosol layers optically dominated by non-spherical particles over the measurement period. The layer-integrated

attenuated color ratios for the Puyehue case study were also higher ($\chi' = 0.53 \pm 0.08$; Table 2) than the Kasatochi and Sarychev case studies ($\chi' = 0.32\text{--}0.35$). In general, changes in the Puyehue lidar ratios (S_p mean of 69 ± 13 sr and median of 67 sr) with time were quite similar to the changes in lidar ratio with time for Kasatochi and Sarychev case studies.”

The mean values reported in Sect. 4 correspond to the whole time period for each case study. Given that the distributions of δ_p and χ' have equal (or very close to equal) means and medians, and appear to be Gaussian (see Fig. 2 of revised manuscript), we report the means and standard deviations for these properties in Sect. 4 of the revised manuscript. As the lidar ratio distributions are positively skewed (Fig. 2 of revised manuscript), we now report both the median and mean values for each case study in Sect. 4 of the revised manuscript.

Section 4.3: How is a valid lidar ratio profile defined (time/length)? The number of cases/profiles resulting into the mean values should also be given for the other cases. Information about the CALIOP measurements (number, time, days, and location) should be given for the different cases should.

Response:

The lidar ratio retrievals are of a single value for any profile of attenuated backscatter and are constrained by the measurement of effective transmittance. It is not possible to retrieve a “lidar ratio profile” with that single constraint. Valid lidar ratio retrievals are those which satisfy constrained conditions i.e. that are constrained by an estimate of the effective two-way transmittance. We now explicitly define what we mean by ‘valid’ lidar ratio retrievals in Section 2.2:

“To ensure constrained conditions for the lidar ratio retrieval (i.e. clear air above and below a lofted layer with acceptable SNR), only stratospheric volcanic aerosol layers that had an extinction quality control flag equal to 1, a valid two-way transmittance measurement (i.e. $0 < T_e^2 < 1$) and a horizontal averaging value of 5 km were included in the analysis. We refer to ‘valid’ lidar ratio retrievals hereafter as having satisfied these criteria.”

The number of (valid) lidar ratio retrievals resulting in the means are reported for each case study in the revised manuscript (Sections 4.1, 4.2 and 4.3). The time period for each case study and geographic region/locations analysed are also stated in these sections. The number of layers contributing to the mean geometric and optical properties are reported in Tables 1 and 2 of the revised manuscript and the specific measurement time periods for each case study are discussed Section 6.2 of the revised manuscript.

Section 4.3: Standard deviation of color ratio does not agree with the value given in Table 2.

Response:

This error has been corrected in the revised manuscript.

Section 5.1: What is meant by the aerosol scattering ratio?

Response:

The terms “aerosol scattering ratio”, “particulate scattering ratio”, “backscatter ratio” and “scattering ratio” all appear in the literature and usually have the same definition. Here, the aerosol scattering ratio, $R_p(r)$, reported in Vernier et al. (2009), is defined in the present notation as

$$R_p(r) = \frac{\beta_m(r) + \beta_p(r)}{\beta_m(r)}. \quad (5)$$

This is distinct from the attenuated scattering ratio, $R'(r)$, which has not been corrected for molecular, particulate and ozone attenuation. We refer to it as the particulate (aerosol) scattering ratio in the revised manuscript for consistency:

“Vernier et al. (2009) highlighted how this issue would impact the CALIOP calibration region, concluding that undetected aerosols up to 35 km lead to an underestimation of the particulate (aerosol) scattering ratio (an average relative error of 6%), with the effects most pronounced in the tropics (20°N–20°S).”

Section 5.3: Why did you use the error calculation according to Equation 9? This formula is used for the calculation of random (statistical) errors. To my understanding, the errors considered in this manuscript are not random errors and thus the total error should be calculated from the absolute error values of the considered parameters.

Response:

Equation 9 is used in the standard procedure for calculating perturbation errors (see, for example, Chapter 4 of Hughes and Hase, 2010). We consider the errors discussed in Sect. 5 as being systematic i.e. they are errors that are constant through a given profile and cannot be reduced from averaging. This is the same definition used (and explained in detail) in Young et al. (2013). Specifically, we investigate how the errors in different key variables propagate into the lidar ratio retrieval when they are perturbed. If it is assumed that the error in each perturbation variable is uncorrelated then the total error is calculated from the absolute errors by summing them together in quadrature (i.e. the square root of the sum of the squares of the errors). This is because we assume that the total error makes up an error surface composed of the independent component errors. Thus we use Pythagoras' theorem in N dimensions to construct the total error from the component errors (Hughes and Hase, 2010).

Figures 5-7: Please indicate the aerosol free regions below and above the volcanic layer.

Response:

Thank you for this comment. The regions above the layers are assumed to be aerosol free. We account for and discuss errors that may be introduced by this assumption in Sect. 5.2.

We have now indicated the clear air regions below each layer on Figs. 5–7 of the revised manuscript.

Section 6.1: The mean values of the lidar ratio for the Kasatochi and Sarychev layers shown in this case studies are smaller than the mean values reported for the whole measurements for these layers. Can you give more information about the changes over the time? Maybe give a time series of the lidar ratio for the different volcanic layers to illustrate the changes and / or variability over time. Otherwise the mean values of the case studies or the mean values over all suffer the loss of significance.

Response:

The purpose of Sect. 6.1 is to give the reader an idea for the spatial variation of lidar ratio across well-defined volcanic ash and sulfate layers. It also illustrates (Figs. 5–7 of original manuscript) the conditions under which the lidar ratio retrievals are successful and how the volcanic layers correlate with the AI and SI. In the revised manuscript, we have added text to emphasise this point as follows:

“Figures 5–7 show how the CALIOP/AIRS analysis performed for an individual AIRS granule selected

from each case study; illustrating the conditions under which the lidar ratio retrievals are successful and how the volcanic layers correlate with the AI and SI. The times of each of the selected observations (Figs. 5–7) are also indicated on Figs. 8a–c, which show the overall times series of the aerosol optical properties (S_p , δ_p and χ') for each case study. For the Kasatochi and Sarychev layers (5 and Fig. 6, respectively), the lidar ratio is relatively constant throughout the strongly backscattering regions of the stratospheric layers. The AIRS SO₂ signals also collocate well with these aerosols, suggesting that they are largely composed of sulfates. The curtain-average value of the lidar ratio for the two sulfate-rich layers are also very similar ($\overline{S_p} \sim 53$ sr), but lower than the median values of the corresponding lidar ratio distributions (~ 60 sr; Figs. 2a, b). The Kasatochi observation corresponds to an aerosol layer that had resided in the stratosphere for ~ 7 days whereas the Sarychev observation corresponds to a layer approximately twice the age (~ 14 days) of the Kasatochi layer. The mean particulate and volume depolarization ratios for the sulfate-rich layers are both relatively low ($\overline{\delta_p}$, $\overline{\delta_v} \sim 0.05$ – 0.10) indicating that these layers are dominated by spherical particles. The curtain-mean attenuated color ratio for the Kasatochi observation ($\overline{\chi'} = 0.37$; Fig. 5) was higher than the Sarychev observation ($\overline{\chi'} = 0.33$; Fig. 6) although both were smaller than the Puyehue observation ($\overline{\chi'} = 0.54$; Fig. 7) indicating that the sulfate-rich layers were composed of smaller particles than the ash-rich layers.

The Puyehue layers (Fig. 7) are quite similar to the sulfate-rich layers in terms of the geometric thickness; however, the curtain-mean particulate depolarization ratio ($\overline{\delta_p} = 0.32$), along with the AIRS ash signal, unambiguously identify this layer as being optically dominated by non-spherical ash particles. The variability in the lidar ratio for the Puyehue observation generally increases as features become more tenuous, reflecting an increase in sensitivity in the lidar ratio retrieval for transmissive layers (as discussed in Sect. 5.3). The lidar ratios are also more variable than the sulfate ratios, which may be an indication of greater inhomogeneity in the Puyehue layer observations. The curtain-mean lidar ratios for the Puyehue observation are also quite high ~ 68 sr and we note that this may be due to the age of the layers (~ 17 days; discussed in more detail in Sect. 6.2)."

Section 6.2: It is right that the measurements of the different volcanic layers correspond to different stages / ages of the volcanic layer. However the way it is described here could lead to misinterpretation of this information, as one could think that the measurements of the three volcanic layers can be related to each other and show an alteration of volcanic aerosol layers during time.

Response:

The authors did not intend to give this impression. Section 6.2 has been revised to make it clear that the aerosol layers should not be related to each other directly in terms of aerosol evolution. The revised description is:

"As volcanic aerosol layers evolve and disperse into the atmosphere their microphysical properties are expected to change with time. The Kasatochi and Puyehue layers were observable for a duration of ~ 12 days, while the Sarychev observations covered a time period of ~ 17 days. Figures 8a–c show that all observations were made more than three days after eruption onset. The Kasatochi and Puyehue volcanic aerosols were observed for a similar time period (~ 12 days); however, for the Puyehue case study, the aerosol layers had resided in the stratosphere for more than 11 days before the measurement period began. The Sarychev case study covered the longest observational time period, providing observations of sulfate-rich aerosols for over two weeks. All volcanic aerosol layers were subject to long-range transport across the globe as shown by the spatial distribution of observations plotted in Figs. 8j–l."

Section 6.2: The increase of the Puyehue ash layer with time is small compared to the uncertainties

of the retrieved property, thus the statement derived from this changes is very speculative.

Response:

The authors agree. Indeed, the revised version of Fig. 8 (Figure 1 of this document) shows that this statement is even more speculative than first thought. We have therefore removed it from the revised manuscript. The revised statement is

“The particulate lidar ratios for all three case studies were quite variable with time (Figs. 8a–c). Over these time scales (1–2 weeks) it is likely that the volcanic aerosol layers are mixing with ambient aerosol, resulting in fluctuations in the lidar ratio with time. Changes in the lidar ratio may also be a result of sampling different parts of an inhomogeneous aerosol cloud.”

Section 6.3, discussion about high lidar ratios for Puyehue: Should not the loss of the large particles also be reflected in the depolarization ratio? No changes are obvious there.

Response:

For the Puyehue case study, the ash layers had already resided in the atmosphere for ~11 days before the CALIOP measurements were available. This means that the larger particles would have already sedimented out before the measurement period began (see Rose and Durant, 2009, for discussion on atmospheric residence times of volcanic ash). We therefore do not capture the fall out of larger particles in the depolarization ratio, but instead observe layers composed of small, irregular (depolarising) ash particles.

Page 8, lines 7-8: This statement about the volume and the particle depolarization ratio is misleading.

Response:

We assume the reviewer is referring to the statement on page 18 lines 7–8:

“Note that δ_v is not strictly a particle property, but for layers dominated by aerosols it can be used as a first approximation to the particulate depolarization ratio, δ_p (Wiegner et al., 2012).”

We agree and have removed it from the revised manuscript.

Response to RC4

General

The paper is well written. Carefully analysed CALIOP observations are presented. The paper is appropriate for ACP.

The only negative and confusing point is that obviously the volume depolarization ratio and volume color ratio are used instead of the particle depolarization ratio and particle color ratio. But I am not sure what is shown. The authors have to clarify that when discussing equations 1 and 2, see details.

Minor revisions are at least required. However, major revisions (switch to particle depolarization ratio) would significantly improve the paper.

Response:

The authors thank the reviewer for their comments on the manuscript.

As suggested, we have now included the particulate depolarization ratios.

The 1064 nm lidar ratio ($S_{p,1064}$) and layer-effective particulate color ratio (χ_p) can be simultaneously retrieved using the two-color method of Vaughan (2004). We went to considerable effort to set up such an analysis scheme to perform the calculations. However, we found that the method was rather insensitive to variations in $S_{p,1064}$ because of the relatively weak signals and low optical depths of the volcanic aerosol layers. We therefore decided that these results added nothing to the value of the paper. We have added this comment in the revised manuscript as follows:

“We also note that the layer-effective particulate color ratio, χ_p , can be retrieved using the two-color method of Vaughan (2004). This approach seeks to minimise a non-linear function by simultaneously varying $S_{p,1064}$ and χ_p using the method of non-linear least squares. However, for the case studies considered here, we found that the method was rather insensitive to variations in the 1064 nm particulate lidar ratio; often resulting in non-physical solutions for $S_{p,1064}$. We expect that this was due to the relatively weak signals and low optical depths of the volcanic aerosol layers under examination. As these results were inconclusive, and require a more complete treatment of the sources of error, we decided this analysis was outside of the scope of the present analysis and therefore do not report the results here.”

Upon implementing the $S_{p,1064}$ retrieval code we noticed an error in the $S_{p,532}$ retrieval. The error was due to the way the initial lidar ratio (defined by Eq. (7) in the original manuscript) was calculated. In the original code, η values of 0.6 were used in Eq. (7) and η values of 0.90 (for Puyehue) and 0.95 (for Kasatochi and Sarychev) were used in Eq. (3) when we should have been using the same η values in both Eq. (7) and Eq. (3).

We have now corrected this error by using an η value of 0.95 for Kasatochi and Sarychev and 0.90 for Puyehue in both Eqs. (3) and (7) (Eqs. (14) and (15) of the revised manuscript).

We have found that this error resulted in lidar ratios that were biased high by $\sim 4\%$. To illustrate this, we have plotted the original dataset against the η corrected dataset in Figure 2 of this document.

During this process we also found a bug in the lidar ratio retrieval code. The bug was due to the way the trapezoidal integration procedure (used to evaluate the integral term in the denominator of

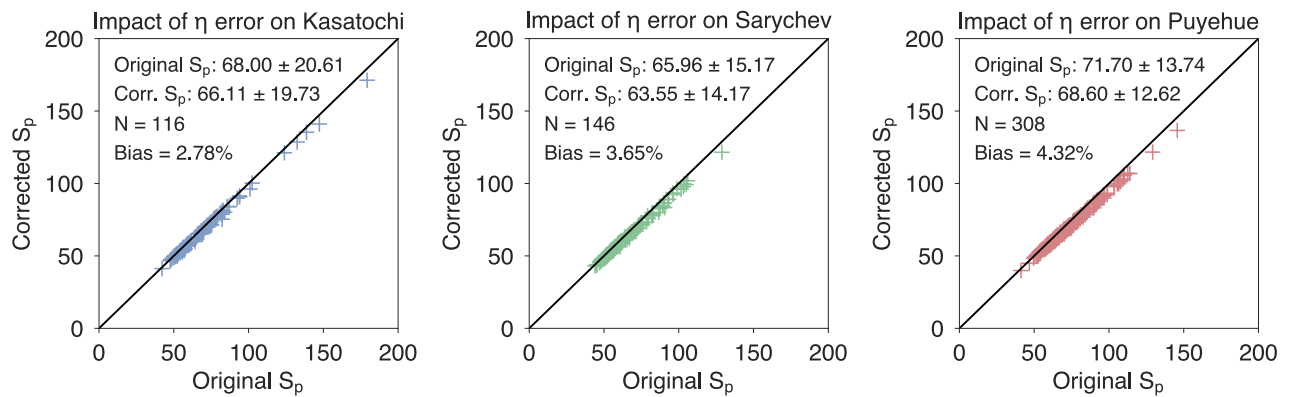


Figure 2: Comparison of S_p for the original dataset and the dataset corrected for the η error.

Eq. (3) of the original manuscript) handled masked values. Specifically, if there was at least one masked value in an array then the integral of the array would be evaluated as being masked; leading to a masked lidar ratio retrieval, which was rejected from the analysis. We have revised the code now so that an array containing masked values will still be evaluated. This is achieved using the cumulative trapezoidal integration module from the Scipy library (<https://docs.scipy.org/doc/scipy/reference/generated/scipy.integrate.cumtrapz.html>). The result of this revision on the analysis is that more data points (more valid lidar ratio retrievals) are now analysed. The results presented in the revised manuscript do not, however, differ significantly from the results presented in the original manuscript and so the main conclusions drawn from the original manuscript have been retained. The impact of this correction on the analysis is shown for a specific example of an observation of an ash layer for the Puyehue case study (Figure 3 of this document). Here the added data points are in red and lidar ratios that have been corrected for the η error are in blue (Figure 3d of this document). Figure 4 (of this document) shows how the correction impacts the overall lidar ratio PDFs.

In the revised manuscript, Figs. 2–10 of the original manuscript have been corrected for the η error and the integration bug (corresponding to η + integration values that are annotated on the subplots of Figure 4 of this document). The values in Tables 1–3 have also been corrected in the revised manuscript.

Details:

Abstract:

P1, L9: Please state the wavelength (532 nm) again in the case of the volume depolarization ratio.

Response:

Accepted.

P1, L10-12: A volume depolarization ratio of 0.08, 0.05, 0.25 tells us almost nothing as long as we do not know the backscatter ratio (total-to-Rayleigh backscatter). So again, why not trying to determine the particle depolarization ratio? At least for a few examples.

Response:

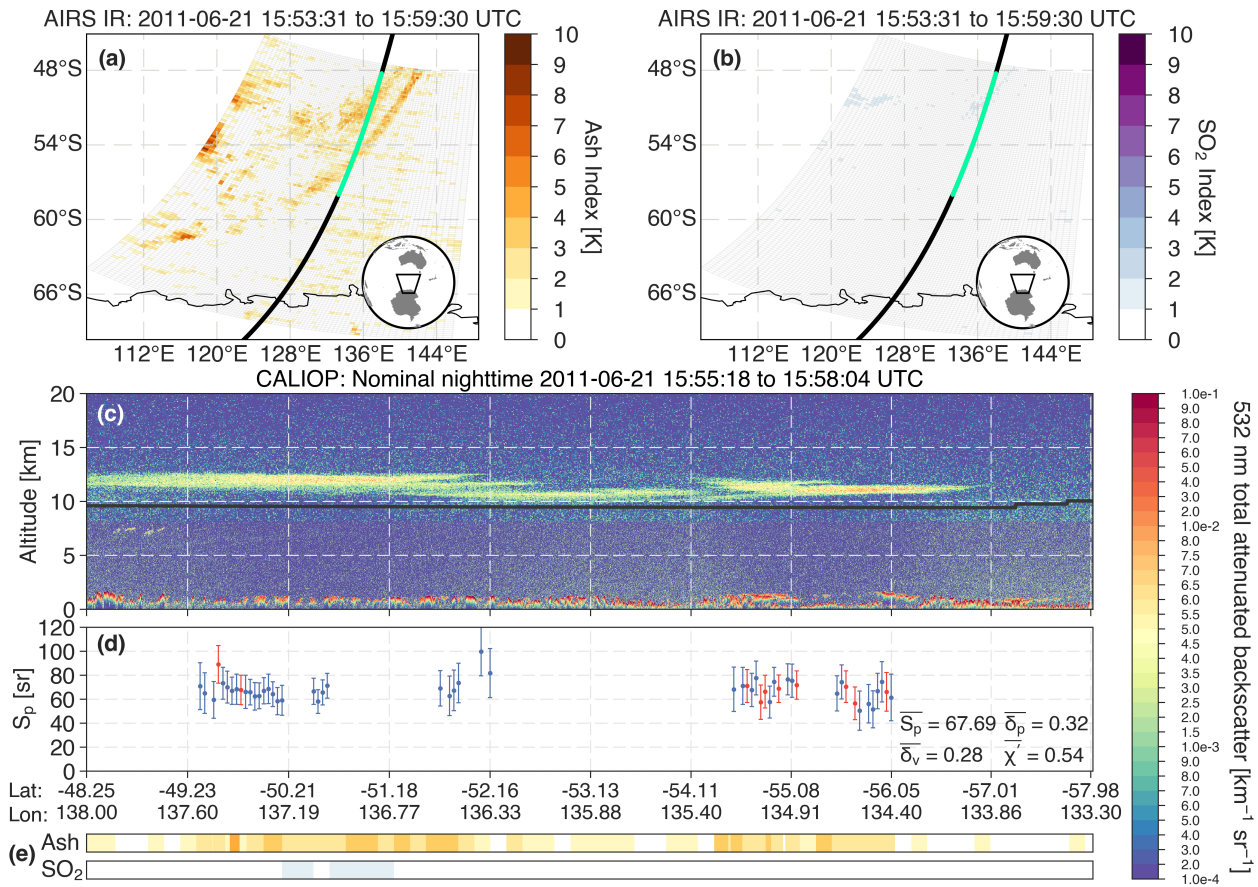


Figure 3: Revised version of Fig. 7 of original manuscript. Red data points on panel (d) indicate retrievals that were added after the integration bug was corrected.

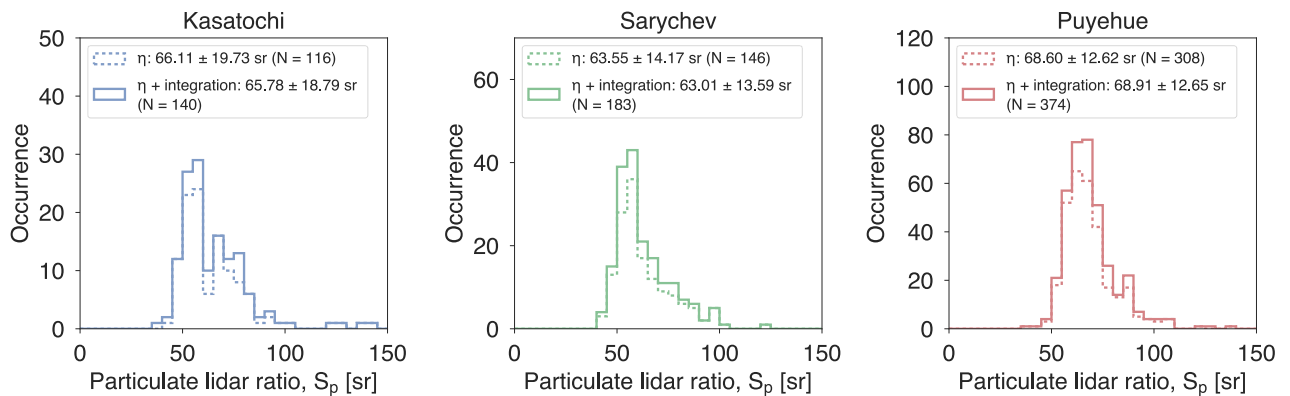


Figure 4: Impact of integration bug on S_p for each case study. The mean and standard deviation of S_p for the η correction and the η + integration correction are annotated on each plot.

The authors disagree that the volume depolarization ratios tell us “almost nothing” without the scattering ratio. The volume depolarization ratios presented do show distinctions between the layers identified as sulfates and the layers identified as volcanic ash (Fig. 9 of the original manuscript). One could argue that, for CALIOP, the volume depolarization ratios are more useful than the particulate depolarization ratio as the volume depolarization ratios are direct measurements (i.e. do not require a lidar ratio retrieval). This is in fact the reason why we focussed on the volume depolarization ratios in the initial submission. However, we agree that the particulate depolarization ratios provide useful intrinsic information on volcanic aerosols and have included them in the revised manuscript as follows:

“The value of δ_p can be derived from the layer-integrated volume depolarization ratio, δ_v , by adapting the approach of Tesche et al. (2009) to integrated quantities:

$$\delta_p = \frac{\gamma_m(\delta_v - \delta_m) + \gamma_p\delta_v(1 + \delta_m)}{\gamma_m(\delta_m - \delta_v) + \gamma_p(1 + \delta_m)}, \quad (6)$$

where

$$\gamma_m = \int_{r_t}^{r_b} \beta_m(r) dr \quad (7)$$

and

$$\gamma_p = \int_{r_t}^{r_b} \beta_p(r) dr. \quad (8)$$

Here the particulate backscatter profile, $\beta_p(r)$, is calculated using the retrieved 532-nm particulate lidar ratio and the numerical integration procedure of Fernald (1984). We also define δ_m as the layer-integrated molecular depolarization ratio. Due to CALIOP’s narrow band optical filter, δ_m is the depolarization ratio at the central Cabannes line, which can be assumed to be a constant; $\delta_m \approx 0.003656$ (Hostetler et al., 2006).”

We also note that in our initial response to RC4 we had an error in the way the molecular depolarization ratio was defined. In the original response we had incorrectly multiplied δ_m by $(r_t - r_b)$. This has been corrected in the present response and the revised manuscript as shown in green above.

Introduction:

P2, L22: Later on, in this paper, you mention the Mattis paper which also deals with the same volcanic eruptions in the high northern latitudes in 2008 and 2009. I checked that paper and found lidar ratios and depolarization ratios for 355 and 532 nm for high- northern-latitude volcanic aerosol in the upper troposphere and stratosphere.

So, I was surprized that you did not give any reference to this paper in the introduction. Is there a specific reason, or did you simply forget? Mattis found lidar ratios of 30-40sr for 532nm and 60-80 sr for 355nm in August 2008 (upper troposphere, clearly related to volcanic aerosol), and 30-50sr for both wavelength between 14-18 km height one year later. And, by the way, Mattis found volume depolarization ratios of 0.015. Such low numbers really indicate spherical particles, in contrast to your high numbers of 0.05 to 0.08 for the volume depolarization ratio, so that I started to think about the particle depolarization ratio.

So, please give proper reference to that Mattis paper in the introduction!

Response:

Thank you for bringing our attention to this. Reference to the Mattis paper has now been included in the introduction. We note Mattis et al. (2010) were using Raman observations of the volcanic layers which have a much higher signal-to-noise ratio than the native CALIOP measurements. And so we question whether it would be possible, in practice, to measure volume depolarization ratios as low as 0.015 using CALIOP.

Instead, you mention papers that deal with volcanic layers in the lower troposphere. Please give the heights of these volcanic layers so that the reader can make his/her own conclusion how useful such information is in a paper dealing with stratospheric volcanic layers.

Response:

The tropospheric layers mentioned in the introduction were describing previously reported lidar ratios for ash-rich volcanic layers. To our knowledge, there are no reported lidar ratio retrievals for ash-rich layers residing in the stratosphere. When discussing sulfate-rich aerosol layers, we gave reference to Sawamura et al. (2012) who report lidar ratios for stratospheric aerosols produced by the Nabro eruption, O'Neill et al. (2012) who report stratospheric lidar ratios for Sarychev and Hoffmann et al. (2010) who report stratospheric lidar ratios for Kasatochi. However, we agree that the heights of the layers should be reported and have included them in the revised manuscript as follows:

“Previously reported observations of the volcanic ash lidar ratio vary. Ansmann et al. (2010) and Groß et al. (2012) reported values in the range from 44–60 sr (at 532 nm), based on observations of the Eyjafjallajökull ash clouds in the free troposphere (~2.5–4.5 km) over Germany. Wang et al. (2008) report lidar ratios from 42–65 sr for fine ash/sulfate mixed aerosol layers between 1.5 and 7 km produced by the 2001 and 2002 eruptions of Mt Etna. For sulfate-rich volcanic aerosols, the lidar ratio was determined to be 48 sr for volcanic aerosol layers at 16 km produced by the 2011 Nabro eruption (Sawamura et al., 2012). For the Sarychev volcanic aerosols, the lidar ratio was determined to be 55 ± 4 sr for layers measured between 10 and 15 km (O'Neill et al., 2012) and for Kasatochi a lidar ratio of 65 ± 10 sr was determined for a layer at 11 km (Hoffmann et al., 2010). Mattis et al. (2010) also retrieved lidar ratios for Sarychev and Kasatochi, reporting values in the range from 30–50 sr at 532 nm for layers observed between 14 and 18 km.”

P4, L19-20: Again, I am not very happy that you do not make any attempt to provide particle depolarization ratios.

Response:

Particle depolarization ratios have now been included.

Section3: I appreciate the careful consideration of potential multiple scattering effects!

Response:

Thank you.

Now, I got confused! Equation 1 leads, to my opinion, to the particle depolarization ratio. Right? Please clarify that! Are these cross and co-polarized backscatter coefficients for particles???? or for the total (Rayleigh plus particle) backscattering. Please make that very very clear!

If that is for the total backscatter then please put an index p to the ones in equation 2!... or are these total (Rayleigh plus particle) backscatter coefficients as well???

Response:

Equation 1 does not lead to the particulate depolarization ratio. β'_{\perp} and β'_{\parallel} are used to indicate the cross and co-polarised channels of the **total** (molecular + particulate) attenuated backscatter and therefore Eq. 1 leads to the layer-integrated **volume** depolarization ratio. The volume depolarization ratio is taken from the level 2 layer products, and is defined as the ratio of the summation of the co and cross-polarised channels (Vaughan et al., 2005).

This definition has been included in the revised manuscript as follows:

“All products are calculated relative to the base (r_b) and top (r_t) of a given aerosol layer. As in Vaughan et al. (2005), δ_v is calculated as

$$\delta_v = \frac{\sum_{k=top}^{base} \beta'_{532,\perp}(r_k)}{\sum_{k=top}^{base} \beta'_{532,\parallel}(r_k)}, \quad (9)$$

where $\beta'_{532,\perp}(r)$ and $\beta'_{532,\parallel}(r)$ are the perpendicular and parallel components of the attenuated backscatter at 532 nm. The perpendicular and parallel components of attenuated backscatter make up the total attenuated backscatter at 532 nm such that

$$\beta'_{532}(r) = \beta'_{532,\perp}(r) + \beta'_{532,\parallel}(r).” \quad (10)$$

We note that in our original response to RC4 there was an error in the way the above definition was written. We had originally stated that $\beta'_{532,\perp} = \beta'_{m,532,\perp} + \beta'_{p,532,\perp}$ and $\beta'_{532,\parallel} = \beta'_{m,532,\parallel} + \beta'_{p,532,\parallel}$. These definitions are in fact incorrect. This is because the molecular and particulate components are both affected by both molecular and particulate transmittances. The correct definition is given in the revised manuscript as shown in green above.

I got confused because equation 3 deals with the Fernald 1972 approach! So, you have the potential to compute particle backscatter coefficients and particle depolarization ratios when using the later Fernald method (Appl. Opt.I, 1984). So, why not presenting particle related quantities: lidar ratio, depolarization ratio, color ratio?

Response:

Indeed, we had originally calculated the particulate depolarization ratio. We wanted to focus on the volume, rather than particulate, properties as they are direct measurements from the CALIOP instrument and are operationally used in the level 2 aerosol classification scheme (Omar et al., 2009). It is not trivial to calculate the particulate color ratio. To retrieve it you need the particulate backscatter profile at 1064 nm. This requires knowledge of the particulate lidar ratio at 1064 nm, which cannot be retrieved using the two-way transmittance method as the 1064 channel is ~ 16 times less sensitive to molecular backscatter than the 532 nm channel. The 1064 nm lidar ratio and particulate color ratio can be retrieved using the two color method of Vaughan (2004); however, as discussed above, we found that the method was rather insensitive to changes in $S_{p,1064}$.

Figure 2 is very nice, but I am missing the particle depolarization ratio, and obviously the color ratio is also for Rayleigh plus particle backscatter coefficients, and thus not very helpful. . . . But, at the moment, I am not sure what is shown.

Response:

Thank you.

We have now included the particle depolarization ratio, for all three case studies, in a revised Fig. 2.

The particulate color ratios are not shown for reasons discussed above. The authors disagree with the notion that the layer-integrated volume color ratio is “not very helpful”. The value of χ' does show some distinction between the sulfate-rich (Kasatochi and Sarychev) layers and the volcanic ash-rich layers (Puyehue). The χ' parameter is also used in the aerosol classification scheme for CALIOP and thus it is a valuable piece of information when attempting to classify volcanic aerosols in CALIOP observations. Indeed, Vernier et al. (2013) use χ' measurements to separate ash from ice.

All the results in the figures are nice (figures 5,6,7,8 ,9), but I am still confused to see PARTICLE lidar ratios together with information on VOLUME depolarization ratios and VOLUME color ratio.

Correlations (Fig.9) of PARTICLE lidar ratio versus VOLUME depolarization ratio are poor!!! Apples and oranges are correlated, to my opinion.

Response:

Figure 9b has been revised to compare the particulate lidar ratio against the particulate depolarization ratio.

However, Fig. 9a that shows the volume color and volume depolarization ratios has been retained as the relationship between these parameters, we argue, is an important source of information for the classification of volcanic aerosols in CALIOP observations.

Maybe it is simply not easy to compute particle depolarization ratios and particle color ratios. But at least a figure showing both, the volume and particle depolarization ratio and maybe the same for the color ratio is required to convince the reader that such correlations as in Figure 9 are useful.

Response:

As previously discussed, the color ratio requires knowledge of the particulate lidar ratio at 1064 nm. While methods do exist to retrieve the 1064 nm lidar ratio (e.g. Vaughan, 2004) we believe that to include this retrieval method would be outside the scope of the present study.

However, we are able to calculate the layer-integrated particulate depolarization ratio and have included a new figure comparing the particulate lidar ratio to the particulate depolarization ratio for each case study (Fig. 9b of revised manuscript).

As the reviewer is aware, CALIOP is not a Raman lidar and cannot measure extinction and lidar ratios directly and must retrieve particulate quantities using lidar ratios that are either retrieved using transmittance constraints or default values for each aerosol subtype (Omar et al., 2009). Even if it were a Raman system, travelling at ~ 7.5 km / second would not permit the long averaging times that improve the SNR in ground-based Raman systems, and spatial inhomogeneity and limited horizontal extent of features do not always permit CALIOP to increase its SNR by averaging over long along-track paths. So deriving particulate properties is dependent on SNR, as we have seen in this paper. Until we have operational HSRLs in space, we are limited then to using the elastic backscattering signals from CALIOP and analytical techniques using this form of lidar data.

Additional changes

(1) Due to the major revisions of the manuscript we have re-written the conclusions section to reflect the relevant changes. These changes can be viewed in the attached track changes document.

(2) All previous occurrences of the word "depolarisation" have been changed to "depolarization" and "colour" has been changed to "color".

(3) The original discussion of high depolarization ratios and multiple scattering (Sect. 6.4 of the original manuscript, now Sect. 6.5 of the revised manuscript) was misleading. The original discussion implied that depolarization causes multiple scattering. In fact, it is depolarization that arises from multiple scattering. This has been clarified in the revised manuscript as follows:

"The impact of multiple scattering on CALIOP measurements can also be indicated by high depolarization ratios. Liu et al. (2011) found that effective lidar ratios ($S^* = \eta S_p$), derived from CALIOP measurements of opaque African dust layers, decrease as the volume depolarization ratio increases, an effect they ascribe to the impact of multiple scattering in denser layers. For layers with optical depths greater than 3, they found that volume depolarization ratios increased from a value of ~ 0.3 , typical for African dust, to ~ 0.36 , while the effective lidar ratios decreased to 30.5 sr from a typical value of 40 sr, implying a multiple scattering factor of ~ 0.75 . For low to moderately dense layers, they found multiple scattering to be negligible. Since the volcanic aerosol layers in this study were generally optically thin ($\tau_e < 0.8$, Fig. 4), multiple scattering effects are also expected to be small, consistent with our assumption of $\eta = 0.90\text{--}0.95$ for the ash-rich volcanic layers considered here."

References

- Ansmann, A., Tesche, M., Groß, S., Freudenthaler, V., Seifert, P., Hiebsch, A., Schmidt, J., Wandinger, U., Mattis, I., Müller, D., and Wiegner, M.: The 16 April 2010 major volcanic ash plume over central Europe: EARLINET lidar and AERONET photometer observations at Leipzig and Munich, Germany, *Geophys. Res. Lett.*, 37, L13810, 2010.
- Fernald, F. G.: Analysis of atmospheric lidar observations: some comments., *Appl. Opt.*, 23, 652–652, 1984.
- Fernald, F. G., Herman, B. M., and Reagan, J. A.: Determination of Aerosol Height Distributions by Lidar., *J. Appl. Meteorol.*, 11, 482–489, 1972.
- Groß, S., Freudenthaler, V., Wiegner, M., Gasteiger, J., Geiß, A., and Schnell, F.: Dual-wavelength linear depolarization ratio of volcanic aerosols: Lidar measurements of the Eyjafjallajökull plume over Maisach, Germany, *Atmos. Environ.*, 48, 85–96, 2012.
- Hoffmann, A., Ritter, C., Stock, M., Maturilli, M., Eckhardt, S., Herber, A., and Neuber, R.: Lidar measurements of the Kasatochi aerosol plume in August and September 2008 in Ny-Ålesund, Spitsbergen, 115, D00L12, 2010.
- Hostetler, C. A., Liu, Z., Reagan, J. A., Vaughan, M. A., Osborn, M. T., Hunt, W. H., Powell, K. A., and Trepte, C. R.: CALIOP Algorithm Theoretical Basis Document Part 1: Calibration and Level 1 Data Products [Available online at <https://www-calipso.larc.nasa.gov/resources/pdfs/PC-SCI-201v1.0.pdf>], 2006.

- Hughes, I. G. and Hase, T. P. A.: Measurements and their Uncertainties: A Practical Guide to Modern Error Analysis, Oxford University Press, 2010.
- Liu, Z., Winker, D., Omar, A., Vaughan, M., Trepte, C., Hu, Y., Powell, K., Sun, W., and Lin, B.: Effective lidar ratios of dense dust layers over North Africa derived from the CALIOP measurements, *J. Quant. Spectrosc. Radiat. Transf.*, 112, 204–213, 2011.
- Mattis, I., Siefert, P., Müller, D., Tesche, M., Hiebsch, A., Kanitz, T., Schmidt, J., Finger, F., Wandinger, U., and Ansmann, A.: Volcanic aerosol layers observed with multiwavelength Raman lidar over central Europe in 2008–2009, *J. Geophys. Res.*, 115, D00L04–9, 2010.
- Omar, A. H., Winker, D. M., Vaughan, M. A., Hu, Y., Trepte, C. R., Ferrare, R. A., Lee, K.-P., Hostetler, C. A., Kittaka, C., Rogers, R. R., Kuehn, R. E., and Liu, Z.: The CALIPSO Automated Aerosol Classification and Lidar Ratio Selection Algorithm, *J. Atmos. Ocean. Tech.*, 26, 1994–2014, 2009.
- O'Neill, N. T., Perro, C., Saha, A., Lesins, G., Duck, T. J., Eloranta, E. W., Nott, G. J., Hoffman, A., Karumudi, M. L., Ritter, C., Bourassa, A., Abboud, I., Carn, S. A., and Savastiouk, V.: Properties of Sarychev sulphate aerosols over the Arctic, *J. Geophys. Res.*, 117, D04 203–21, 2012.
- Platt, C.: Lidar and Radiometric Observations of Cirrus Clouds, *J. Atmos. Sci.*, 30, 1191–1204, 1973.
- Prata, A. T., Siems, S. T., and Manton, M. J.: Quantification of volcanic cloud top heights and thicknesses using A-train observations for the 2008 Chaitén eruption, *J. Geophys. Res. Atmos.*, 120, 2928–2950, 2015.
- Rose, W. I. and Durant, A. J.: Fine ash content of explosive eruptions, *J. Volcanol. Geoth. Res.*, 186, 32–39, 2009.
- Sawamura, P., Vernier, J. P., Barnes, J. E., Berkoff, T. A., Welton, E. J., Alados-Arboledas, L., Navas-Guzmán, F., Pappalardo, G., Mona, L., Madonna, F., Lange, D., Sicard, M., Godin-Beekmann, S., Payen, G., Wang, Z., Hu, S., Tripathi, S. N., Cordoba-Jabonero, C., and Hoff, R. M.: Stratospheric AOD after the 2011 eruption of Nabro volcano measured by lidars over the Northern Hemisphere, *Environ. Res. Lett.*, 7, 034 013, 2012.
- Tackett, J. L., Omar, A. H., Vaughan, M. A., Kar, J., Trepte, C. R., Winker, D. M., and Magill, B.: New Stratospheric Aerosol Subtypes Implemented in CALIOP Version 4 Level 2, in: CALIPSO/CloudSat Science Team Meeting. 1-3 March 2016., 2016.
- Tesche, M., Ansmann, A., Müller, D., Althausen, D., Engelmann, R., Freudenthaler, V., and Groß, S.: Vertically resolved separation of dust and smoke over Cape Verde using multiwavelength Raman and polarization lidars during Saharan Mineral Dust Experiment 2008, *J. Geophys. Res.*, 114, D13 202–14, 2009.
- Vaughan, M.: Algorithm for retrieving lidar ratios at 1064 nm from space-based lidar backscatter data, in: Proc. SPIE, pp. 104–115, NASA Langley Research Ctr., USA, 2004.
- Vaughan, M. A., Winker, D. M., and Powell, K. A.: CALIOP Algorithm Theoretical Basis Document Part 2: Feature Detection and Layer Properties Algorithms [Available online at http://www-calipso.larc.nasa.gov/resources/pdfs/PC-SCI-202_Part2_rev1x01.pdf], 2005.
- Vaughan, M. A., Powell, K. A., Kuehn, R. E., Young, S. A., Winker, D. M., Hostetler, C. A., Hunt, W. H., Liu, Z., McGill, M. J., and Getzewich, B. J.: Fully Automated Detection of Cloud and Aerosol Layers in the CALIPSO Lidar Measurements, *J. Atmos. Ocean. Tech.*, 26, 2034–2050, 2009.

- Vaughan, M. A., Liu, Z., McGill, M. J., Hu, Y., and Obland, M. D.: On the spectral dependence of backscatter from cirrus clouds: Assessing CALIOP's 1064 nm calibration assumptions using cloud physics lidar measurements, *J. Geophys. Res. Atmos.*, 115, D14 206, 2010.
- Vernier, J. P., Pommereau, J. P., Garnier, A., Pelon, J., Larsen, N., Nielsen, J., Christensen, T., Cairo, F., Thomason, L. W., Leblanc, T., and McDermid, I. S.: Tropical stratospheric aerosol layer from CALIPSO lidar observations, 114, D00H10, 2009.
- Vernier, J. P., Fairlie, T. D., Murray, J. J., Tupper, A., Trepte, C., Winker, D., Pelon, J., Garnier, A., Jumelet, J., Pavolonis, M., Omar, A. H., and Powell, K. A.: An Advanced System to Monitor the 3D Structure of Diffuse Volcanic Ash Clouds, *J. Appl. Meteorol. Climatol.*, 52, 2125–2138, 2013.
- Vernier, J.-P., Fairlie, T. D., Deshler, T., Natarajan, M., Knepp, T., Foster, K., Weinhold, F. G., Bedka, K. M., Thomason, L., and Trepte, C.: In situ and space-based observations of the Kelud volcanic plume: The persistence of ash in the lower stratosphere, *J. Geophys. Res. Atmos.*, 2016.
- Wang, X., Boselli, A., D'Avino, L., Pisani, G., Spinelli, N., Amodeo, A., Chaikovsky, A., Wiegner, M., Nickovic, S., Papayannis, A., Perrone, M. R., Rizi, V., Sauvage, L., and Stohl, A.: Volcanic dust characterization by EARLINET during Etna's eruptions in 2001–2002, *Atmos. Environ.*, 42, 893–905, 2008.
- Wiegner, M., Gasteiger, J., Groß, S., Schnell, F., Freudenthaler, V., and Forkel, R.: Characterization of the Eyjafjallajökull ash-plume: Potential of lidar remote sensing, *Phys. Chem. Earth*, 45-46, 79–86, 2012.
- Winker, D. M., Hostetler, C. A., Vaughan, M. A., and Omar, A. H.: CALIOP Algorithm Theoretical Basis Document, Part 1: CALIOP Instrument, and Algorithms Overview, Release, 2006.
- Young, S. A. and Vaughan, M. A.: The Retrieval of Profiles of Particulate Extinction from Cloud-Aerosol Lidar Infrared Pathfinder Satellite Observations (CALIPSO) Data: Algorithm Description, *J. Atmos. Ocean. Tech.*, 26, 1105–1119, 2009.
- Young, S. A., Vaughan, M. A., Kuehn, R. E., and Winker, D. M.: The Retrieval of Profiles of Particulate Extinction from Cloud-Aerosol Lidar and Infrared Pathfinder Satellite Observations (CALIPSO) Data: Uncertainty and Error Sensitivity Analyses, *J. Atmos. Ocean. Tech.*, 30, 395–428, 2013.

Lidar ratios of stratospheric volcanic ash and sulfate aerosols retrieved from CALIOP measurements

Andrew T. Prata¹, Stuart A. Young², Steven T. Siems¹, and Michael J. Manton¹

¹School of Earth, Atmosphere and Environment, Monash University, Clayton, Victoria 3800, Australia.

²CSIRO Oceans and Atmosphere, Aspendale, Victoria 3195, Australia.

Correspondence to: Andrew T. Prata (andrew.prata@monash.edu)

Abstract. We apply a two-way transmittance constraint to nighttime CALIOP (Cloud-Aerosol Lidar with Orthogonal Polarization) observations of volcanic aerosol layers to retrieve estimates of the particulate lidar ratio (S_p) at 532 nm. This technique is applied to three volcanic eruption case studies that were found to have injected aerosols directly into the stratosphere. Numerous lidar observations permitted characterisation of the optical and geometric properties of the volcanic aerosol layers over a time period of 1–2 weeks. For the volcanic ~~ash-ash-rich~~ layers produced by the Puyehue-Cordón Caulle eruption (June 2011) we obtain mean and median particulate lidar ratios of ~~72–69~~ \pm ~~14 sr and 70–13 sr and 67 sr~~, respectively. For the ~~sulfates sulfate-rich aerosol layers~~ produced by Kasatochi (August 2008) and Sarychev Peak (June 2009), the ~~mean-means~~ of the retrieved lidar ratios were ~~68–66~~ \pm ~~21–19 sr~~ (median ~~62–60 sr~~) and ~~66–63~~ \pm ~~15–14 sr~~ (median ~~61–59 sr~~), respectively.

~~The The 532-nm~~ layer-integrated ~~volume depolarisation ratios (δ_v)~~ ~~particulate depolarization ratios (δ_p)~~ observed for the Puyehue ~~ash layers (δ_v)~~ layers ($\delta_p = 0.28\text{--}0.33 \pm 0.03$) were much larger than those found for the ~~sulfate-volcanic aerosol~~ layers produced by the Kasatochi ($\delta_v\text{--}\delta_p = 0.08\text{--}0.09 \pm 0.03$) and Sarychev ($\delta_v\text{--}\delta_p = 0.05 \pm 0.04$) eruptions. However, for the Sarychev layers we observe an exponential decay (e -folding time of ~~1 week~~) ~~in δ_v 3.6 days~~ ~~in δ_p~~ with time from ~~0.25 to 0.05~~. ~~The 0.27 to 0.03. Similar decreases in the~~ layer-integrated attenuated ~~colour ratios for the Puyehue ash layers~~ ~~color ratios with time were observed for the Sarychev case. In general, the Puyehue layers exhibited larger color ratios~~ ($\chi' = 0.54\text{--}0.53 \pm 0.07$) ~~were also~~ larger than what was observed for the Kasatochi ($\chi' = 0.35 \pm 0.07$) and Sarychev ($\chi' = 0.32 \pm 0.07$) ~~sulfate~~-layers, indicating that the Puyehue ~~ash~~-layers were generally composed of larger particles. These observations are particularly relevant to the new stratospheric aerosol subtyping classification scheme, which has been incorporated into version 4 of the level 2 CALIPSO data products.

1 Introduction

Stratospheric volcanic aerosols are formed when explosive volcanic eruptions inject SO_2 gas and silicate (SiO_2) ash particles into the stratosphere. The volcanic SO_2 can subsequently convert to sulfate aerosols (radii from 0.1–1 μm) to form stratospheric aerosol clouds with their radiative effects persisting from weeks to years depending on the timing, location and amount of precursory SO_2 gas (Carn et al., 2016; Kremser et al., 2016). According to the observational record, stratospheric sulfates formed as a result of major volcanic eruptions can cause abrupt changes in global stratospheric aerosol optical depth (SAOD;

Sato et al., 1993; Bourassa et al., 2012; Rieger et al., 2015). Following the eruption of Pinatubo (Philippines, 1991), this change in SAOD led to a warming of the stratosphere (Labitzke and McCormick, 1992) and cooling of the troposphere (Dutton and Christy, 1992). Small-to-moderate eruptions also have the ability to perturb SAOD (Vernier et al., 2011) and the cumulative effect of enhanced volcanism over the previous decade may have induced a volcanic forcing large enough to temporarily slow global warming (Solomon et al., 2011; Ridley et al., 2014; Santer et al., 2014).

Volcanic ash particles, although more short-lived than sulfates, can cause localised shortwave heating (Gerstell et al., 1995), generate regional-scale temperature anomalies (Mass and Robock, 1982) and pose a serious threat to civil aviation (Prata, 2016). In a modelling study, Niemeier et al. (2009) found that the radiative heating due to stratospheric fine ash particles, released at high latitude (60°N), influenced the regional wind flow. They argued that the combination of weak local flow, a strong Coriolis force and thermal expansion of air due to volcanic ash radiative heating led to the generation of localised vortices. The study highlighted the importance of characterising the optical properties of volcanic ash, especially during the first few weeks of an eruption.

Satellite measurements allow us to determine how volcanic ash and sulfates (collectively referred to here as ‘volcanic aerosols’) interact with solar and terrestrial radiation. Since 2006, the CALIOP instrument aboard the Cloud-Aerosol Lidar and Infrared Pathfinder Satellite Observations (CALIPSO) satellite has been making global, vertically resolved, attenuated backscatter measurements of the Earth’s atmosphere (Winker et al., 2010). CALIOP observations have been used to identify stratospheric volcanic sulfates (Carn et al., 2007; Thomason and Pitts, 2008) as well as volcanic ash in the troposphere (Prata and Prata, 2012; Winker et al., 2012; Prata et al., 2015) and stratosphere (Vernier et al., 2013; Kristiansen et al., 2015).

The lidar equation for elastic backscatter lidars, which governs the CALIOP return signal, includes both molecular and particulate components. While the molecular terms can be estimated or modelled from atmospheric data, we are left with two unknowns (particulate backscatter and extinction) and one equation. This problem is usually overcome, as in the Fernald algorithm (Fernald et al., 1972; Fernald, 1984) (Fernald, 1984) by employing an extinction-to-backscatter ratio, which is now commonly referred to as the ‘lidar ratio’.

Previously reported observations of the volcanic ash lidar ratio vary. Ansmann et al. (2010) and Groß et al. (2012) reported values in the range from 44–60 sr (at 532 nm), based on observations of the Eyjafjallajökull ash clouds in the free troposphere (~2.5–4.5 km) over Germany. Wang et al. (2008) report lidar ratios from 42–65 sr for fine ash/sulfate mixed aerosol layers between 1.5 and 7 km produced by the 2001 and 2002 eruptions of Mt Etna. For sulfate-rich layers volcanic aerosols, the lidar ratio was determined to be ~ 48 sr for Nabro (Sawamura et al., 2012), volcanic aerosol layers at 16 km produced by the 2011 Nabro eruption (Sawamura et al., 2012). For the Sarychev volcanic aerosols, the lidar ratio was determined to be 55 ± 4 sr for Sarychev (O’Neill et al., 2012) and layers measured between 10 and 15 km (O’Neill et al., 2012) and for Kasatochi a lidar ratio of 65 ± 10 sr for Kasatochi (Hoffmann et al., 2010), was determined for a layer at 11 km (Hoffmann et al., 2010). Mattis et al. (2010) also retrieved lidar ratios for Sarychev and Kasatochi, reporting values in the range from 30–50 sr at 532 nm for layers observed between 14 and 18 km.

Since CALIOP is an elastic backscatter lidar, in most cases the lidar ratio must be chosen *a priori* in order to retrieve the extinction profile. Based on extensive ground-based sun photometer measurements taken from the Aerosol Robotic Network

(AERONET; Holben et al., 1998), Omar et al. (2009) have defined six aerosol subtypes for use with CALIOP measurements in version 3 of the data products; clean continental, polluted continental, polluted dust, desert dust, clean marine and smoke. In the version 4 release there will also be a dusty marine aerosol type in the troposphere and there will be four stratospheric types. The CALIOP scene classification algorithm (SCA; Omar et al., 2009), uses optical layer properties, surface type and layer height information to identify CALIOP feature layers as one of the predefined aerosol subtypes. By assigning each aerosol subtype with a characteristic lidar ratio, the extinction profile can be retrieved from CALIOP data (Young and Vaughan, 2009).

While the ~~lidar ratio~~ particulate lidar ratio (S_p) must be assigned *a priori* in the majority of cases, under certain conditions, ~~Fernald's equations~~ the equations of Fernald et al. (1972) can be used to determine S_p from CALIOP measurements. This occurs when the lidar ratio solution is constrained by an estimate of the two-way transmittance (Young, 1995) (Fernald et al., 1972; Young, 1995). Reliable estimates of the two-way transmittance are possible when sufficient clear air exists above and below a lofted cloud/aerosol layer. The transmittance method has previously been applied to optically thin cirrus layers (Sassen and Cho, 1992; Young, 1995), desert dust (Omar et al., 2010) and smoke plumes (Cook et al., 1972).

Stratospheric volcanic ash and sulfate layers are often observed as semi-transparent, laminar features (e.g. Winker and Osborn, 1992a; Vernier et al., 2013). Moreover, the stratosphere is generally free of meteorological clouds, desert dust, biomass burning and continental aerosols; providing the necessary clear-air conditions. The CALIOP backscatter signal-to-noise ratio (SNR), however, is significantly degraded by sunlight during the day. Thus, nighttime observations are generally required to perform a constrained retrieval on stratospheric volcanic aerosols.

Recently it has been shown that sulfate layers can be identified in CALIOP profiles using collocated measurements of SO_2 gas (Carboni et al., 2016). Since CALIOP is insensitive to SO_2 , the underlying assumption is that volcanic SO_2 gas and SO_4^{2-} aerosols are generally collocated. This is a reasonable assumption for the eruptions considered in the present study. Clarisse et al. (2013) showed that sulfate aerosols were detectable from the very onset of the Sarychev Peak eruption and that the infrared SO_2 and $\text{H}_2\text{SO}_4/\text{SO}_4$ signatures were collocated in space and time for the first month. Similarly, Karagulian et al. (2010) demonstrated that the Kasatochi SO_2 cloud was collocated with sulfates for more than one month after the eruption.

This study uses the transmittance method and ~~the Fernald solutions~~ equations of Fernald et al. (1972) to characterise and explore the variability of the lidar ratio for stratospheric volcanic ~~ash and sulfate layers~~ aerosol layers dominated by either ash or sulfate aerosols. We ~~Specifically, we~~ present CALIOP-derived lidar ratios for the ~~ash~~ ash-rich layers produced by the 2011 Puyehue-Cordón Caulle (hereafter Puyehue) eruption and the ~~sulfate~~ sulfate-rich layers produced by the Kasatochi and Sarychev Peak (hereafter Sarychev) eruptions in 2008 and 2009, respectively. We use independent, passive infrared detection from the Atmospheric Infrared Sounder (AIRS) to identify volcanic ash in CALIOP profiles following the method presented by Prata et al. (2015). We also extend this method to sulfates using SO_2 as a proxy for SO_4^{2-} .

2 Satellite data

2.1 AIRS

The AIRS instrument is a part of the Afternoon-train (A-train; Stephens et al., 2002) and is aboard the Aqua satellite in sun-synchronous orbit at 705 km altitude. The AIRS spectrometer disperses upwelling radiation across highly sensitive detector arrays, which results in 2378 spectral samples (nominal spectral resolution of $\lambda/\Delta\lambda = 1200$). These high-spectral resolution measurements cover three infrared wavebands (3.74–4.61 μm , 6.20–8.22 μm and 8.8–15.4 μm ; Aumann et al., 2003) and can be used to detect volcanic ash (Prata et al., 2015) and SO_2 (Hoffmann et al., 2014). An individual AIRS granule comprises 90×135 pixels (1800 km \times 2700 km) with a spatial resolution of $13.5 \times 13.5 \text{ km}^2$ at nadir.

The data products used in the present study are the level 1B geolocated and calibrated radiances version 5.0.23. Only channels suitable for retrievals were used to calculate brightness temperatures (i.e. with L2_ignore flag set to zero; see <http://disc.sci.gsfc.nasa.gov/AIRS/documentation>).

2.2 CALIOP

The CALIPSO satellite is also a member of the A-train and carries the CALIOP instrument as its primary payload (Winker et al., 2010). Following closely behind Aqua (~ 73 s), the space-borne lidar measures elastically backscattered light at 532 and 1064 nm using a three-channel receiver subsystem (Hunt et al., 2009). The ratio of the backscatter measured at these wavelengths (i.e. the attenuated ~~colour~~-color ratio) can be used to infer information about particle size (Liu et al., 2009). The ~~532-nm~~-532-nm signal is also split into two linear polarisation states, which enable ~~depolarisation~~-depolarization measurements to distinguish between irregular (e.g. ash, ice, dust) and spherical (e.g. sulfates) particles.

The CALIOP level 1 version 4, ~~532-nm~~-532-nm total attenuated backscatter profiles (L1-Standard-V4-00) were used to generate attenuated backscatter curtain plots. At a given wavelength, λ , the total attenuated backscatter profile, $\beta'_\lambda(r)$, is related to the particulate and molecular components of backscatter by (Vaughan et al., 2009)

$$\beta'_\lambda(r) = [\beta_{m,\lambda}(r) + \beta_{p,\lambda}(r)] T_{m,\lambda}^2(0,r) T_{e,\lambda}^2(0,r) T_{O_3,\lambda}^2(0,r), \quad (1)$$

where r is the range from the lidar, $\beta_{m,\lambda}(r)$ and $\beta_{p,\lambda}(r)$ are the molecular and particulate backscatter profiles, respectively, and $T_{m,\lambda}^2(0,r)$, $T_{e,\lambda}^2(0,r)$ and $T_{O_3,\lambda}^2(0,r)$ are the molecular, effective and ozone two-way transmittance profiles, respectively.
We note that the effective two-way transmittance profile, $T_{e,\lambda}^2(0,r)$, is related to the particulate two-way transmittance profile via $T_{e,\lambda}^2(0,r) = T_{p,\lambda}^{2\eta}(0,r)$, where η is defined here as the multiple scattering factor (Platt, 1973). The vertical resolutions of the level 1 backscatter profiles are altitude dependent and are broken down into five range intervals. For the altitudes ranges shown here (0–20 km), the relevant vertical resolutions are 30 m and 60 m for the altitude ranges from -0.5 to 8.2 km and 8.2 to 20.2 km, respectively.

The Geometric and optical properties of layers were obtained from the level 2 aerosol layer ~~product-version-3~~(L2_05kmALay) was used to report geometric and optical layer properties. product version 3. (Version 4, level 2 data had not been released at the time of writing.) The vertical resolution was 60 m ~~as for~~ all volcanic layer observations ~~as they~~ were within the 8.2–20.2

km altitude range interval. To ensure constrained conditions for the lidar ratio retrieval (i.e. clear air above and below a lofted layer with acceptable SNR), only stratospheric volcanic aerosol layers that had an extinction quality control flag equal to 1, a valid two-way transmittance measurement (i.e. $0 < T_e^2(r_t, r_b) < 1$) and a horizontal averaging value of 5 km were included in the analysis. We refer to ‘valid’ lidar ratio retrievals hereafter as having satisfied these criteria. We note that the operational 5 lidar ratio data (Final_532_Lidar_Ratio) were not used because we wanted to adjust the multiple scattering factor (η) in the lidar ratio retrieval presented in Sect. 3.2.

As in Winker et al. (2012), the The level 2 optical products used in the present analysis are the effective two-way transmittance ($T_e^2(r_t, r_b)$), the integrated attenuated backscatter (γ'_p), the layer-integrated volume ~~depolarisation ratio~~ (δ_v ~~depolarization ratio~~ (δ_v) and layer-integrated attenuated ~~colour~~ color ratio (χ') are defined. All products are calculated relative to the base (r_b) and 10 ~~top~~ (r_t) of a given aerosol layer. As in Vaughan et al. (2005), δ_v is calculated as

$$\delta_v = \frac{\int_{r_t}^{r_b} \beta'_{\perp}(r) dr}{\int_{r_t}^{r_b} \beta'_{\parallel}(r) dr}$$

and

$$\chi' = \frac{\int_{r_t}^{r_b} \beta'_{1064}(r) dr}{\int_{r_t}^{r_b} \beta'_{532}(r) dr} \frac{\sum_{k=top}^{base} \beta'_{532,\perp}(r_k)}{\sum_{k=top}^{base} \beta'_{532,\parallel}(r_k)}, \quad (2)$$

where r is the range from the lidar, r_t and r_b are the ranges from the lidar to layer-top and layer-base, respectively, $\beta'_{\perp}(r)$ 15 and $\beta'_{\parallel}(r)$ are the $\beta'_{532,\perp}(r)$ and $\beta'_{532,\parallel}(r)$ are the perpendicular and parallel components of the attenuated backscatter at 532 nm. The perpendicular and parallel components of the attenuated backscatter, respectively, and $\beta'_{532}(r)$ and $\beta'_{1064}(r)$ are the attenuated backscatter profiles measured at 532 and 1064 nm, respectively.

The attenuated backscatter make up the total attenuated backscatter at 532 nm such that

$$\beta'_{532}(r) = \beta'_{532,\perp}(r) + \beta'_{532,\parallel}(r). \quad (3)$$

20 The layer-integrated attenuated color ratio, χ' , is calculated as

$$\chi' = \frac{\sum_{k=top}^{base} B_{1064}(r_k)}{\sum_{k=top}^{base} B_{532}(r_k)}, \quad (4)$$

where, $B_{1064}(r)$ and $B_{532}(r)$ are the total attenuated backscatter coefficients corrected for molecular and ozone transmittance:

$$B_{\lambda}(r) = \frac{\beta'_{\lambda}(r)}{T_{m,\lambda}^2(0,r)T_{O_3,\lambda}^2(0,r)} = [\beta_{m,\lambda}(r) + \beta_{p,\lambda}(r)] T_{e,\lambda}^2(0,r). \quad (5)$$

25 In general, the 1064-nm backscattering component will be less than the 532-nm component for small particles and so the attenuated color ratio will also be small. Indeed, the attenuated color ratio is generally greater than 1 for cloud layers and is

less than 1 for aerosols (Liu et al., 2009). The particulate integrated attenuated backscatter, γ'_p , and the is defined as

$$\gamma'_p = \int_{r_t}^{r_b} \beta_p(r) T_p^2(r_t, r) dr \quad (6)$$

and is approximated using the clear air trapezoid technique in the level 2 layer products (Vaughan et al., 2005). This quantity is used in the lidar ratio retrieval described in Sect. 3.2. Finally, the effective two-way transmittance at 532 nm, T_e^2 , were also taken from the, $T_e^2(r_t, r_b)$, is calculated by taking the ratio of the mean attenuated scattering ratio profiles over regions of clear air detected above and below the layer (Vaughan et al., 2009):

$$T_e^2(r_t, r_b) = \langle R'_{\text{below}}(r) \rangle / \langle R'_{\text{above}}(r) \rangle, \quad (7)$$

where the attenuated scattering ratio profile is defined as $R'(r) = \beta'_{532}(r) / \beta'_{m,532}(r)$. We note that only the top layer in a given profile was considered in the present study so that measurements of $T_e^2(r_t, r_b)$ were not degraded by signal attenuation introduced by overlying cloud/aerosol layers. For the top layer, the operational retrieval assumes a purely molecular atmosphere (i.e. $\langle R'_{\text{above}} \rangle = 1$), and so the effective two-way transmittance is calculated as $T_e^2(r_t, r_b) = \langle R'_{\text{below}} \rangle$. The clear air region is defined by the ‘clear air analysis depth’, which is determined via an iterative process in the CALIPSO level 2 layer products as they are required for the lidar ratio retrieval feature detection algorithm (Vaughan et al., 2005). It should also be noted that $T_e^2(r_t, r_b)$ can only be calculated at 532 nm as the molecular scattering signal at 1064 nm is too small (~ 16 times weaker than at 532 nm).

The CALIOP level 2 profile products (L2_05kmAPro) were also used to obtain the normalised, ozone-corrected, total attenuated backscatter coefficient, $\beta'_N(r)$, which is also required as input into the lidar ratio retrieval (discussed in Sect. 3.2). The reason for calculating $\beta'_N(r)$ from the level 2 operational products is so that a new value for η that is, more representative of volcanic ash/sulfates could, can be used in the lidar ratio retrieval.

20 3 Methods

3.1 Volcanic aerosol detection in CALIOP profiles

In order to identify sulfate-sulfate-rich aerosol layers in CALIOP profiles, we assume SO_2 is collocated with SO_4^{2-} and adopt the SO_2 Index (SI) defined in Hoffmann et al. (2014). The SI is defined as the difference between brightness temperatures measured at 7.1 μm and 7.3 μm and exploits the strong absorption signature of SO_2 at 7.3 μm . It is defined such that positive values indicate the presence of SO_2 in the atmosphere. For ash layer detection:

$$SI = BT(1407.2 \text{ cm}^{-1}) - BT(1371.5 \text{ cm}^{-1}), \quad (8)$$

where $BT(\nu)$ is the brightness temperature measured at wavenumber, ν . For detection of volcanic aerosols dominated by ash particles, we use the BTD algorithm defined in Prata et al. (2015). To be consistent with the terminology used in Hoffmann

et al. (2014), the ash BTD algorithm is referred to hereafter as the Ash Index (AI). The AI is a 12-channel BTD algorithm designed to exploit the reverse absorption signature of volcanic ash from 10.4–11.7 μm and 8.8–9.2 μm .

$$\text{AI} = \text{BT}_1 - \text{BT}_2 + \text{BT}_3 - \text{BT}_4, \quad (9)$$

where

$$\text{BT}_1 = \frac{1}{4} [\text{BT}(856.44 \text{ cm}^{-1}) + \text{BT}(856.75 \text{ cm}^{-1}) + \text{BT}(857.06 \text{ cm}^{-1}) + \text{BT}(857.37 \text{ cm}^{-1})],$$

$$\text{BT}_2 = \frac{1}{4} [\text{BT}(964.25 \text{ cm}^{-1}) + \text{BT}(965.04 \text{ cm}^{-1}) + \text{BT}(965.44 \text{ cm}^{-1}) + \text{BT}(966.24 \text{ cm}^{-1})],$$

$$\text{BT}_3 = \frac{1}{2} [\text{BT}(1131.79 \text{ cm}^{-1}) + \text{BT}(1133.96 \text{ cm}^{-1})]$$

and

$$\text{BT}_4 = \frac{1}{2} [\text{BT}(1080.92 \text{ cm}^{-1}) + \text{BT}(1082.41 \text{ cm}^{-1})].$$

We note that Prata et al. (2015) also introduced a temperature threshold (T_h) to remove false detections due to variable surface emissivity over land; however, it became clear that CALIOP detections of weak ash layers were removed by this threshold condition and so it was relaxed for the present study. As with the SI, the AI is defined such that positive values indicate the presence of volcanic ash.

~~Ash and sulfate layers~~ Volcanic ash and sulfate aerosols are identified in CALIOP profiles based on collocated AIRS pixel values of the AI and SI, respectively. The collocation is achieved by calculating the minimum distance between a given CALIOP profile and the centre of each AIRS pixel. For the Puyehue case study, this set of collocated AIRS pixels is scanned for an AI greater than or equal to 1 K and SI below 1 K. ~~For the~~ These conditions were set to ensure that the volcanic aerosol layers analysed for the Puyehue case study were dominated by an ash signal and, importantly, did not exhibit an SO_2 signal. Similarly, to ensure that observations of volcanic layers for the Kasatochi and Sarychev case studies were dominated by sulfates (and not an ash), the algorithm ~~requires a~~ required an SI greater than or equal to 1 K and an AI below 1 K. We also note that CALIOP profiles located south of 65°S were removed from the Puyehue analysis as conditions over Antarctica during the Southern Hemisphere winter (June/July) are conducive to polar stratospheric cloud (PSC) formation (Pitts et al., 2009).

3.2 The ~~Fernald solutions~~ two-component lidar ratio solution for CALIOP

~~In order to retrieve the particulate lidar ratio,~~ We develop our lidar ratio retrieval procedure following Fernald et al. (1972) and use the same notation as Young and Vaughan (2009) and Young et al. (2013). The elastic backscatter lidar equation for the normalised, ozone-corrected, total attenuated backscatter coefficient can be written as

$$\beta'_N(r) = \left[\beta_m(r) + \beta_p(r) \right] T_m^2(r_t, r) T_e^2(r_t, r), \quad (10)$$

where

$$T_e^2(r_t, r) = \exp \left[-2\eta S_p \int_{r_t}^r \beta_p(r') dr' \right] \quad (11)$$

and

$$T_m^2(r_t, r) = \exp \left[-2S_m \int_{r_t}^r \beta_m(r') dr' \right]. \quad (12)$$

- 5 Here S_m and S_p , we use the are the molecular and particulate lidar ratios, which are assumed to be constant throughout the aerosol layer. Following Fernald et al. (1972), Eq. (10) leads to the following first-order differential equation;

$$\frac{dT_e^2(r_t, r)}{dr} - 2\eta S_p \beta_m(r) T_e^2(r_t, r) = -\frac{2\eta S_p \beta'_N(r)}{T_m^2(r_t, r)}. \quad (13)$$

Solving Eq. (13) and rearranging for S_p results in the solution of the two-component Fernald lidar ratio solution (Fernald et al., 1972), lidar equation;

$$10 \quad S_p = \frac{1 - T_e^2(r_t, r_b) T_m^{2\eta S_p/S_m}(r_t, r_b)}{2\eta \int_{r_t}^{r_b} \beta'_N(r) T_m^{2(\eta S_p/S_m - 1)}(r_t, r) dr}. \quad (14)$$

- where r is the range from the lidar, r_t and r_b are the ranges from lidar to layer top and base, respectively, η is the Equation (14) is essentially Eq. (15) of Fernald et al. (1972), but using the notation of Young and Vaughan (2009) and the multiple scattering factor, η , has been included. Since Eq. (14) is transcendental, we apply an iterative solution to retrieve S_p (Fernald et al., 1972). In order to initialise Eq. (14), the solution to the single-component lidar equation could be used to calculate an initial estimate of the lidar ratio (Eq. (7) of Fernald et al. (1972)). However, for the top-most layer in the atmospheric column, CALIOP measurements can be used to make a reasonable approximation of the particulate component of the integrated attenuated backscatter γ'_p (obtained from the level 2 data products) and an initial value of S_p can then be obtained using

$$S_p = \frac{1 - T_e^2(r_t, r_b)}{2\eta \gamma'_p}. \quad (15)$$

- This value is then substituted into Eq. (14) to calculate a refined estimate of S_p . The refined estimate is then compared with the previous value of S_p and the iteration continues until consecutive solutions converge to within a threshold of 0.01% (Fernald et al., 1972).

3.2.1 Using the level 2 products to retrieve S_p

Table 1. Mean and standard deviation of the geometric layer properties for the Kasatochi, Sarychev and Puyehue case studies.

Eruption	Number of layers	Layer-top (km)	Layer-base (km)	Layer-thickness (km)
Kasatochi	116 140	13.60-13.69 ± 1.99 2.03	12.59-12.62 ± 1.98 2.04	1.01-1.06 ± 0.43 0.47
Sarychev	146 183	13.73-13.80 ± 1.89 1.85	12.45-12.40 ± 1.73 1.76	1.40 \pm 0.41
Puyehue	308 374	12.44-12.45 ± 0.82 0.81	10.65-10.63 ± 0.62 0.63	1.79-1.82 ± 0.54 0.55

In order to evaluate Eq. (14), the normalised, ozone-corrected total attenuated backscatter coefficient, $\beta'_N(r)$, must be known. In order to obtain $\beta'_N(r)$ from the level 2 products, we evaluate Eqs. (10)–(12) using the operational values of S_m is the molecular lidar ratio and $T_m^2(r_t, r)$ and $T_e^2(r_t, r)$ are the molecular and effective two-way transmittance profiles, respectively.

The effective two-way transmittance constraint, $T_e^2(r_t, r_b)$, S_p , $\beta_m(r)$, $\beta_p(r)$ and η . The values of S_p and η are obtained from the level 2 aerosol layer product (L2_05kmALay) and $\beta_p(r)$ is obtained from aerosol profile product (L2_05kmAPro). The molecular backscatter profile, $\beta_m(r)$, is calculated by taking the ratio of the mean scattering ratio below layer-base and above layer-top (Vaughan et al., 2009). We only considered the top layer in a given profile so that measurements of $T_e^2(r_t, r_b)$ were not degraded by signal attenuation introduced by overlying cloud from the Global Modelling and Assimilation Office (GMAO; Rienecker et al., 2008) meteorological data provided with the level 2 aerosol profile product and S_m is assumed to be a constant. Note that the molecular lidar ratio is often assumed to be $8\pi/3$. However, this does not include the effects of molecular polarisability. Additionally, the narrow bandwidth of CALIOP's optical filter means that it does not see all of the scattered wavelengths near the central elastic wavelength and the appropriate value of S_m for use with CALIOP data at 532 nm is 8.70447 sr rather than $8\pi/\text{aerosol layers} \cdot 3 \approx 8.37758$ sr.

The

3.2.2 Multiple scattering considerations

The reason for calculating $\beta'_N(r)$ from the level 2 operational products (as above) is so that S_p can be re-calculated, via Eqs. (14) and (15), using a new value for η that is more representative of volcanic ash or sulfates. The multiple scattering factor, η , by definition, varies from 0 to 1 (Platt, 1973). Single scattering is represented by $\eta = 1$ while lower values of η represent increased multiple scattering. In the CALIPSO level 2 version 3 datasets, η is set to 0.6 for all stratospheric features. However, we argue that this approximation may overestimate the effect of multiple scattering in the volcanic aerosols layers considered here. Winker (2003) demonstrated that the value of η for aerosols was a strong function of geometric thickness. Essentially, as the geometric thickness of the aerosol layer is increased the value of η asymptotes towards unity (layers thicker than 500 m correspond to $\eta \geq 0.85$). Given that the mean geometric thickness of the Puyehue ash layers was 1.79 layers was 1.82 ± 0.54 0.55 km (Table 1), η was assumed to be 0.90 ± 0.05 . Accordingly, this value was set higher than the multiple scattering factor used for the Eyjafjallajökull ash layers (0.85 ± 0.05 ; Winker et al., 2012), which were reported to have a mean geometric thicknesses of 0.75 km (Winker et al., 2012). The multiple scattering effects of volcanic sulfates are expected to be similar to that of spherical, fine mode, sulfurous aerosols; analogous to the polluted continental aerosol subtype defined in

Omar et al. (2009). For the polluted continental class, multiple scattering is also expected to have a small effect on [optical depth](#) ([Young et al., 2008](#)) and, therefore, the retrieved lidar ratio ([Young et al., 2008](#)). Considering also that the mean thicknesses of the Kasatochi and Sarychev layers were $1.01\text{--}1.06 \pm 0.43\text{--}0.47$ km and 1.40 ± 0.41 km, respectively (Table 1), η was set to 0.95 ± 0.05 for sulfate aerosols.

- 5 ~~The normalised, ozone-corrected, total attenuated backscatter profile, $\beta'_N(r)$, can be calculated from the level 2 operational products using Eq. (10) of Young and Vaughan (2009):-~~

~~$$\beta'_N(r) = \beta_m(r) + \beta_p(r) T_m^2(r_t, r) T_e^2(r_t, r);$$~~

~~where $\beta_m(r)$ and $\beta_p(r)$ are the molecular and particulate backscatter profiles, respectively, and the transmittance profiles are defined as-~~

~~$$10 \quad T_m^2(r_t, r) = \exp \left[-2S_m \int_{r_t}^r \beta_m(r') dr' \right]$$~~

~~and-~~

~~$$T_e^2(r_t, r) = \exp \left[-2\eta S_p \int_{r_t}^r \beta_p(r') dr' \right].$$~~

- ~~Here $\beta'_N(r)$ is calculated from the operational values of S_p , η and $\beta_p(r)$ provided in the level 2 aerosol layer and profile products. As noted previously, the reason for calculating $\beta'_N(r)$ from the level 2 operational products is so that S_p can be re-calculated, via Eq. , using a new value for η that is more representative of volcanic ash or sulfates. We also compared the re-calculated lidar ratio against the operational lidar ratio using the operational value for η as a check on our method and found that the average difference was $\sim 1\%$.~~

- ~~The molecular backscatter profile, $\beta_m(r)$, is calculated from the Global Modelling and Assimilation Office (GMAO; Rienecker et al., 2008) meteorological data provided with the CALIPSO datasets, and S_m is the molecular lidar ratio. Note that the molecular lidar ratio is generally assumed to be $8\pi/3$. However, the narrow bandwidth of CALIOP's optical filter means that it does not see all the scattered wavelengths near the central elastic wavelength. It also includes the molecular polarisability term giving an actual value at 532 nm of $S_m = 8.70447$ sr rather than $8\pi/3 \approx 8.37758$ sr.~~

3.2.3 An iterative solution for the particulate lidar ratio

~~Since Eq. is transcendental, we apply an iterative solution to retrieve-~~

- 25 **3.3 [Retrieving the particulate depolarization ratio](#)**

~~As we can use the value of S_p (Fernald et al., 1972). In order to initialise Eq. obtained from Eq. (14) , the solution to the single-component lidar equation (see Eq. (7) of Fernald et al. (1972)) is used to calculate an initial estimate of the lidar ratio; to retrieve the profile of particulate backscatter, $\beta_p(r)$, we are also able to retrieve the layer-integrated particulate depolarization ratio, δ_p , which is an intrinsic property of the aerosol layer. The value of δ_p can be derived from the layer-integrated volume~~

depolarization ratio, δ_v , by adapting the approach of Tesche et al. (2009) to integrated quantities:

$$\underline{S}_p \delta_p = \frac{1 - T_e^2(r_t, r_b)}{2\eta\gamma_p'} \frac{\gamma_m(\delta_v - \delta_m) + \gamma_p\delta_v(1 + \delta_m)}{\gamma_m(\delta_m - \delta_v) + \gamma_p(1 + \delta_m)}, \quad (16)$$

where

$$\underline{\gamma_p'}\gamma_m = \int_{r_t}^{r_b} \underline{\beta_p}\beta_m(r) \underline{T_p^2(r_t, r)dr} \quad (17)$$

5 and

$$\underline{\gamma_p} = \int_{r_t}^{r_b} \underline{\beta_p}(r)dr. \quad (18)$$

Here $\underline{\gamma_p'}$ is the particulate integrated attenuated backscatter, which is taken from the level 2 aerosol layer products. In the operational products, $\underline{\gamma_p'}$ is approximated using the clear-air trapezoid technique (Vaughan et al., 2005). The initial value of \underline{S}_p , derived from Eq. , is then substituted into the right-hand side of Eq. to calculate a refined estimate of \underline{S}_p . The refined estimate is then compared with the previous value of \underline{S}_p and the iteration continues until consecutive solutions converge to within a threshold of 0.01%. This refinement is necessary for tenuous aerosol layers where the molecular component of backscatter becomes significant (Young, 1995). the particulate backscatter profile, $\beta_p(r)$, is calculated using the retrieved 532-nm particulate lidar ratio and the numerical integration procedure of Fernald (1984). We also define δ_m as the layer-integrated molecular depolarization ratio. Due to CALIOP's narrow band optical filter, δ_m is the depolarization ratio at the central Cabannes line, which can be assumed to be a constant; $\delta_m \approx 0.003656$ (Hostetler et al., 2006).

We also note that the layer-effective particulate color ratio, χ_p , can be retrieved using the two-color method of Vaughan (2004). This approach seeks to minimise a non-linear function by simultaneously varying $S_{p,1064}$ and χ_p using the method of non-linear least squares. However, for the case studies considered here, we found that the method was rather insensitive to variations in the 1064-nm particulate lidar ratio, often resulting in non-physical solutions for $S_{p,1064}$. We expect that this was due to the relatively weak signals and low optical depths of the volcanic aerosol layers under examination. As these results were inconclusive, and require a more complete treatment of the sources of error, we decided this analysis was outside of the scope of the present analysis and therefore do not report the results here.

4 Case studies and results

4.1 Kasatochi

25 Activity at the Aleutian Island volcano, Kasatochi (52.18°N, 175.51°W) began over a period from 7–8 August 2008 (Waythomas et al., 2010) with SO₂ detectable in the atmosphere for at least a month (Krotkov et al., 2010). Using the SI, it was found that the Kasatochi signature was detectable in AIRS measurements until 28 August 2008. All of the available nighttime CALIOP

Table 2. Mean, median and standard deviation of the optical layer properties for the Kasatochi, Sarychev and Puyehue case studies. The symbols used for the particulate lidar ratio, particulate depolarization ratio, volume depolarisation-depolarization ratio and volume-colour attenuated color ratio are S_p , δ_p , δ_v and χ' , respectively.

Eruption	Number of layers	S_p - S_p (sr)			δ_p (δ_v)			χ'		
		Mean	Median	Std. Dev.	Mean	Median	Std. Dev.	Mean	Median	Std. Dev.
Kasatochi	116-140	68.00 ± 20.61-65.78	59.81	18.79	0.09 (0.08 ±)	0.08 (0.08)	0.03 (0.03)	0.35 ±	0.34	0.07
Sarychev	146-183	65.96 ± 15.17-63.01	58.96	13.59	0.05 ± (0.05)	0.04 (0.04)	0.33 ± 0.09-0.04 (0.03)	0.32	0.31	0.07
Puyehue	308-374	71.70 ± 13.74-68.91	0.29 ± 66.87	12.65	0.33 (0.28)	0.33 (0.28)	0.03 (0.03)	0.53	0.54 ±	0.08

and AIRS data from 8–28 August covering a geographic region from 30°N to 90°N to 180°W to 180°E were included in the present analysis. As seen in Fig. 1a, the SO₂ dispersion was extremely complex, with the SO₂ cloud being dispersed into the atmosphere over a period of ~3 weeks until it became well-mixed and undetectable by AIRS. In total, ~~116-140~~ valid lidar ratio retrievals were made for the Kasatochi ~~volcanic sulfate~~-layers. The mean layer-top height and thickness of the Kasatochi layers were ~~13.60-13.69 ± 1.99 km and 1.01-2.03 km and 1.06 ± 0.43-0.47~~ km, respectively. The mean ~~depolarisation and colour ratios were 0.08-particulate depolarization and attenuated color ratios were 0.09 ± 0.03 and 0.35 ± 0.07~~, respectively, indicating observations of ~~sulfate layers aerosols layers optically dominated by sulfates~~; composed of small, spherical particles. The mean and standard deviation of the lidar ratios for the Kasatochi ~~sulfate~~-layers retrieved over a time period from 8–28 August were ~~68-66 ± 21-19~~ sr (median of ~~62-60~~ sr). The lidar ratios (S_p) and color ratios (χ') were quite variable with time; making it difficult to infer any clear trends in these parameters. The particulate depolarization ratios (δ_p) remained largely unchanged during the measurement time period (Fig. 8d). Figure 2 shows the respective distributions of the optical properties for each eruption case study. The layer-mean properties are given in Tables 1 and 2.

4.2 Sarychev

Sarychev (48.09°N, 153.20°E), which is one of the most active volcanoes in the Kuril Island chain (Russia), began to erupt on 11 June 2009 (Rybin et al., 2011). AIRS detected an ash and SO₂ signature on June 12; however, CALIOP data was not available from 12–14 June 2009. According to surface observations, no more ash or SO₂ was seen emanating from the volcano after 24 June, but SO₂ was still detectable in the atmosphere (Williams and Thomas, 2011). Data for the Sarychev case study were therefore collected from 15 June to 12 July 2009, covering the same geographic region as the Kasatochi case study. Figure 1b provides an overview of the Sarychev SO₂ dispersion. Unlike Kasatochi, the Sarychev SO₂ signature initially separated into two distinct SO₂ clouds that dispersed toward the east and northwest. The eastward-traveling SO₂ cloud remained over the Alaskan peninsula for several days, while the northwestward SO₂ cloud travelled south as it crossed back over the volcano. In total, ~~146-183~~ valid lidar ratio retrievals were obtained. The mean optical properties of the Sarychev ~~sulfate~~-layers shared many similarities with the Kasatochi layers (Fig. 2). ~~The mean depolarisation- 2); however, the Sarychev particulate depolarization ratio exhibited an exponential decrease with time over 3.6 days. A similar decreasing trend was also observed for the attenuated color ratio. The time evolution of all optical properties are discussed in Sect. 6.2 and are shown in Fig. 8. The mean particulate~~

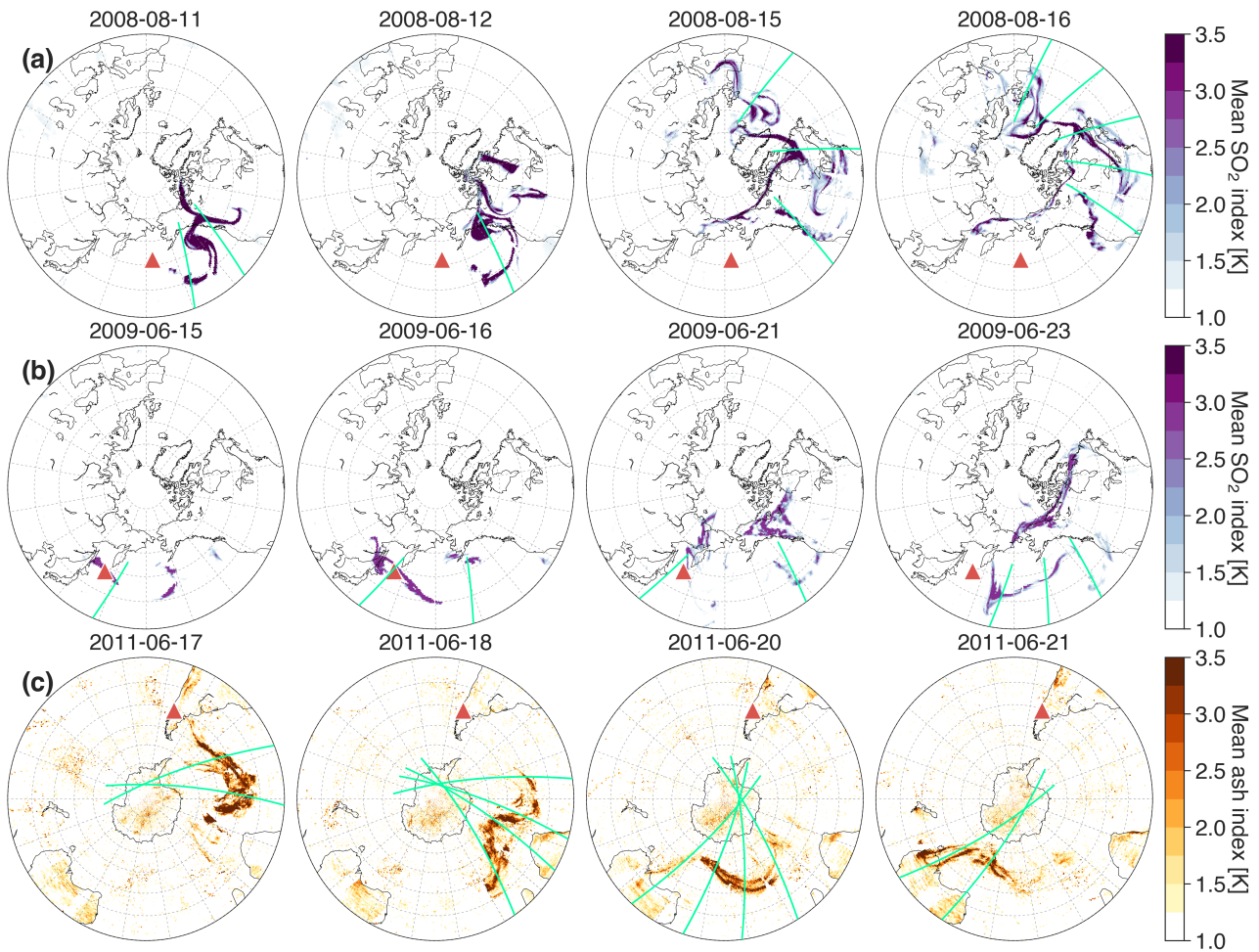


Figure 1. CALIOP/AIRS overview for a selected number of days for each of the case studies analysed; Kasatochi (a), Sarychev (b) and Puyehue (c). The locations of each volcano are plotted as red triangles. The AI (Ash Index) and SI (SO₂ Index) have been re-gridded into $0.5^\circ \times 0.5^\circ$ grid boxes and have been averaged by the number of data points falling into a given grid box and therefore represent AI and SI means. Over-plotted green lines indicate CALIOP overpasses that contained valid lidar ratio retrievals.

depolarization ratio was 0.05 ± 0.04 and mean colour-attenuated color ratio was 0.32 ± 0.07 (Table 2). The mean lidar ratio for the Sarychev layers was 66.63 ± 15.14 sr (median of 61.59 sr), corresponding to a layer-mean height and thickness of 13.73 ± 1.89 – 1.85 km and 1.40 ± 0.41 km, respectively (Table 1).

4.3 Puyehue

- 5 ~~The eruption~~ The eruptions of Chilean volcano, Puyehue (40.59°S , 72.12°W) ~~was the first VEI 5~~
(Volcanic Explosivity Index; Newhall and Self, 1982) eruption since Cerro Hudson in 1991. ~~The eruptions~~ began on 4 June
2011 and resulted in wide-spread and far-reaching ash layers that caused flight cancellations in Australia and New Zealand.
Vernier et al. (2013) analysed CALIOP observations of the ~~Puyehue ash clouds and found the volcanic aerosol~~ volcanic aerosols
10 produced by Puyehue and found that the layers were primarily made up of ash particles ~~and that sulfates contributed with~~
sulfates contributing to less than 10% of the total attenuated backscatter. In the present analysis, we avoid ice-rich layers
and identify ash-rich layers using passive infrared detection from collocated AIRS pixels (i.e. $\text{AI} \geq 1$ K and $\text{SI} < 1$ K). The
CALIPSO analysis presented by Vernier et al. (2013) also showed that the ash clouds remained near the tropopause as they
were driven around the Southern Hemisphere by a strong westerly polar jet. This spatial description of the Puyehue ~~ash clouds~~
aerosols has been corroborated by several other authors (Klüser et al., 2013; Hoffmann et al., 2014; Theys et al., 2014).
- 15 CALIOP was switched into safe mode on 4 June, and again from 6–14 June 2011 (with 46.8% coverage on 15 June). During
this time period the ~~ash layers~~ volcanic aerosols made their first circuit around the Southern Hemisphere. The observations
included in the present analysis are therefore representative of aged (~ 2 weeks) ~~ash~~ ash-rich volcanic aerosol layers. The AIRS
observations were analysed over a time period from 16 June to 4 July and a geographical area from 20°S to 90°S and 180°E to
20 180°W (Fig. 1c). The CALIOP profiles were restricted to latitudes north of or equal to 65°S to avoid PSCs (as noted in Sect.
3). In total, ~~308–374~~ valid lidar ratio retrievals were applied to CALIOP profiles containing stratospheric ~~ash~~ aerosol layers. The
mean layer-top height and thickness of the Puyehue layers were ~~12.44–12.45~~ ± 0.82 km and ~~1.79–0.81~~ km and 1.82 ± 0.54 – 0.55
km, respectively (Table 1). In contrast to the optical properties of the Kasatochi and Sarychev layers, the Puyehue ~~ash layers~~
~~showed significant depolarisation~~ (δ_p layers exhibited consistently high depolarization ratios ($\delta_p = 0.29$ – 0.33 ± 0.03 ; Table 2),
25 indicating aerosol layers optically dominated by non-spherical particles ~~. The colour ratios of the Puyehue ash layers over the~~
measurement period. The layer-integrated attenuated color ratios for the Puyehue case study were also higher ($\chi' = 0.54$ – 0.53
 ± 0.07 – 0.08 ; Table 2) than the ~~sulfates~~ Kasatochi and Sarychev case studies ($\chi' = 0.32$ – 0.35). ~~The~~ In general, changes in the
Puyehue lidar ratios (S_p mean of ~~72–69~~ ± 14 – 13 sr and median of ~~70 sr~~) ~~were similar in magnitude to the sulfate lidar ratios of~~
67 sr) with time were quite similar to the changes in lidar ratio with time for Kasatochi and Sarychev case studies. The lidar
ratio distributions for the three case studies were similar in shape and were all positively skewed. We therefore provide both
30 the mean and median lidar ratios (annotated on each histogram of Fig. 2).

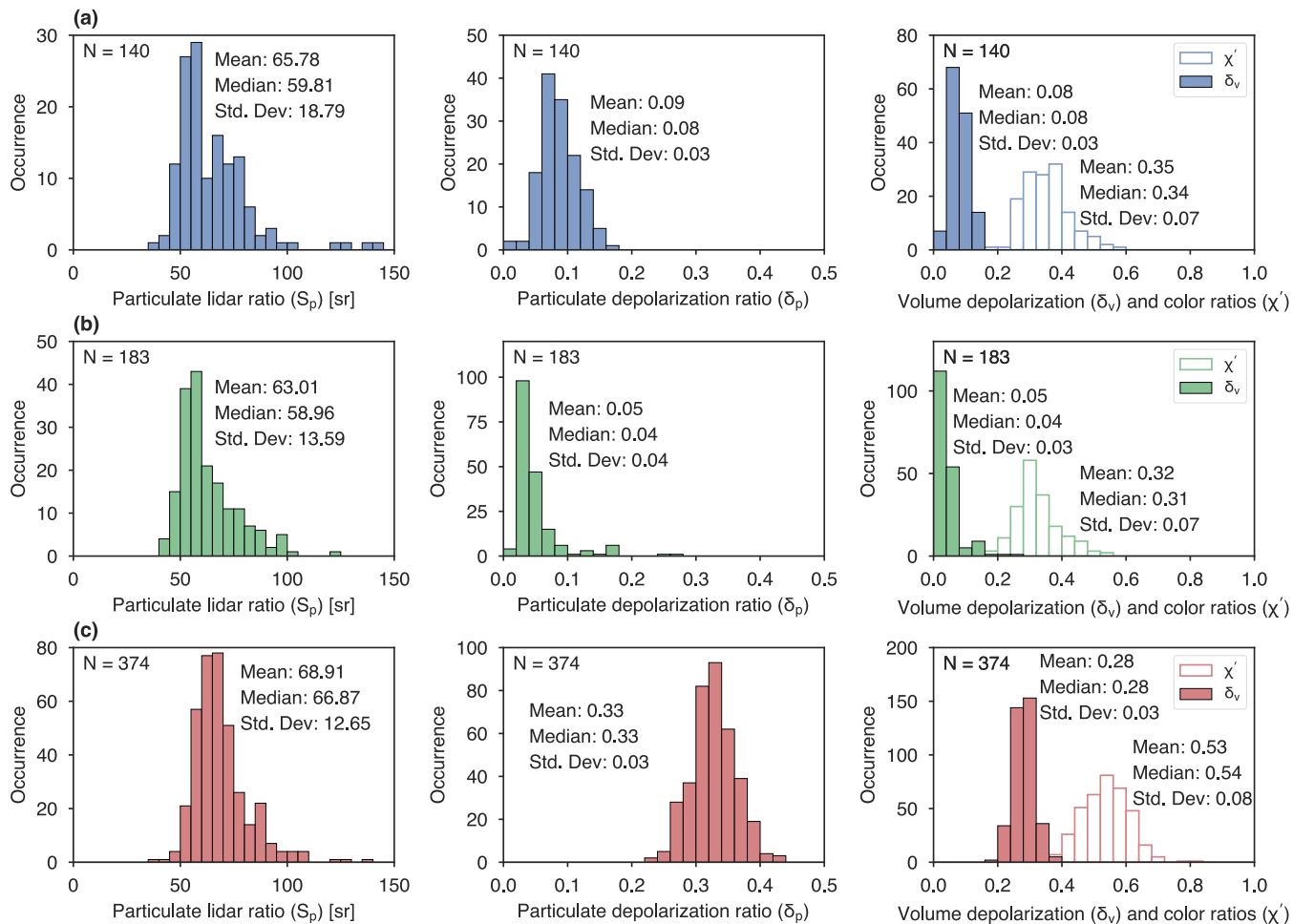


Figure 2. Histograms of the particulate lidar ratio (left column), layer-integrated volume depolarisation-particulate depolarization ratio (middle column) and layer-integrated volume depolarization and attenuated colour-ratio-color ratios (right column) for the three case studies; (a) Kasatochi plotted in blue, (b) Sarychev plotted in green and (c) Puyehue in red.

5 Error sensitivity and propagation analysis

As discussed in Young et al. (2013), errors in a constrained retrieval of S_p can be broken down into two main categories: calibration/renormalisation error, $\epsilon(\beta'_N)$, and error in the transmittance constraint, $\epsilon(T_e^2)$. We also consider possible errors in the choice of the multiple scattering factor, $\epsilon(\eta)$. We do not, however, consider the impact of random noise on the lidar ratio retrieval. Essentially, we assume that error due to random noise will be negligibly small after 5 km averaging and thus insignificant in comparison to the other sources of error.

5.1 Errors in calibration/normalisation

Rogers et al. (2011) provide a comprehensive assessment of the version 3.01 CALIOP ~~532-nm~~532-nm total attenuated backscatter calibration. For nighttime measurements under clear-air conditions the mean relative error was reported to be $2.7\% \pm 2.1\%$ when compared against airborne HSRL measurements. One of the main sources of error that is particularly relevant here, can arise in the case of an undetected (background) stratospheric aerosol layer. Vernier et al. (2009) highlighted how this issue would impact the CALIOP calibration region, concluding that undetected aerosols up to 35 km ~~lead-led~~ to an underestimation of the ~~aerosol-particulate~~(aerosol) scattering ratio (an average relative error of 6%), with the effects most pronounced in the tropics (20°N – 20°S). Although the observations presented here are confined to middle–high latitude regions, they directly coincide with ongoing volcanic eruption events, and so we must consider errors introduced by aerosol contamination (which have not been corrected for in the version 3 datasets).

Considering the $\sim 5\%$ calibration error suggested by Rogers et al. (2011) and the 6% aerosol contamination error suggested by Vernier et al. (2009), we anticipated a relative error of 10% in the normalised, attenuated backscatter profile (i.e. $\epsilon(\beta'_N)/\beta'_N = 10\%$).

5.2 Errors in transmittance

The CALIOP level 2 aerosol products provide an estimate of the measured two-way transmittance error, which is calculated as the standard deviation of the attenuated scattering ratio in the clear air region below the detected layer (Vaughan et al., 2005). For the case studies considered, the means (and standard deviations) of the two-way transmittance relative errors were ~~+15.91~~16.04 $\% \pm 2.79\%$, ~~+16.76~~2.94 $\%$, 16.69 $\% \pm 2.72\%$, and ~~+16.93~~16.70 $\% \pm 4.08$ 3.84 $\%$ for Kasatochi, Sarychev and Puyehue, respectively. However, since the operational algorithm (Vaughan et al., 2009) assumes pure Rayleigh scattering above the top layer of a given CALIOP profile, it is assumed that there is no attenuation by undetected layers aloft and that all of the attenuation is in the detected layer. In this case the estimate of T_e^2 will be too low and S_p will be too high. Rogers et al. (2011) considered the possible influence of volcanic aerosols affecting the two-way transmittance between 8–30 km. Based on volcanic stratospheric optical depths from Mattis et al. (2010), they estimated a maximum bias in the two-way transmittance of 3%. Considering the mean transmittance errors for the three case studies ($\sim 17\%$) and the error introduced by undetected volcanic aerosols ($\sim 3\%$), a relative error of 20% in the effective two-way transmittance constraint was assumed (i.e. $\epsilon(T_e^2)/T_e^2 = 20\%$).

5.3 Error propagation analysis

To estimate how the errors in β'_N , T_e^2 and η propagate into errors in S_p a multi-variable functional approach (Hughes and Hase, 2010) was applied to Eq. (14) to calculate a perturbation error for each variable. As discussed in the previous sections, β'_N and T_e^2 were perturbed by 10% and 20%, respectively, and η was perturbed by 0.05. If any variable was perturbed outside of its physical bounds then it was set to the relevant upper or lower bound. Each perturbation error was then summed in quadrature to calculate the absolute error in the particulate lidar ratio:

$$\epsilon(S_p) = \pm \sqrt{\epsilon(S_{p,\beta'_N})^2 + \epsilon(S_{p,T_e^2})^2 + \epsilon(S_{p,\eta})^2}, \quad (19)$$

where $\epsilon(S_{p,\beta'_N})$, $\epsilon(S_{p,T_e^2})$ and $\epsilon(S_{p,\eta})$ represent the three components of error in S_p . The subscripts represent the variable that was perturbed while holding the other two variables constant. Figure 3 illustrates, for each case study, how each of the three perturbation errors propagated into the error in S_p . The assumed relative errors in β'_N and T_e^2 , translated into mean absolute component errors of ~ 6 sr and ~ 14 sr, respectively, while the assumed error perturbations of 0.05 in η corresponded to errors in S_p of ~ 3 sr. Overall, the perturbation errors, when summed in quadrature, corresponded to a mean absolute error in S_p of ~ 15 sr.

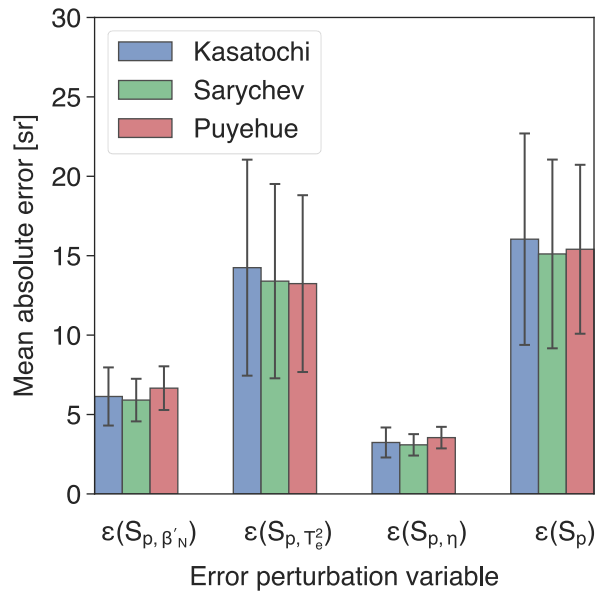


Figure 3. Perturbation errors for each case study; Kasatochi (blue), Sarychev (green) and Puyehue (red). The standard deviations for each perturbation error are plotted as whiskers over each bar plot.

As T_e^2 was considered to be the largest source of error in S_p , we examined how the relative error in the lidar ratio, $\epsilon(S_p)/S_p$, varied as a function of T_e^2 (Fig. 4). Here we see that the relative error in S_p asymptotes toward $\sim 10\%$ as T_e^2 approaches zero

and increases exponentially as T_e^2 approaches unity. In other words, for non-transmissive (optically thick) layers, error in the retrieved value of S_p will be limited by errors in β'_N and η . For highly transmissive (optically thin) layers, error in T_e^2 will become the dominant source of error in S_p .

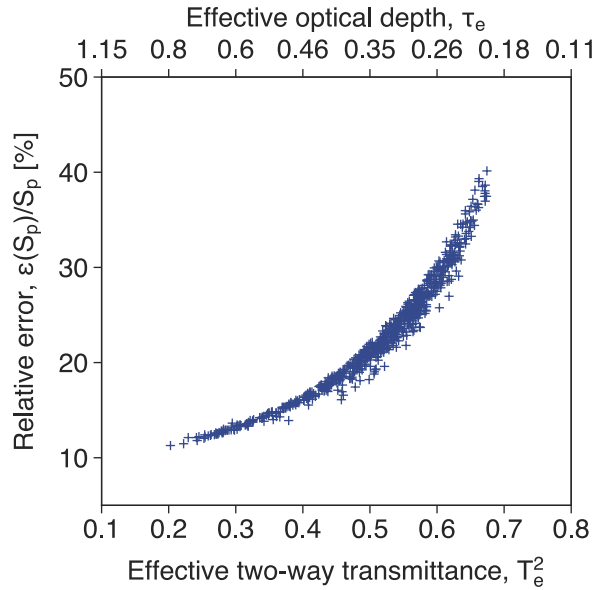


Figure 4. Relationship between T_e^2 and the relative error in the particulate lidar ratio, $\epsilon(S_p)/S_p$.

6 Discussion

6.1 Lidar ratio retrievals for selected observations

Figures 5–7 illustrate show how the CALIOP/AIRS analysis performed for an individual granule-AIRS granule selected from each case study; illustrating the conditions under which the lidar ratio retrievals are successful and how the volcanic layers correlate with the AI and SI. The times of each of the selected observations (Figs. 5–7) are also indicated on Figs. 8a–c, which show the overall times series of the aerosol optical properties (S_p , δ_p and χ') for each case study. For the Kasatochi and Sarychev sulfate-layers (Fig. 5 and Fig. 6, respectively), the lidar ratio is relatively constant throughout the strongly backscattering regions of the stratospheric layers. The AIRS SO₂ signals also collocate well with the sulfate-layersthese aerosols, suggesting that they are largely composed of sulfates. The curtain-average value of the lidar ratio for the two-sulfate-two sulfate-rich layers are also very similar ($S_p \sim 54$ sr), $\overline{S_p} \sim 53$ sr), but lower than the median values of the corresponding lidar ratio distributions (~ 60 sr; Figs. 2a, b). The Kasatochi observation corresponds to an aerosol layer that had resided in the stratosphere for ~ 7 days whereas the Sarychev observation corresponds to a layer approximately twice the age (~ 14

days) of the Kasatochi layer. The mean ~~volume depolarisation-particulate and volume depolarization~~ ratios for the ~~sulfates sulfate-rich layers~~ are both relatively low ($\delta_v < 0.2\bar{\delta}_p$, $\bar{\delta}_v \sim 0.05-0.10$) indicating that these layers are dominated by spherical particles. ~~The low mean depolarisation ratio ($\bar{\delta}_v = 0.04$) and strong SO₂ signature implies that the Sarychev layer is dominated by spherical sulfate particles.~~The attenuated colour ratios for the sulfate observations are also quite similar ($\chi' =$ ~~The curtain-mean attenuated color ratio for the Kasatochi observation ($\bar{\chi}' = 0.37$; Fig. 5) was higher than the Sarychev observation ($\bar{\chi}' = 0.33-0.37$) and indicate that these aerosol layers are made up of small particles; Fig. 6) although both were smaller than the Puyehue observation ($\bar{\chi}' = 0.54$; Fig. 7) indicating that the sulfate-rich layers were composed of smaller particles than the ash-rich layers.~~

The Puyehue ~~ash~~ layers (Fig. 7) are quite similar to the ~~sulfate-sulfate-rich~~ layers in terms of the geometric thickness; however, the ~~layer-integrated optical properties~~curtain-mean particulate depolarization ratio ($\bar{\delta}_p = 0.32$), along with the AIRS ash signal, unambiguously identify this layer as being ~~made up of optically dominated by~~ non-spherical ash particles. The variability in the lidar ratio for the Puyehue observation generally increases as features become more tenuous, reflecting an increase in sensitivity in the lidar ratio retrieval for transmissive layers (as discussed in Sect. 5.3). ~~The lidar ratios are also more variable than the sulfate ratios, which may be an indication of greater inhomogeneity in the Puyehue layer observations.~~ The curtain-mean lidar ratios for the Puyehue observation are also quite high ~ 68 sr and we note that this may be due to the age of the layers (~ 17 days; discussed in more detail in Sect. 6.2).

6.2 Time evolution of volcanic aerosol optical properties

As volcanic aerosol layers evolve and disperse into the atmosphere their microphysical properties are expected to change with time. The Kasatochi and Puyehue layers were observable for a duration of $\sim 5-12$ days, while the Sarychev observations covered a time period of $\sim 12-17$ days. ~~Figure 8 shows~~ Figures 8a-c show that all observations were made more than three days after eruption onset. The Kasatochi ~~observations are representative of the earlier stages of volcanic sulfate layer evolution and the Puyehue observations are more representative of long-range transported ash layers that~~ and Puyehue volcanic aerosols were observed for a similar time period (~ 12 days); however, for the Puyehue case study, the aerosol layers had resided in the stratosphere for more than ~~2 weeks~~ 11 days before the measurement period began. The Sarychev case study ~~provided covered~~ the longest observational time period ~~of volcanic aerosol layer evolution of the three case studies considered.~~

~~, providing observations of sulfate-rich aerosols for over two weeks. All volcanic aerosol layers were subject to long-range transport across the globe as shown by the spatial distribution of observations plotted in Figs. 8j-l.~~

The particulate lidar ratios for ~~Kasatochi show a steady decrease with time from 75 sr to 55 sr over the first 4 days of observations, followed by an increase to 65 sr from day 7-8 (Fig. 8a).~~ The lidar ratio observations were more variable with time for the Sarychev case study; however, when averaged over the total observation period the lidar ratios generally increased with time from 60 sr to 70 sr. The Puyehue lidar ratios were the least variable and exhibited a linear increase with time over ~ 5 days from 65 to 70 sr.

~~The triangles corresponding to the right hand axis of Fig. all three case studies were quite variable with time (Figs. 8a-c demonstrate how changes in S_p with time are inversely related to the integrated attenuated backscatter, γ'_p . As an SO₂-rich~~

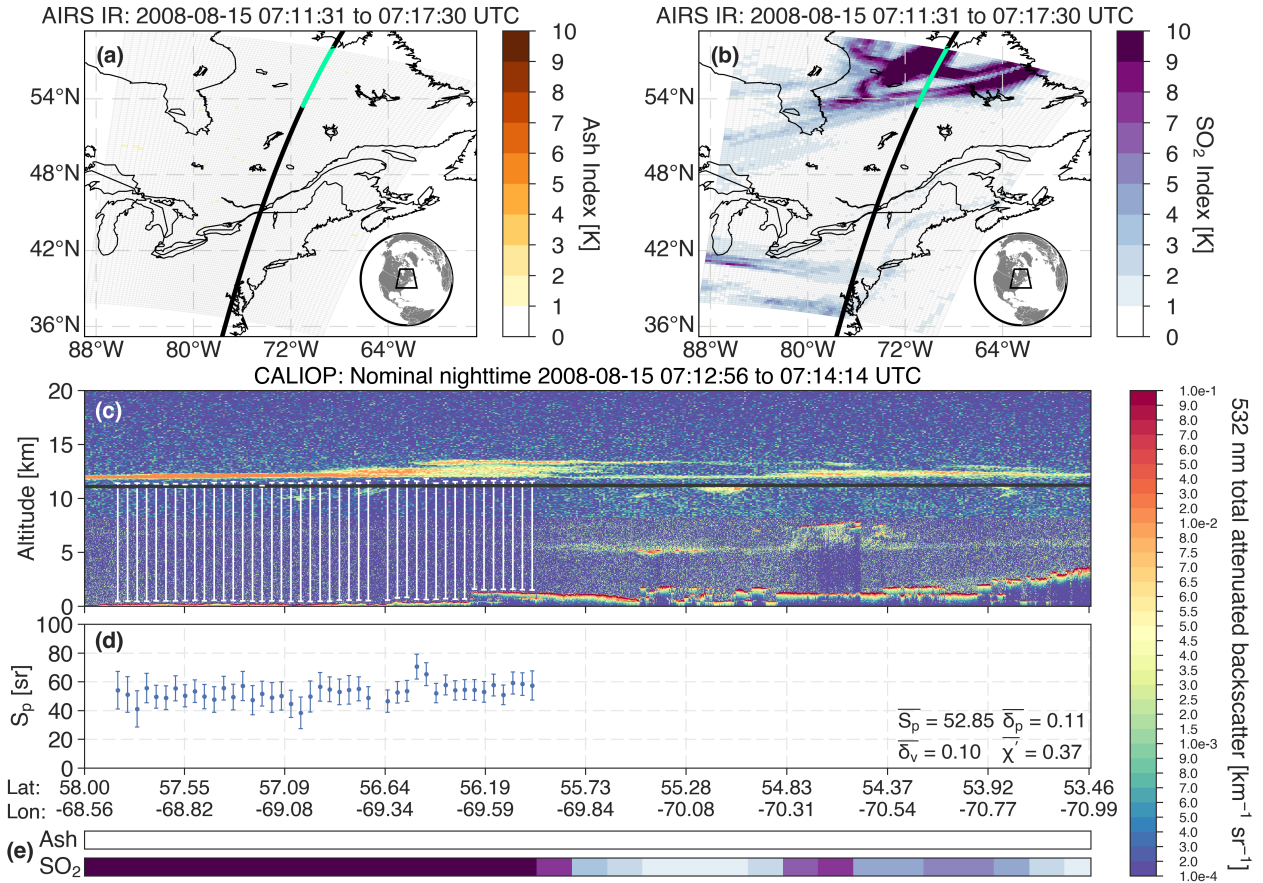


Figure 5. CALIOP/AIRS observations of a stratospheric volcanic sulfate-sulfate-rich layer produced by the 2008 Kasatochi eruption. (a) AIRS swath with the AI (Ash Index) plotted. The CALIOP trace (black line) is over-plotted and the section of the CALIOP trace corresponding to the CALIOP curtain panel, plotted in (c), is highlighted in green. (b) Same as (a) but for the SI (SO₂ Index). (c) CALIOP curtain plot (longitude/latitude/longitude vs. total attenuated backscatter) with the GMAO tropopause height over-plotted in black and clear air analysis depths over-plotted in white. (d) Particulate lidar ratio retrievals (error bars are calculated from Eq. (19)). The curtain-mean values of the particulate lidar ratio ($\overline{S_p}$), layer-integrated depolarisation-particulate depolarization ratio ($\overline{\delta_p}$), volume depolarization ratio ($\overline{\delta_v}$) and colour-attenuated color ratio ($\overline{\chi'}$) are annotated on the right-hand side of the plot. (e) AI and SI AIRS pixels that have been collocated along the CALIOP track.

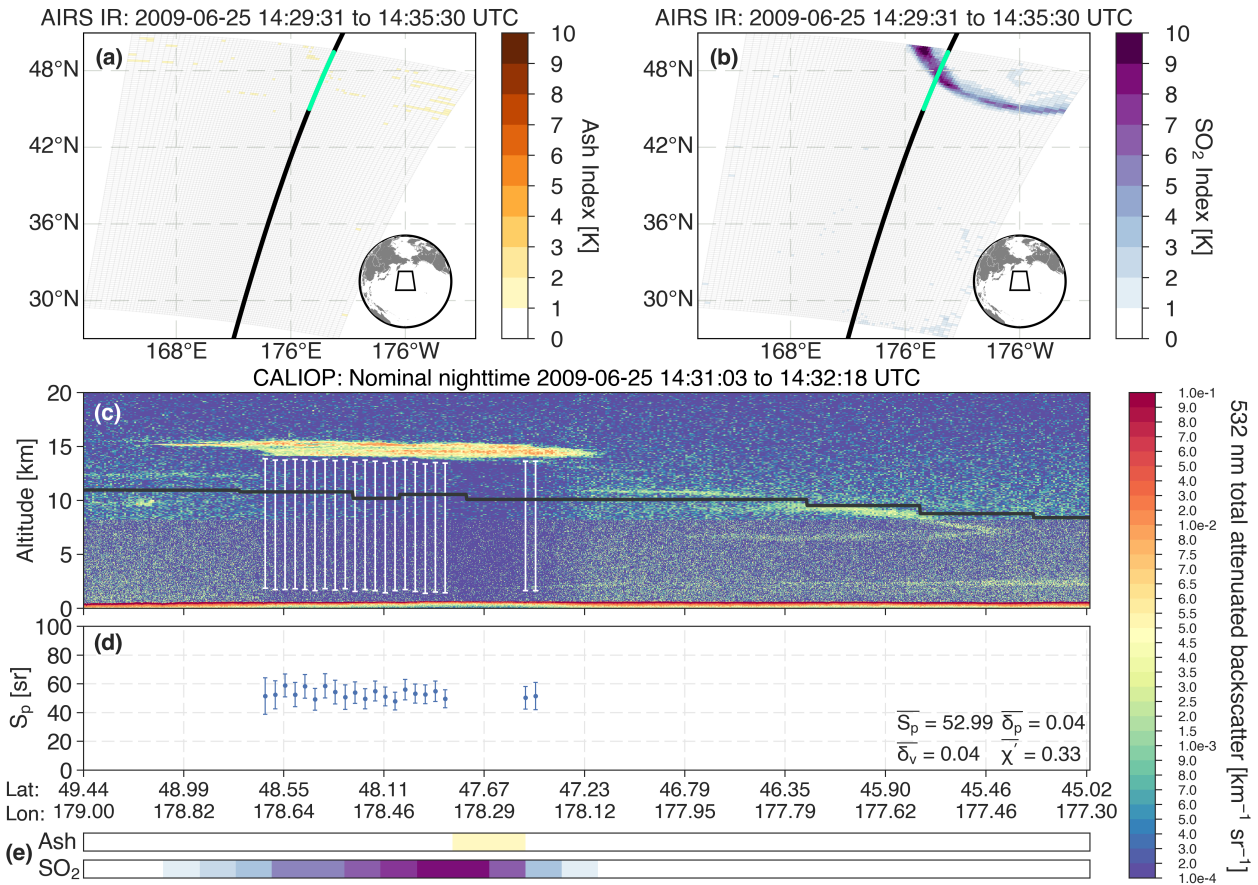


Figure 6. Same as Fig. 5 but for a stratospheric volcanic sulfate-sulfate-rich layer produced by the 2009 Sarychev eruption.

volcanic cloud develops, the integrated attenuated backscatter would be expected to initially increase as SO_2 molecules are oxidised and hydrated to form sulfate particles. Since the particulate lidar ratio is inversely proportional to backscatter, this process would lead to a reduction in S_p . Over these timescales (1–2 weeks) it is likely that the volcanic aerosol layers are mixing with ambient aerosol, resulting in fluctuations in the lidar ratio with time. On the other hand, as layers mature and particles fall out of the atmosphere due to sedimentation processes, γ_p' will decrease leading to an increase in S_p toward the later stages of layer development. For the ash-rich layers of Puyehue, it is likely that the increase in S_p with time is being driven by particle sedimentation processes (i. e. a decrease in γ_p' with time). Changes in the lidar ratio may also be a result of sampling different parts of an inhomogeneous aerosol cloud.

The Puyehue lidar ratios (65–70 sr) are relatively high in comparison to previously reported volcanic ash lidar ratios (40–60 sr; Ansmann et al., 2010; Groß et al., 2012). In fact, the Puyehue lidar ratios share interesting similarities with long-range transported Saharan desert dust lidar ratios (40–75 sr; Mattis et al., 2002). Mattis et al. (2002) provide two main reasons for high lidar ratios of long-range transported dust particles. The first is an increase in the fine to coarse mode particle ratio due to

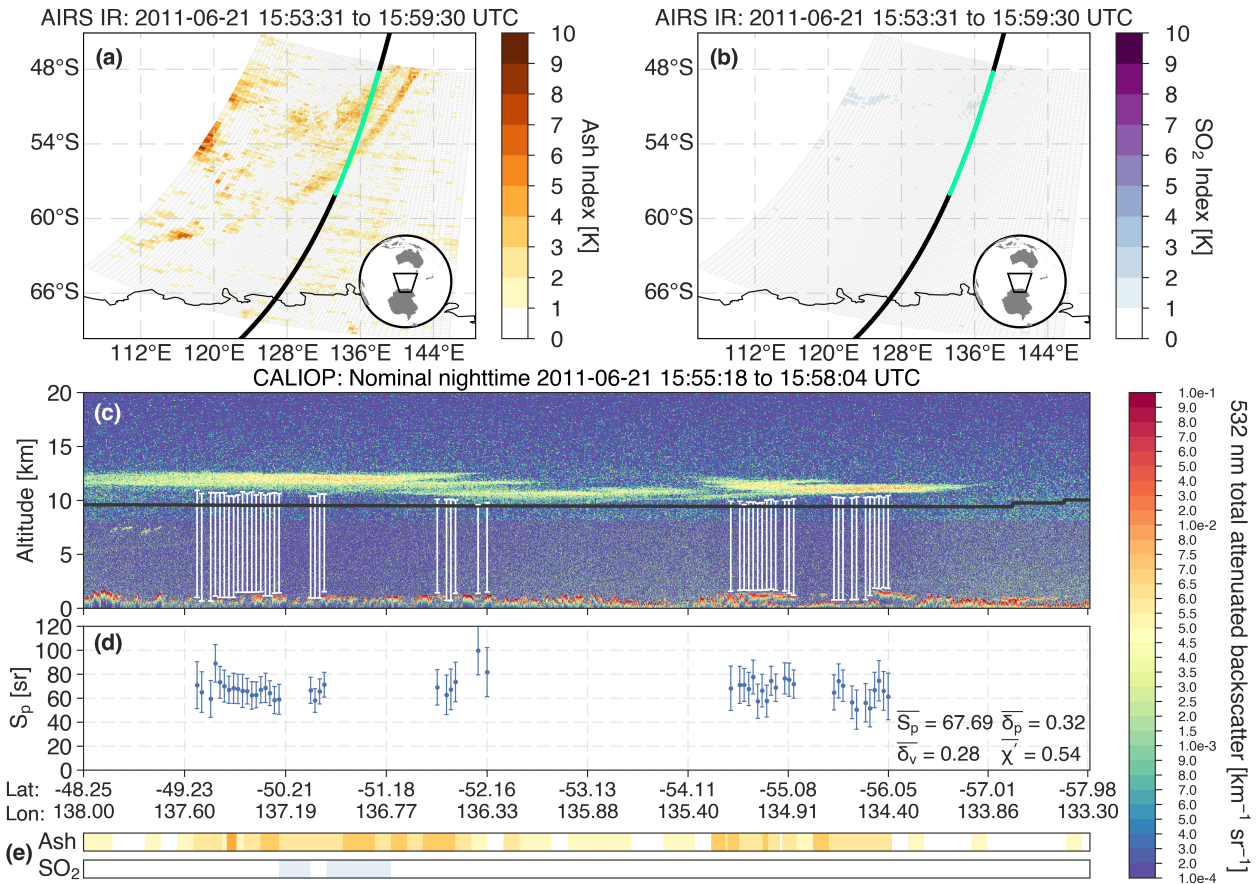


Figure 7. Same as Fig. 5 but for a stratospheric ash-rich volcanic ash-aerosol layer produced by the 2011 Puyehue eruption.

gravitational settling of coarse mode (diameters $>1 \mu\text{m}$) particles. The second is a large reduction in backscattering efficiency due to the non-sphericity of the particles. Both explanations are consistent with the Puyehue observations. The ash-rich aerosol layers were observed after 12-11 days of long-range transport (providing the necessary time for coarse mode particles to fall out) and the layers were also dominated by irregular, highly depolarising ($\delta_v \sim \delta_p \geq 0.30$) particles.

- 5 The volume-depolarisation-particulate depolarization ratios of the Puyehue ash-layers were generally much larger-higher than the Kasatochi and Sarychev layers (Figs. 8d-f). Note that δ_v is not strictly a particle property, but for layers dominated by aerosols it can be used as a first approximation to the particulate depolarisation ratio, d-i. Winker and Osborn (1992b) report similar depolarization ratios (δ_p (Wiegner et al., 2012). The Puyehue depolarisation ratios were higher than expected ~ 0.30 for aged (~ 2 weeks) ash particles as there are few observations of aged ash layers with depolarisation ratios higher than 0.30
- 10 (e.g. Pinatubo; Winker and Osborn, 1992b). 27 days), stratospheric (~ 22 km) volcanic aerosol layers produced by the 1991 Pinatubo eruption. Ansmann et al. (2010), Groß et al. (2012) and Wiegner et al. (2012) reported particulate depolarisation

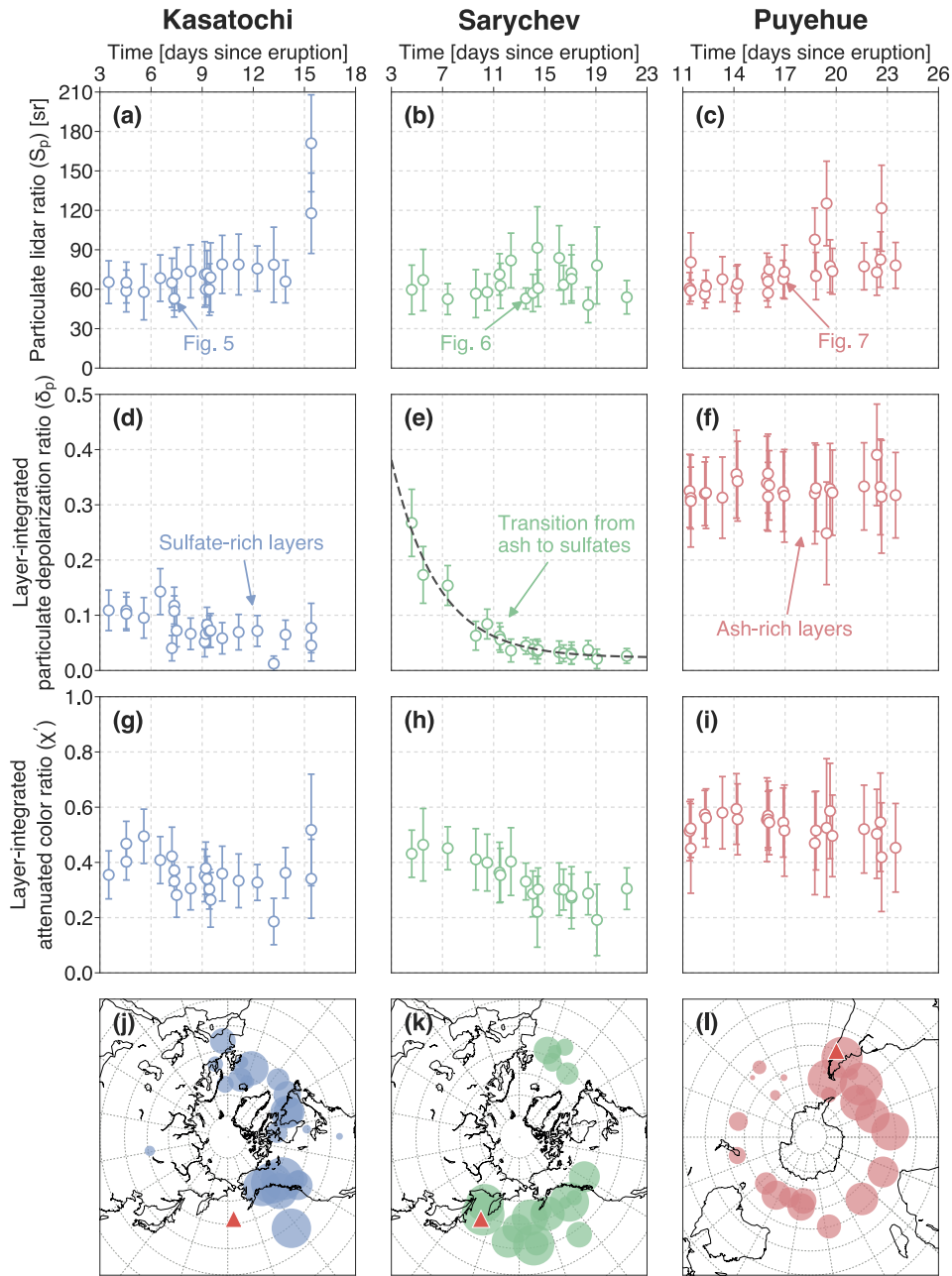


Figure 8. Time evolution of the optical properties for Kasatochi (left column), Sarychev (middle column) and Puyehue (right column). (a)–(c) Left axis corresponds to CALIOP curtain mean and standard deviation root mean squared error (error bars) of S_p (plotted as circles) and right axis corresponds γ_p' (plotted as triangles). (d)–(f) The same as (a)–(c) but for the layer-integrated volume depolarisation particulate depolarization ratio (δ_p). Also plotted, on (e), is an exponential fit (black dashed line) corresponding to an e -folding time of 1-week 3.6 days. (g)–(i) The same as (a)–(c) but for the layer-integrated-attenuated colour-color ratio (χ'). (j)–(l) Geographic representation of the data plotted on panels (a)–(i) with where the size of the data points sealed to be are negatively proportional to the residence time of the volcanic aerosol layers aerosols. Locations of volcanoes are plotted as red triangles.

report even higher particulate depolarization ratios from 0.35–0.40 for Eyjafjallajökull ash observed over Germany; however, these were observations of young (1–3 days old) tropospheric ash layers.

Over the ~~~2–2.5~~ weeks of Sarychev CALIOP observations, δ_v – δ_p is seen to decay from ~~0.25 to 0.05~~ 0.27 to 0.03 exponentially with time. ~~This decay~~ A decrease in χ' is also observed (Fig. 8h). The decay in δ_p corresponds to an e -folding time of ~~1-week~~ 3.6 days (dashed line; Fig 8e) and may indicate that ash particles were being removed from the atmosphere during the measurement period for the Sarychev case study. Since the Sarychev layers were only analysed if the CALIOP observations were collocated with an AI < 1 K and SI \geq 1 K, it is possible that the CALIOP instrument is detecting ash layers–particles with a very weak reverse absorption signature that have not been removed by the AI threshold criterion. ~~Papayannis et al. (2012) reported changes in depolarisation from 0.30 to 0.10 with time for the Eyjafjallajökull ash layers, suggesting humidity uptake (Latham et al., 2011) as a mechanism for increasing the overall sphericity of the volcanic aerosols with time. Sulfate coating has also been offered as a mechanism for altering depolarisation with time (e.g. Povey et al., 2014). Humidity uptake is unlikely to explain the decay in δ_v for the Sarychev observations due to the lack of water vapour in the stratosphere. Also note that volume depolarisation will decrease ($\delta_v \rightarrow \delta_m$) with time as the scattering ratio (ratio of total backscatter to molecular backscatter) decreases ($R \rightarrow 1$) even if the particulate depolarisation remains constant. The results presented here suggest that~~

Figure 8h demonstrates that χ' also decreased with time over the measurement period. Changes in χ' can be due to changes in the size, complex refractive index and shape of the aerosols being measured. It is difficult to infer, quantitatively, what the volcanic aerosol particle sizes are without assuming more about the complex refractive index and size distribution of the earlier particles; however, we note that O'Neill et al. (2012) report effective radii of 0.25 μm for the Sarychev aerosols over the Arctic. As the attenuated color ratio is constructed based on two measurements (532 and 1064 nm attenuated backscatter) we can only use it to infer relative changes in particle size. We speculate that ash particles were present in the initial observations of the Sarychev layers contained irregular ash particles and as the layer evolved, SO_2 converted to sulfate, ash particles sedimented out and the layers became dominated by spherical (sulfate) particles.

~~This physical process might also explain the time evolution of the layer-integrated attenuated colour ratio, χ' (Figs. 8g–i) . For the Sarychev layers an overall CALIOP measurements and so a combination of the sedimentation (contributing to a reduction in particle size) and sulfate formation (contributing to a change in the imaginary part of the refractive index) led to a decrease in χ' is observed, suggesting a transition to smaller particles. Interestingly, the Kasatochi colour ratios show an initial increase, before gradually decreasing with time. This increase in χ' may indicate coagulation/condensation processes leading to particle growth at the earlier stages of layer development.~~

Overall, the Puyehue ~~ash colour~~ color ratios reported here ($\chi' = 0.54 \pm 0.07$) are in agreement with the values reported by Vernier et al. (2013). These ~~colour~~–color ratios are at the low end of values reported for the free-tropospheric ash layers produced by Eyjafjallajökull (0.47–0.77; Winker et al., 2012) and considering the high particulate lidar ratios ($S_p \sim 70$ sr) and ~~significant depolarisation ratios ($\delta_v \sim 0.30$)~~ particulate depolarization ratios ($\delta_p = 0.33 \pm 0.03$) these results suggest that the CALIOP observations of the Puyehue aerosol layers are representative of layers dominated by fine mode, ash particles. The Kasatochi ($\chi' = 0.35 \pm 0.07$) and Sarychev ($\chi' = 0.32 \pm 0.07$) ~~colour~~–color ratios were, on average, quite similar but both were

lower than those found for the Puyehue case study. This indicates that the Puyehue ~~ash particles aerosol layers were composed of particles that~~ were larger than ~~those in~~ the Kasatochi and Sarychev ~~sulfates. The sulfate colour aerosol layers. The Kasatochi and Sarychev color~~ ratios ($\chi' = 0.30 \sim 0.32$ – 0.35) were also lower than typical ~~colour-color~~ ratios for desert dust ($\chi' \sim 0.45$; Liu et al., 2009), while the Puyehue ~~ash-colour-color~~ ratios ($\chi' \sim 0.55$) ~~were 0.53~~ were generally higher. Both classes of volcanic aerosols had smaller ~~colour-color~~ ratios than those CALIOP typically observes for ice ($\chi' = 0.7$ – 1.2) and water clouds ($\chi' = 1$ – 1.4 ; Hu et al., 2009).

6.3 Discriminating properties of CALIOP layer-products

Figure 9a compares the optical properties of the Kasatochi and Sarychev ~~sulfates-sulfate-rich aerosols~~ with the Puyehue ~~ash retrievals ash-rich aerosols~~. When combined, the ~~depolarisation-ratio and colour-ratio plots~~ ~~volume depolarization ratios and attenuated color ratios~~ emphasise distinctive differences between the two classes of volcanic aerosol. These optical properties are relevant to the new stratospheric aerosol classification scheme that considers δ_v , χ' and γ'_p (Tackett et al., 2016). The results of the present analysis ~~are in support of support~~ a sub-classification scheme, also suggested by O'Neill et al. (2012) that categorises stratospheric sulfate layers having volume ~~depolarisation-depolarization~~ ratios of $0 < \delta_v \leq 0.2$ (Fig. 9a; dashed line). Further classification could potentially be achieved using the ~~colour-color~~ ratios (e.g. $\chi' \leq 0.4 =$ sulfates, $0.4 < \chi' \leq 0.7 =$ ash). However, ~~distinctions between ash and sulfates based on the aerosol layers under examination here, distinctions between ash-rich and sulfate-rich layers~~ using χ' are less ~~obvious-clear~~ than distinctions made with δ_v .

We point out that our suggested δ_v threshold of 0.2 has been optimised for the eruption case studies considered here and that a slightly different threshold might be found for a different or larger data set. For example, Tackett et al. (2016) found a slightly lower threshold of $\delta_v = 0.15$ for the cases they examined. We also note that, for the depolarization ratio range $0.075 < \delta_v \leq 0.15$, Tackett et al. (2016) use $\chi' < 0.5$ to identify stratospheric smoke. As volcanic aerosols are often composed of a complex mixture of both ash and sulfate, which changes with time, strict classification using a single threshold is challenging. In the case of ambiguous depolarization ratios ($\delta_v \sim 0.2$), supplementary information from collocated AIRS measurements may provide more insight into the likely composition of stratospheric volcanic aerosol layers.

Figure 9b shows the relationship between the particulate lidar ratio and the ~~volume depolarisation-particulate depolarization~~ ratio. As previously noted, the particulate lidar ratios for the Puyehue ~~ash and the sulfates ash-rich aerosol layers and the sulfate-rich layers~~ of Kasatochi and Sarychev were similar. This would make it difficult to discriminate between ~~ash and sulfates-a volcanic layer dominated by ash versus a volcanic layer dominated by sulfate~~ using S_p alone. Nevertheless, these lidar ratio retrievals provide important information for distinguishing volcanic aerosols from water ($S_p \approx 20$ sr) and ice ($S_p \approx 25$ sr) clouds and could potentially be utilised in new lidar aerosol classification schemes (e.g. Groß et al., 2014).

6.4 ~~Multiple scattering considerations~~ Deriving an optical depth times series

In cases where the lidar ratio cannot be retrieved directly, the CALIPSO extinction retrieval (Young and Vaughan, 2009) relies on a predefined lidar ratio that is associated with a predefined type. Classification of volcanic aerosols into ash-rich and sulfate-rich layers is therefore important as the lidar ratio may change depending on the composition of the layers. The

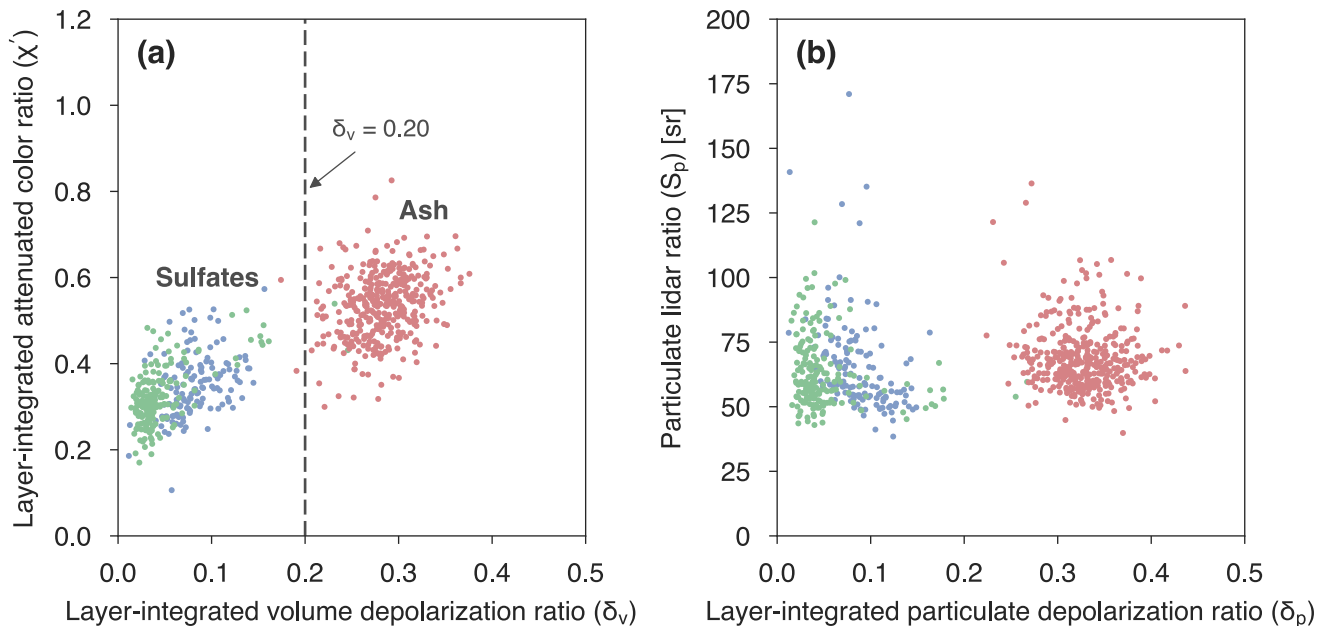


Figure 9. Optical properties of the Kasatochi (blue), Sarychev (green) and Puyehue (red) volcanic aerosols. (a) The relationship between the layer-integrated volume ~~depolarisation~~ ~~depolarization~~ ratio and the layer-integrated attenuated ~~colour~~ ~~color~~ ratio. (b) The relationship between the particulate lidar ratio and the layer-integrated volume ~~depolarisation~~ ~~depolarization~~ ratio.

depolarization ratio appears to be the most appropriate parameter for determining whether a stratospheric volcanic layer is sulfate-rich or ash-rich. As we have shown, the lidar ratio varied with time for the case studies presented here and so the assumption of a constant lidar ratio will likely introduce errors in the retrieval of extinction profiles. Optimum results for a volcanic aerosol optical depth time series could be obtained by following the method presented here and only accepting cases
 5 where an extinction retrieval was constrained by an estimate of the two-way transmittance (i.e. extinction quality control flag equal to 1). This would most likely restrict observations to nighttime measurements of layers with optical depths > 0.2 (Fig. 4). In cases where the two-way transmittance method fails, a predefined lidar ratio would have to be used. One could use the the PDFs presented in Fig. 2 to constrain the choice of the lidar ratio. As the PDFs for the lidar ratios are positively skewed, the median lidar ratio would be best suited for this approach. For example, 60 sr for sulfate-rich ($\delta_v < 0.2$) and 67 sr for ash-rich
 10 ($\delta_v > 0.2$) layers.

6.5 Choice of the multiple scattering factor

In order to facilitate interpretation of the results presented in Sect. 4, η was held constant for each case study. However, since the ‘true’ value of η for volcanic aerosols is unknown we provide S_p calculated for a range of different η values in Table 3.

Table 3. Mean, median and standard deviation of the particulate lidar ratio for different values of the multiple scattering factor for the Kasatochi, Sarychev and Puyehue case studies.

Multiple scattering factor, η	Kasatochi S_p (sr)			Sarychev S_p (sr)			Puyehue S_p (sr)											
	Mean	Median	Std. Dev.	Mean	Median	Std. Dev.	Mean	Median	Std. Dev.									
0.50	121.41	121.53	112.58	113.46	27.18	26.91	120.75	119.71	111.99	112.01	26.92	25.83	123.46	124.05	119.71	120.36	22.71	22.77
0.55	112.61	112.32	103.30	103.21	29.69	28.67	109.77	108.83	101.81	101.83	24.47	23.48	112.24	112.77	108.83	109.42	20.64	20.7
0.60	103.22	102.96	94.69	94.61	27.22	26.28	100.63	99.76	93.33	93.35	22.43	21.52	102.9	103.37	99.76	100.3	18.92	18.98
0.65	95.47	96.15	87.55	87.42	25.15	27.47	93.14	92.08	86.47	86.17	20.77	19.87	95.27	95.42	92.45	92.59	17.51	17.52
0.70	90.28	89.28	81.72	81.17	26.97	25.51	86.99	85.51	80.70	80.01	19.50	18.45	89.17	88.6	86.59	85.97	16.50	16.27
0.75	84.64	83.33	76.58	75.76	25.35	23.81	81.66	79.81	75.70	74.68	18.40	17.22	83.93	82.7	81.47	80.24	15.66	15.18
0.80	79.70	78.12	72.09	71.03	23.94	22.32	77.00	74.82	71.25	70.01	17.44	16.14	79.34	77.53	76.98	75.23	14.94	14.23
0.85	75.34	73.52	68.12	66.85	22.70	21.0	72.89	70.42	67.24	65.89	16.59	15.19	75.29	72.97	73.09	70.8	14.30	13.4
0.90	71.47	69.44	64.65	63.13	21.60	19.84	69.23	66.51	63.73	62.23	15.84	14.35	71.70	68.91	69.54	66.87	13.74	12.65
0.95	68.00	65.78	61.54	59.81	20.61	18.79	65.96	63.01	60.74	58.96	15.17	13.59	68.48	65.29	66.45	63.35	13.23	11.99
1.00	64.88	62.49	58.74	56.82	19.72	17.85	63.02	59.86	58.10	56.01	14.57	12.91	65.58	62.02	63.46	60.18	12.78	11.39

The relationship between η and S_p for the three case studies is also shown in Fig. 10. As expected from Eq. (15), the mean particulate lidar ratio decreased as the assumed multiple scattering factor was increased.

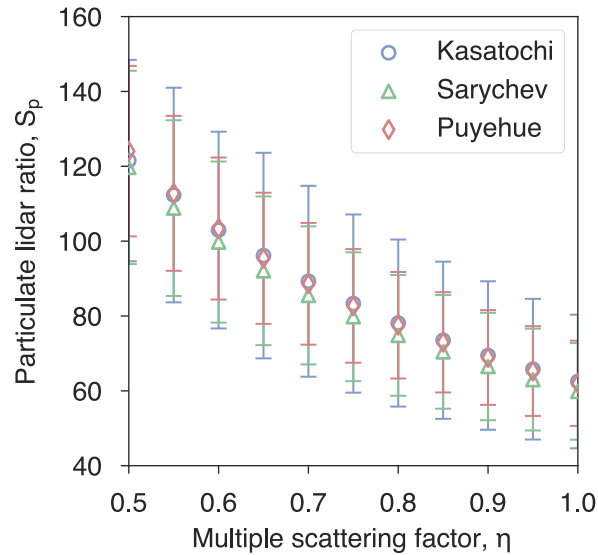


Figure 10. Mean particulate lidar ratios (S_p) for Kasatochi, Sarychev and Puyehue as a function of the multiple scattering factor, η . Error bars represent the standard deviation of S_p for each case study.

Previously reported values of the lidar ratio (at 532 nm) provide insight into the likely range of S_p for case studies considered here. The reported lidar ratios (at 532 nm) for Kasatochi and Sarychev range from 40–65 sr (Mattis et al., 2010). Although it

is difficult to make direct comparisons (due to a lack of coincident observations), these values support a choice of η closer to unity for [sulfates/sulfate-rich aerosols](#).

To our knowledge there have been no lidar ratio observations reported in the scientific literature for the Puyehue [ash layers/volcanic aerosols](#). However, ground-based lidar observations were made at Lauder, New Zealand. Nakamae et al. (2014) applied the Fernald (1984) algorithm to ground-based lidar measurements to derive aerosol (particulate) extinction profiles. They assumed a lidar ratio of 50 sr, but noted better agreement with independently derived optical depths when they set S_p to 60 sr. Their initial choice of lidar ratio was based on previous reports of the lidar ratio for the Eyjafjallajökull ash layers. According to Fig. 10, a lidar ratio of 60 sr corresponds to a multiple scattering factor close to unity (Fig. 10).

~~Another factor that can contribute to multiple scattering in CALIOP measurements is high depolarisation ($\delta_v > 0.3$). Liu et al. (2011) demonstrated through observations of desert dust that it is the increase in depolarisation ratio with depth into the layer that ultimately determines the magnitude of its multiple scattering effect. For dense desert dust, an increase in depolarisation with depth can lead to a~~

~~The impact of multiple scattering on CALIOP measurements can also be indicated by high depolarization ratios. Liu et al. (2011) found that effective lidar ratios ($S^* = \eta S_p$), derived from CALIOP measurements of opaque African dust layers, decrease as the volume depolarization ratio increases, an effect they ascribe to the impact of multiple scattering in denser layers. For layers with optical depths greater than 3, they found that volume depolarization ratios increased from a value of ~ 0.3 , typical for African dust, to ~ 0.36 , while the effective lidar ratios decreased to 30.5 sr from a typical value of 40 sr, implying a multiple scattering factor of $\eta \sim 0.75$ (Liu et al., 2011). However, for moderately dense layers multiple scattering is expected to be small, they found multiple scattering to be negligible. Since the volcanic aerosol layers presented here in this study were generally optically thin ($\tau_e < 0.8$; Fig. 4), the change in depolarisation with layer depth is multiple scattering effects are also expected to be small. This argument supports, consistent with our assumption of minor multiple scattering effects (i.e. $\eta = 0.90-0.95$) in the volcanic ash for the ash-rich volcanic layers considered here.~~

7 Conclusions

By applying a two-way transmittance constraint to nighttime CALIOP observations, the [Fernald solutions equations of Fernald et al. \(1972\)](#) were used to derive particulate lidar ratios (S_p) for two classes of volcanic aerosols (fine ash and sulfates). The combination of CALIOP and AIRS measurements has permitted the identification and characterisation of numerous stratospheric volcanic [sulfates and fine ash aerosol](#) layers produced by three recent eruptions. The [mean median](#) lidar ratios of the Kasatochi and Sarychev [sulfates aerosols](#) were found to be [68-60 sr \(mean 66 \$\pm\$ 21 sr \(median 62-19 sr\) and 66-59 sr \(mean 63 \$\pm\$ 15 sr \(median 61-14 sr\), respectively. The \[mean median\]\(#\) lidar ratios are \[broadly in agreement with the sulfate higher than the sulfate/other\]\(#\) lidar ratio of \[70 sr of the new 50 sr to be used in the new, version-4\]\(#\), stratospheric aerosol scheme \(\[Tackett et al., 2016\]\(#\)\). ~~However, the~~ \[Further, the median\]\(#\) lidar ratios of the aged, \[fine mode ash fine mode ash-rich\]\(#\) layers produced by Puyehue were found to be \[much higher \\(72 significantly higher \\(67 sr; mean 69 \\$\pm\\$ 14 sr; median 70-13 sr\\)\]\(#\)](#)

than the value of 44 sr to be used for volcanic ash. This discrepancy suggests that ash layers could potentially be considered as two subtypes: fine (~~70-67~~ sr) and coarse (44 sr) mode ash.

Errors in the lidar ratio retrieval were most sensitive to errors in the effective two-way particulate transmittance constraint (T_e^2) when layers were optically thin. However, as T_e^2 approaches zero, the error in S_p is limited to the error in the multiple scattering factor (η) and normalised attenuated backscatter profile ($\beta'_N(r)$). Considering the three main sources of error in the lidar ratio retrieval ($\epsilon(\beta'_N)$, $\epsilon(T_e^2)$ and $\epsilon(\eta)$), a relative error of ~~less than up to~~ 40% is expected for the particulate lidar ratio retrievals presented here (Fig. 4).

~~Since the operational lidar ratio retrieval already utilises the CALIOP's stratospheric aerosol retrievals use a~~ two-way transmittance constraint ~~where one is available, but~~ it is expected that the retrievals of the extinction profiles of stratospheric volcanic aerosols could be improved by setting η to a value closer to unity. While 0.6 is a good approximation for cirrus layers (Garnier et al., 2015), ~~an underestimate in multiple scattering it is probably an underestimate for most stratospheric volcanic layers, which tend to have low to moderate optical depths.~~ An underestimate of the multiple scattering factor translates to an overestimate in the particulate lidar ratio (Fig. 10). ~~Quantification of the~~ 10) in constrained retrievals, which attempt to match the retrieved and measured two-way particulate transmittances. The use of an overestimated lidar ratio would then cause the calculated particulate extinction and optical depths to be overestimated. Determination of appropriate values for the multiple scattering factor for volcanic aerosols ~~may further reduce uncertainty in~~ would further improve the accuracy of CALIOP derived lidar ratios. This ~~can be achieved, in theory, could be achieved~~ by comparing visible ~~with and~~ infrared optical depth retrievals (e.g. Platt, 1973; Lamquin et al., 2008; Josset et al., 2012; Garnier et al., 2015).

Several differences in the optical properties of the ~~sulfates versus ash sulfate-rich aerosol layers versus ash-rich layers~~ were identified through the analysis of layer-integrated optical properties. The low mean layer-integrated volume ~~depolarisation ratios~~ (δ_v) ~~found for and particulate~~ (δ_p) depolarization ratios found for the Kasatochi and Sarychev layers indicate that the assumption of collocated SO_2 and SO_4^{2-} , used to identify ~~sulfate sulfate-rich~~ layers, appears to be effective and well-founded for the case studies considered. It was also shown that δ_v can be used to discriminate ~~sulfates from ash particles sulfate-rich aerosol layers from ash-rich aerosol layers~~, and when supplemented with the layer-integrated attenuated colour ratio (χ') these optical properties provide useful information for new stratospheric aerosol classification schemes.

The time evolution of volcanic aerosol optical properties was also investigated. The ~~particulate lidar ratios, for all three case studies, increased with time toward the later stages of aerosol layer development. This can largely be attributed to a decrease in the integrated attenuated backscatter, γ'_p , with time.~~ The δ_v - δ_p values were consistently low (≤ 0.10) for the Kasatochi ~~sulfate sulfate-rich~~ layers and consistently high ($\sim \geq 0.30$) for the Puyehue ~~ash ash-rich~~ layers. This suggested little change in layer composition ~~with time over the measurement period~~ for the Kasatochi and Puyehue ~~layers case studies~~. In contrast, an exponential decay (e -folding time of ~~1 week) in δ_v from 0.25 to 0.05 3.6 days) in δ_p from 0.27 to 0.03 was observed in the Sarychev layers. A transition from non-spherical to spherical aerosol particles suggested that CALIOP may have captured the formation of sulfate particles as larger irregular particles (ash) were removed. This behaviour was also characterised by a decrease in the layer-integrated attenuated colour ratio (χ') with time.~~

~~Finally, the methodology presented here was designed to maximise the quality of CALIOP observations of volcanic aerosols. While only stratospheric aerosols were considered, this analysis could be extended to carefully selected observations of tropospheric ash layers. Since the tropospheric ash layers of Eyjafjallajökull were observed by ground-based lidars, this retrieval technique could potentially be validated using coincident CALIOP/AIRS observations.~~

- 5 *Acknowledgements.* The authors would like to acknowledge Monash University for supporting this research through the Post-graduate Publication Award (PPA). The CALIPSO and AIRS teams are thanked for the provision of the data used in this study. The CALIPSO data were obtained from the NASA Langley Research Center Atmospheric Science Data Center. We also thank [Dr Zhaoyan Liu](#) for helpful comments on [the manuscript and four anonymous reviewers whose comments helped to significantly improve](#) the manuscript.

References

- Ansmann, A., Tesche, M., Groß, S., Freudenthaler, V., Seifert, P., Hiebsch, A., Schmidt, J., Wandinger, U., Mattis, I., Müller, D., and Wiegner, M.: The 16 April 2010 major volcanic ash plume over central Europe: EARLINET lidar and AERONET photometer observations at Leipzig and Munich, Germany, *Geophys. Res. Lett.*, 37, L13 810, 2010.
- 5 Aumann, H. H., Chahine, M. T., Gautier, C., Goldberg, M. D., Kalnay, E., McMillin, L. M., Revercomb, H., Rosenkranz, P. W., Smith, W. L., Staelin, D. H., Strow, L. L., and Susskind, J.: AIRS/AMSU/HSB on the aqua mission: design, science objectives, data products, and processing systems, *IEEE Trans. Geosci. Remote Sens.*, 41, 253–264, 2003.
- Bourassa, A. E., Rieger, L. A., Lloyd, N. D., and Degenstein, D. A.: Odin-OSIRIS stratospheric aerosol data product and SAGE III inter-comparison, *Atmos. Chem. Phys.*, 12, 605–614, 2012.
- 10 Carboni, E., Grainger, R. G., Mather, T. A., Pyle, D. M., Thomas, G. E., Siddans, R., Smith, A. J. A., Dudhia, A., Koukouli, M. E., and Balis, D.: The vertical distribution of volcanic SO₂ plumes measured by IASI, *Atmos. Chem. Phys.*, 16, 4343–4367, 2016.
- Carn, S. A., Krotkov, N. A., Yang, K., Hoff, R. M., Prata, A. J., Krueger, A. J., Loughlin, S. C., and Levelt, P. F.: Extended observations of volcanic SO₂ and sulfate aerosol in the stratosphere, *Atmos. Chem. Phys.*, 7, 2857–2871, 2007.
- Carn, S. A., Clarisse, L., and Prata, A. J.: Multi-decadal satellite measurements of global volcanic degassing, *J. Volcanol. Geoth. Res.*, 311, 99–134, 2016.
- 15 Clarisse, L., Coheur, P. F., Prata, F., Hadji-Lazaro, J., Hurtmans, D., and Clerbaux, C.: A unified approach to infrared aerosol remote sensing and type specification, *Atmos. Chem. Phys.*, 13, 2195–2221, 2013.
- Cook, C. S., Bethke, G. W., and Conner, W. D.: Remote measurement of smoke plume transmittance using lidar., *Appl. Opt.*, 11, 1742–1748, 1972.
- 20 Dutton, E. G. and Christy, J. R.: Solar radiative forcing at selected locations and evidence for global lower tropospheric cooling following the eruptions of El Chichón and Pinatubo, *Geophys. Res. Lett.*, 19, 2313–2316, 1992.
- Fernald, F. G.: Analysis of atmospheric lidar observations: some comments., *Appl. Opt.*, 23, 652–652, 1984.
- Fernald, F. G., Herman, B. M., and Reagan, J. A.: Determination of Aerosol Height Distributions by Lidar., *J. Appl. Meteorol.*, 11, 482–489, 1972.
- 25 Garnier, A., Pelon, J., Vaughan, M. A., Winker, D. M., Trepte, C. R., and Dubuisson, P.: Lidar multiple scattering factors inferred from CALIPSO lidar and IIR retrievals of semi-transparent cirrus cloud optical depths over oceans, *Atmos. Meas. Tech.*, 8, 2759–2774, 2015.
- Gerstell, M. F., Crisp, J., and Crisp, D.: Radiative Forcing of the Stratosphere by SO₂ Gas, Silicate Ash, and H₂SO₄ Aerosols Shortly after the 1982 Eruptions of El Chichón., *J. Climate*, 8, 1060–1070, 1995.
- Groß, S., Freudenthaler, V., Wiegner, M., Gasteiger, J., Geiß, A., and Schnell, F.: Dual-wavelength linear depolarization ratio of volcanic aerosols: Lidar measurements of the Eyjafjallajökull plume over Maisach, Germany, *Atmos. Environ.*, 48, 85–96, 2012.
- 30 Groß, S., Freudenthaler, V., Wirth, M., and Weinzierl, B.: Towards an aerosol classification scheme for future EarthCARE lidar observations and implications for research needs, *Atmos. Sci. Lett.*, 16, 77–82, 2014.
- Hoffmann, A., Ritter, C., Stock, M., Maturilli, M., Eckhardt, S., Herber, A., and Neuber, R.: Lidar measurements of the Kasatochi aerosol plume in August and September 2008 in Ny-Ålesund, Spitsbergen, 115, D00L12, 2010.
- 35 Hoffmann, L., Griebbach, S., and Meyer, C. I.: Volcanic emissions from AIRS observations: detection methods, case study, and statistical analysis, *Proc. of SPIE*, 9242, 924 214, 2014.

- Holben, B. N., Eck, T. F., Slutsker, I., Tanré, D., and Buis, J. P.: AERONET—A federated instrument network and data archive for aerosol characterization, *Remote Sens. Environ.*, 66, 1–16, 1998.
- Hostetler, C. A., Liu, Z., Reagan, J. A., Vaughan, M. A., Osborn, M. T., Hunt, W. H., Powell, K. A., and Trepte, C. R.: CALIOP Algorithm Theoretical Basis Document Part 1: Calibration and Level 1 Data Products [Available online at <https://www-calipso.larc.nasa.gov/resources/pdfs/PC-SCI-201v1.0.pdf>], 2006.
- 5 Hu, Y., Winker, D., Vaughan, M., Lin, B., Omar, A., Trepte, C., Flittner, D., Yang, P., Nasiri, S. L., Baum, B., Holz, R., Sun, W., Liu, Z., Wang, Z., Young, S., Stamnes, K., Huang, J., and Kuehn, R.: CALIPSO/CALIOP Cloud Phase Discrimination Algorithm, *J. Atmos. Ocean. Tech.*, 26, 2293–2309, 2009.
- Hughes, I. G. and Hase, T. P. A.: *Measurements and their Uncertainties: A Practical Guide to Modern Error Analysis*, Oxford University Press, 2010.
- 10 Hunt, W. H., Winker, D. M., Vaughan, M. A., Powell, K. A., Lucker, P. L., and Weimer, C.: CALIPSO Lidar Description and Performance Assessment, *J. Atmos. Ocean. Tech.*, 26, 1214–1228, 2009.
- Josset, D., Pelon, J., Garnier, A., Hu, Y., Vaughan, M., Zhai, P.-W., Kuehn, R., and Lucker, P.: Cirrus optical depth and lidar ratio retrieval from combined CALIPSO-CloudSat observations using ocean surface echo, *J. Geophys. Res.*, 117, D05 207–14, 2012.
- 15 Karagulian, F., Clarisse, L., Clerbaux, C., Prata, A. J., Hurtmans, D., and Coheur, P. F.: Detection of volcanic SO₂, ash, and H₂SO₄ using the Infrared Atmospheric Sounding Interferometer (IASI), *J. Geophys. Res. Atmos.*, 115, D00L02, 2010.
- Klüser, L., Erbertseder, T., and Meyer-Arnek, J.: Observation of volcanic ash from Puyehue-Cordón Caulle with IASI, *Atmos. Meas. Tech.*, 6, 35–46, 2013.
- Kremser, S., Thomason, L. W., Hobe, M., Hermann, M., Deshler, T., Timmreck, C., Toohey, M., Stenke, A., Schwarz, J. P., Weigel, R., Fueglistaler, S., Prata, F. J., Vernier, J.-P., Schlager, H., Barnes, J. E., Antuña Marrero, J. C., Fairlie, D., Palm, M., Mahieu, E., Notholt, J., Rex, M., Bingen, C., Vanhellefont, F., Bourassa, A., Plane, J. M. C., Klocke, D., Carn, S. A., Clarisse, L., Trickl, T., Neely, R., James, A. D., Rieger, L., Wilson, J. C., and Meland, B.: Stratospheric aerosol—Observations, processes, and impact on climate, *Rev. Geophys.*, 54, 2016.
- 20 Kristiansen, N. I., Prata, A. J., and Stohl, A.: Stratospheric volcanic ash emissions from the 13 February 2014 Kelut eruption, *Geophys. Res. Lett.*, 42, 588–596, 2015.
- 25 Krotkov, N. A., Schoeberl, M. R., Morris, G. A., Carn, S., and Yang, K.: Dispersion and lifetime of the SO₂ cloud from the August 2008 Kasatochi eruption, *J. Geophys. Res. Atmos.*, 115, D00L20, 2010.
- Labitzke, K. and McCormick, M. P.: Stratospheric temperature increases due to Pinatubo aerosols, *Geophys. Res. Lett.*, 19, 207–210, 1992.
- Lamquin, N., Stubenrauch, C. J., and Pelon, J.: Upper tropospheric humidity and cirrus geometrical and optical thickness: Relationships inferred from 1 year of collocated AIRS and CALIPSO data, *J. Geophys. Res.*, 113, D00A08–12, 2008.
- 30 Latham, T. L., Kumar, P., Nenes, A., Dufek, J., Sokolik, I. N., Trail, M., and Russell, A.: Hygroscopic properties of volcanic ash, *Geophys. Res. Lett.*, 38, L11 802, 2011.
- Liu, Z., Vaughan, M., Winker, D., Kittaka, C., Getzewich, B., Kuehn, R., Omar, A., Powell, K., Trepte, C., and Hostetler, C.: The CALIPSO Lidar Cloud and Aerosol Discrimination: Version 2 Algorithm and Initial Assessment of Performance, *J. Atmos. Ocean. Tech.*, 26, 1198–1213, 2009.
- 35 Liu, Z., Winker, D., Omar, A., Vaughan, M., Trepte, C., Hu, Y., Powell, K., Sun, W., and Lin, B.: Effective lidar ratios of dense dust layers over North Africa derived from the CALIOP measurements, *J. Quant. Spectrosc. Radiat. Transf.*, 112, 204–213, 2011.

- Mass, C. and Robock, A.: The Short-Term Influence of the Mount St. Helens Volcanic Eruption on Surface Temperature in the Northwest United States, *Mon. Weather Rev.*, 110, 614–622, 1982.
- Mattis, I., Ansmann, A., Müller, D., Wandinger, U., and Althausen, D.: Dual-wavelength Raman lidar observations of the extinction-to-backscatter ratio of Saharan dust, *Geophys. Res. Lett.*, 29, 1306–1, 2002.
- 5 Mattis, I., Siefert, P., Müller, D., Tesche, M., Hiebsch, A., Kanitz, T., Schmidt, J., Finger, F., Wandinger, U., and Ansmann, A.: Volcanic aerosol layers observed with multiwavelength Raman lidar over central Europe in 2008–2009, *J. Geophys. Res.*, 115, D00L04–9, 2010.
- Nakamae, K., Uchino, O., Morino, I., Liley, B., Sakai, T., Nagai, T., and Yokota, T.: Lidar observation of the 2011 Puyehue-Cordón Caulle volcanic aerosols at Lauder, New Zealand, *Atmos. Chem. Phys.*, 14, 12 099–12 108, 2014.
- Newhall, C. G. and Self, S.: The volcanic explosivity index (VEI): An estimate of explosive magnitude for historical volcanism, *J. Geophys. Res.*, 87, 1231–1238, 1982.
- 10 Niemeier, U., Timmreck, C., Graf, H. F., Kinne, S., Rast, S., and Self, S.: Initial fate of fine ash and sulfur from large volcanic eruptions, *Atmos. Chem. Phys.*, 9, 9043–9057, 2009.
- Omar, A., Liu, Z., Vaughan, M., Thornhill, K., Kittaka, C., Ismail, S., Hu, Y., Chen, G., Powell, K., Winker, D., Trepte, C., Winstead, E., and Anderson, B.: Extinction-to-backscatter ratios of Saharan dust layers derived from in situ measurements and CALIPSO overflights during
15 NAMMA, *J. Geophys. Res.*, 115, D24 217–21, 2010.
- Omar, A. H., Winker, D. M., Vaughan, M. A., Hu, Y., Trepte, C. R., Ferrare, R. A., Lee, K.-P., Hostetler, C. A., Kittaka, C., Rogers, R. R., Kuehn, R. E., and Liu, Z.: The CALIPSO Automated Aerosol Classification and Lidar Ratio Selection Algorithm, *J. Atmos. Ocean. Tech.*, 26, 1994–2014, 2009.
- O’Neill, N. T., Perro, C., Saha, A., Lesins, G., Duck, T. J., Eloranta, E. W., Nott, G. J., Hoffman, A., Karumudi, M. L., Ritter, C., Bourassa, A.,
20 Abboud, I., Carn, S. A., and Savastouk, V.: Properties of Sarychev sulphate aerosols over the Arctic, *J. Geophys. Res.*, 117, D04 203–21, 2012.
- Papayannis, A., Mamouri, R. E., Amiridis, V., Giannakaki, E., Veselovskii, I., Kokkalis, P., Tsaknakis, G., Balis, D., Kristiansen, N. I., Stohl, A., Korenskiy, M., Allakhverdiev, K., Huseyinoglu, M. F., and Baykara, T.: Optical properties and vertical extension of aged ash layers over the Eastern Mediterranean as observed by Raman lidars during the Eyjafjallajökull eruption in May 2010, *Atmos. Environ.*, 48,
25 56–65, 2012.
- Pitts, M. C., Poole, L. R., and Thomason, L. W.: CALIPSO polar stratospheric cloud observations: second-generation detection algorithm and composition discrimination, *Atmos. Chem. Phys.*, 9, 7577–7589, 2009.
- Platt, C.: Lidar and Radiometric Observations of Cirrus Clouds, *J. Atmos. Sci.*, 30, 1191–1204, 1973.
- Povey, A. C., Grainger, R. G., Peters, D. M., and Agnew, J. L.: Retrieval of aerosol backscatter, extinction, and lidar ratio from Raman lidar
30 with optimal estimation, *Atmos. Meas. Tech.*, 7, 757–776, 2014.
- Prata, A. J. and Prata, A. T.: Eyjafjallajökull volcanic ash concentrations determined using Spin Enhanced Visible and Infrared Imager measurements, *J. Geophys. Res. Atmos.*, 117, D00U23, 2012.
- Prata, A. T.: Remote sensing of volcanic eruptions: from aviation hazards to global cooling, in: *Plate Boundaries and Natural Hazards*, edited by Duarte, J. C. and Schellart, W. P., 2016.
- 35 Prata, A. T., Siems, S. T., and Manton, M. J.: Quantification of volcanic cloud top heights and thicknesses using A-train observations for the 2008 Chaitén eruption, *J. Geophys. Res. Atmos.*, 120, 2928–2950, 2015.

- Ridley, D. A., Solomon, S., Barnes, J. E., Burlakov, V. D., Deshler, T., Dolgii, S. I., Herber, A. B., Nagai, T., Neely, R. R., Nevzorov, A. V., Ritter, C., Sakai, T., Santer, B. D., Sato, M., Schmidt, A., Uchino, O., and Vernier, J. P.: Total volcanic stratospheric aerosol optical depths and implications for global climate change, *Geophys. Res. Lett.*, 41, 7763–7769, 2014.
- Rieger, L. A., Bourassa, A. E., and Degenstein, D. A.: Merging the OSIRIS and SAGE II stratospheric aerosol records, *J. Geophys. Res. Atmos.*, 120, 8890–8904, 2015.
- Rienecker, M. M., Suarez, M. J., Todling, R., Bacmeister, J., Takacs, L., Liu, H. C., Gu, W., Sienkiewicz, M., Koster, R. D., Gelaro, R., Stajner, I., and Nielsen, J. E.: The GEOS-5 Data Assimilation System— Documentation of Versions 5.0.1, 5.1.0, and 5.2.0, Technical Report Series on Global Modeling and Data Assimilation, 27, NASA/TM-2008-104606, 1–118, 2008.
- Rogers, R. R., Hostetler, C. A., Hair, J. W., Ferrare, R. A., Liu, Z., Obland, M. D., Harper, D. B., Cook, A. L., Powell, K. A., Vaughan, M. A., and Winker, D. M.: Assessment of the CALIPSO Lidar 532 nm attenuated backscatter calibration using the NASA LaRC airborne High Spectral Resolution Lidar, *Atmos. Chem. Phys.*, 11, 1295–1311, 2011.
- Rybin, A., Chibisova, M., Webley, P., Steensen, T., Izbekov, P., Neal, C., and Realmuto, V.: Satellite and ground observations of the June 2009 eruption of Sarychev Peak volcano, Matua Island, Central Kuriles, *Bull. Volcanol.*, 73, 1377–1392, 2011.
- Santer, B. D., Bonfils, C., Painter, J. F., Zelinka, M. D., Mears, C., Solomon, S., Schmidt, G. A., Fyfe, J. C., Cole, J. N. S., Nazarenko, L., Taylor, K. E., and Wentz, F. J.: Volcanic contribution to decadal changes in tropospheric temperature, *Nat. Geosci.*, 7, 185–189, 2014.
- Sassen, K. and Cho, B. S.: Subvisual-Thin Cirrus Lidar Dataset for Satellite Verification and Climatological Research., *J. Appl. Meteorol.*, 31, 1275–1285, 1992.
- Sato, M., Hansen, J. E., McCormick, M. P., and Pollack, J. B.: Stratospheric Aerosol Optical Depths, 1850–1990, *J. Geophys. Res.*, 98, 22987, 1993.
- Sawamura, P., Vernier, J. P., Barnes, J. E., Berkoff, T. A., Welton, E. J., Alados-Arboledas, L., Navas-Guzmán, F., Pappalardo, G., Mona, L., Madonna, F., Lange, D., Sicard, M., Godin-Beekmann, S., Payen, G., Wang, Z., Hu, S., Tripathi, S. N., Cordoba-Jabonero, C., and Hoff, R. M.: Stratospheric AOD after the 2011 eruption of Nabro volcano measured by lidars over the Northern Hemisphere, *Environ. Res. Lett.*, 7, 034013, 2012.
- Solomon, S., Daniel, J. S., Neely, R. R., Vernier, J. P., Dutton, E. G., and Thomason, L. W.: The persistently variable "background" stratospheric aerosol layer and global climate change., *Science*, 333, 866–870, 2011.
- Stephens, G. L., Vane, D. G., Boain, R. J., Mace, G. G., Sassen, K., Wang, Z., Illingworth, A. J., O'Connor, E. J., Rossow, W. B., Durden, S. L., Miller, S. D., Austin, R. T., Benedetti, A., Mitrescu, C., and CloudSat Science Team, T.: The CloudSat mission and the A-Train: A new dimension of space-based observations of clouds and precipitation, *B. Am. Meteorol. Soc.*, 83, 1771–1790, 2002.
- Tackett, J. L., Omar, A. H., Vaughan, M. A., Kar, J., Trepte, C. R., Winker, D. M., and Magill, B.: New Stratospheric Aerosol Subtypes Implemented in CALIOP Version 4 Level 2, in: CALIPSO/CloudSat Science Team Meeting. 1-3 March 2016., 2016.
- Tesche, M., Ansmann, A., Müller, D., Althausen, D., Engelmann, R., Freudenthaler, V., and Groß, S.: Vertically resolved separation of dust and smoke over Cape Verde using multiwavelength Raman and polarization lidars during Saharan Mineral Dust Experiment 2008, *J. Geophys. Res.*, 114, D13202–14, 2009.
- Theys, N., De Smedt, I., Van Roozendael, M., Froidevaux, L., Clarisse, L., and Hendrick, F.: First satellite detection of volcanic OCIO after the eruption of Puyehue-Cordón Caulle, *Geophys. Res. Lett.*, 41, 667–672, 2014.
- Thomason, L. W. and Pitts, M. C.: CALIPSO observations of volcanic aerosol in the stratosphere, *Proc. SPIE*, 7153, 715300–1–715300–8, 2008.

- Vaughan, M.: Algorithm for retrieving lidar ratios at 1064 nm from space-based lidar backscatter data, in: Proc. SPIE, pp. 104–115, NASA Langley Research Ctr., USA, 2004.
- Vaughan, M. A., Winker, D. M., and Powell, K. A.: CALIOP Algorithm Theoretical Basis Document Part 2: Feature Detection and Layer Properties Algorithms [Available online at http://www-calipso.larc.nasa.gov/resources/pdfs/PC-SCI-202_Part2_rev1x01.pdf], 2005.
- 5 Vaughan, M. A., Powell, K. A., Kuehn, R. E., Young, S. A., Winker, D. M., Hostetler, C. A., Hunt, W. H., Liu, Z., McGill, M. J., and Getzewich, B. J.: Fully Automated Detection of Cloud and Aerosol Layers in the CALIPSO Lidar Measurements, *J. Atmos. Ocean. Tech.*, 26, 2034–2050, 2009.
- Vernier, J. P., Pommereau, J. P., Garnier, A., Pelon, J., Larsen, N., Nielsen, J., Christensen, T., Cairo, F., Thomason, L. W., Leblanc, T., and McDermid, I. S.: Tropical stratospheric aerosol layer from CALIPSO lidar observations, 114, D00H10, 2009.
- 10 Vernier, J. P., Thomason, L. W., Pommereau, J. P., Bourassa, A., Pelon, J., Garnier, A., Hauchecorne, A., Blanot, L., Trepte, C., Degenstein, D., and Vargas, F.: Major influence of tropical volcanic eruptions on the stratospheric aerosol layer during the last decade, *Geophys. Res. Lett.*, 38, L12 807, 2011.
- Vernier, J. P., Fairlie, T. D., Murray, J. J., Tupper, A., Trepte, C., Winker, D., Pelon, J., Garnier, A., Jumelet, J., Pavolonis, M., Omar, A. H., and Powell, K. A.: An Advanced System to Monitor the 3D Structure of Diffuse Volcanic Ash Clouds, *J. Appl. Meteorol. Climatol.*, 52, 2125–2138, 2013.
- 15 Wang, X., Boselli, A., D’Avino, L., Pisani, G., Spinelli, N., Amodeo, A., Chaikovsky, A., Wiegner, M., Nickovic, S., Papayannis, A., Perrone, M. R., Rizi, V., Sauvage, L., and Stohl, A.: Volcanic dust characterization by EARLINET during Etna’s eruptions in 2001–2002, *Atmos. Environ.*, 42, 893–905, 2008.
- Waythomas, C. F., Scott, W. E., Prejean, S. G., Schneider, D. J., Izbekov, P., and Nye, C. J.: The 7–8 August 2008 eruption of Kasatochi Volcano, central Aleutian Islands, Alaska, *J. Geophys. Res.*, 115, B00B06–23, 2010.
- Wiegner, M., Gasteiger, J., Groß, S., Schnell, F., Freudenthaler, V., and Forkel, R.: Characterization of the Eyjafjallajökull ash-plume: Potential of lidar remote sensing, *Phys. Chem. Earth*, 45-46, 79–86, 2012.
- Williams, D. B. and Thomas, H. E.: An assessment of volcanic hazards to aviation – a case study from the 2009 Sarychev Peak eruption, *Geomat. Nat. Haz. Risk.*, 2, 233–246, 2011.
- 25 Winker, D. M.: Accounting for multiple scattering in retrievals from space lidar, in: Proc. SPIE, pp. 128–139, NASA Langley Research Ctr., USA, 2003.
- Winker, D. M. and Osborn, M. T.: Airborne Lidar Observations of the Pinatubo Volcanic Plume, *Geophys. Res. Lett.*, 19, 167–170, 1992a.
- Winker, D. M. and Osborn, M. T.: Preliminary analysis of observations of the Pinatubo volcanic plume with a polarization-sensitive lidar, *Geophys. Res. Lett.*, 19, 171–174, 1992b.
- 30 Winker, D. M., Pelon, J., Coakley Jr., J. A., Ackerman, S. A., Charlson, R. J., Colarco, P. R., Flamant, P., Fu, Q., Hoff, R. M., Kittaka, C., Kubar, T. L., Le Treut, H., McCormick, M. P., MéGie, G., Poole, L., Powell, K., Trepte, C., Vaughan, M. A., and Wielicki, B. A.: The CALIPSO Mission: A Global 3D View of Aerosols and Clouds, *B. Am. Meteorol. Soc.*, 91, 1211–1229, 2010.
- Winker, D. M., Liu, Z., Omar, A., Tackett, J., and Fairlie, D.: CALIOP observations of the transport of ash from the Eyjafjallajökull volcano in April 2010, *J. Geophys. Res.*, 117, D00U15, 2012.
- 35 Young, S. A.: Analysis of lidar backscatter profiles in optically thin clouds., *Appl. Opt.*, 34, 7019–7031, 1995.
- Young, S. A. and Vaughan, M. A.: The Retrieval of Profiles of Particulate Extinction from Cloud-Aerosol Lidar Infrared Pathfinder Satellite Observations (CALIPSO) Data: Algorithm Description, *J. Atmos. Ocean. Tech.*, 26, 1105–1119, 2009.

Young, S. A., Winker, D. M., Vaughan, M. A., Hu, Y., and Kuehn, R. E.: CALIOP Algorithm Theoretical Basis Document Part 4: Extinction Retrieval Algorithms [Available online at http://www-calipso.larc.nasa.gov/resources/pdfs/PC-SCI-202_Part4_v1.0.pdf], 2008.

Young, S. A., Vaughan, M. A., Kuehn, R. E., and Winker, D. M.: The Retrieval of Profiles of Particulate Extinction from Cloud–Aerosol Lidar and Infrared Pathfinder Satellite Observations (CALIPSO) Data: Uncertainty and Error Sensitivity Analyses, *J. Atmos. Ocean. Tech.*, 30,

5 395–428, 2013.